UNIVERSIDAD DE CÓRDOBA

DEPARTAMENTO DE INGENIERÍA FORESTAL

Programa de doctorado

Biociencias y ciencias agroalimentarias

TESIS DOCTORAL

Detección de estrés en coníferas mediante teledetección hiperespectral y térmica de alta resolución y modelos de transferencia radiativa.

PhD THESIS

Stress detection in conifer forest with high resolution hyperspectral and thermal remote sensing and radiative transfer modeling.

PhD Candidate

Rocío Hernández Clemente

PhD Supervisors

Rafael M. Navarro Cerrillo (University of Córdoba)

Pablo J. Zarco Tejada (IAS, Consejo Superior de Investigaciones Científicas)

Memoria presentada en satisfacción de los requisitos necesarios para optar al grado de doctor internacional.

TÍTULO: Detección de estrés en coníferas mediante teledetección hiperespectral y térmica de alta resolución y modelos de transferencia radiativa

AUTOR: Rocío Hernández Clemente

Campus de Rabanales Ctra. Nacional IV, Km. 396 A
14071 Córdoba

www.uco.es/publicaciones
publicaciones@uco.es

Table of contents

List of figures

Figure 2.14. Crown-level relationships obtained between the epoxidation state of the xanthophylls EPS (V+0.5*A)/(V+A+Z) and vegetation indices: NDVI (a), PRI_{570} (b) and PRI_{512} (c). Needle measurements obtained at 12:00 GMT from crowns with different levels of stress on *Pinus sylvestris* and NDVI>0.6. PRI_{570}, PRI_{512} and T obtained from the AHS airborne sensor.

Figure 2.15. Crown-level relationships obtained for *Pinus sylvestris* between the stomatal conductance (Gs) and PRI_{570} (a), PRI_{512} (b) and temperature (T) (c). Crown-level relationships between midday water potential (Ψ) and PRI_{570} (d), PRI_{512} (e) and temperature (T) (f) of trees with NDVI>0.6.

Figure 2.16. PRI_{512}, PRI_{570} and NDVI obtained from the AHS airborne sensor from three study areas of *Pinus nigra* with different levels of stress: SN1, SN2 and SN3. At the bottom of each image, two zoom images of a central plot, one pixel-based displaying 1x1 and 3x3 resolutions and the other at object level.

Figure 2.17. Mean values and standard deviation obtained from the AHS image of PRI_{570}, PRI_{512} and NDVI. Values calculated from twelve trees located in the study areas SN1, SN2 and SN3 of *Pinus nigra* (a) and SS1, SS2 and SS3 of *Pinus sylvestris* (b).

Figure 3.1. (a) Example of imagery acquired with the high resolution narrow-band airborne multispectral camera on board the UAV platform; (b) spectral reflectance extracted from the imagery for pure tree crown, shadow and soil pixels.

Figure 3.2. Leaf-level modeling simulations conducted with the PROSPECT-5 model to assess the effects of *Cx+c* and *Ca+b* content on the spectral signature in the 400-700 nm spectral range. Simulations performed for *Cx+c* variation between 2 and 16 μg cm^{-2} for mean *Ca+b* values of 10, 30 and 60 μg cm^{-2} (a,b,c). Simulations conducted for *Ca+b* variation between 10 and 60 μg cm^{-2} for mean *Cx+c* values of 6, 8 and 14 μg cm^{-2} (d,e,f).

Figure 3.3. High-resolution multispectral image acquired from the UAV platform (a) and the PROSPECT-5+DART simulated image for the same study site (b); zoomed-in image detail of the multispectral image (right) and the simulated image (left) (c); tree crown (d), bare soil (e) and shaded crown (f) spectral reflectance extracted from the multispectral image and the simulated scenes.

Figure 3.4. Canopy reflectance simulated with PROSPECT-5+DART models considering low LAI (LAI=1) and high LAI values (LAI=5) for different concentrations of *Cx+c* (4, 8 and 12 μg cm^{-2}) and a mean *Ca+b* value of 35 μg cm^{-2}.

Figure 3.5. Relationships obtained between *Ca+b, Cx+c* content and the *Ca+b/Cx+c* ratio when compared with vegetation indices proposed for *Cx+c* estimation. Data were simulated at leaf level with PROSPECT-5 model assuming random *Cx+c* (2-16 μg cm^{-2}) and *Ca+b* content (10-60 μg cm^{-2}).

Figure 3.6. Relationships obtained between *Cx+c* content and the simple ratio vegetation indices $R_{510/570}$, $R_{515/570}$, $R_{520/570}$, and $R_{530/570}$ (a) and $R_{510/560}$, $R_{515/560}$, $R_{520/560}$, $R_{530/560}$ (b). Simulations conducted at leaf level with the PROSPECT-5 model considering random *Cx+c* (2-16 μg cm^{-2}) and *Ca+b* content (10-60 μg cm^{-2}).

Figure 3.7. Relationships obtained between *Ca+b, Cx+c* content and the *Ca+b/Cx+c* ratio when compared with vegetation indices proposed for *Cx+c* estimation. Data were simulated at crown level with PROSPECT-5 model coupled with DART assuming random variation of leaf *Cx+c* (2-16 μg cm^{-2}) and *Ca+b* (10-60 μg cm^{-2}) and crown LAI ranging between 1 and 8.

Figure 3.8. Relationships obtained between *Cx+c* and vegetation indices CRI_{550} (a), RNIR*CRI_{550} (b). CRI_{700} (c) and RNIR*CRI_{700} (d) formulated with 10 and 30 nm FWHM at crown level.

Figure 3.9. Relationships obtained between *Cx+c* and vegetation indices R_{515}/ R_{570} (a) and CRI ($1/R_{515}$)-($1/R_{550}$) (b) at leaf level and crown level (c) and (d). Simulations conducted considering random variation of leaf *Cx+c* (2-16 μg cm^{-2}) and *Ca+b* (10-60 μg cm^{-2}) for crown LAI ranging between 1 and 8.

Figure 3.10. Crown-level simulations performed with PROSPECT-5 leaf model coupled with DART considering random leaf *Cx+c* (2-16 μg cm^{-2}) and *Ca+b* (10-60 μg cm^{-2}) values and LAI ranging between

1 and 8 to assess the effects of the canopy density variation on indices ($1/R_{515}$)-($1/R_{550}$) (a), ($1/R_{515}$)-($1/R_{700}$) (b), (R_{515}/R_{570}) (c) and (R_{520}/R_{570}) (d).

Figure 3.11. Canopy-level model simulations conducted with PROSPECT-5 coupled with DART to assess the effect of the *Cx+c* and *Ca+b* content variation on indices used for *Cx+c* estimation such as ($1/R_{515}$)-($1/R_{550}$) (a), (R_{746}/R_{513}) (b), (R_{515}/R_{570}) (c) and (R_{540}/R_{560}) (d). Simulations were performed for LAI ranging 1-6 and tree density variations from 800-2800 trees ha^{-1}. Values normalized to LAI=1.

Figure 3.12. Relationships between *Cx+c* content and the following indices: Gitelson ($1/R_{515}$)-($1/R_{700}$) (a), simple ratio index (R_{515}/R_{570}) (b) and Gitelson ($1/R_{515}$)-($1/R_{550}$)(c). Relationships obtained between EPS and the simple ratio index (R_{515}/R_{570}) (d). Results obtained from leaf-level measurements.

Figure 3.13. Relationships obtained between R_{515}/R_{570} (a) and R_{750}/R_{710} (b) when compared to *Ca+b* content. Results obtained from leaf-level measurements.

Figure 3.14. Relationships obtained between *Cx+c* (a;c) and *Ca+b* content (b;d) when compared to vegetation indices R_{515}/R_{570} (a;b), CRI_{700} (c) and R_{700}/R_{570} (d). Indices calculated at canopy level from the high-resolution multispectral camera on board the UAV platform.

Figure 3.15. Maps showing the spatial variation of *Cx+c* content µg cm^{-2}) using the index R_{515}/R_{570} through scaling-up. Imagery acquired with the narrow-band multispectral camera on board the UAV platform. Maps with different mean values of carotenoid content are shown for 2-6 µg cm^{-2} (a), 6-12 µg cm^{-2}(b), and 12-18 µg cm^{-2} (c).

Figure 4.1. Overview of the area acquired with the AHS instrument and plot locations of the tree measured (a). Single pixel AHS spectra for pure crown pixels of *Pinus sylvestris* and *Pinus nigra* (b).

Figure 4.2. AHS airborne footprint (a). Overview of the area acquired with the AHS instrument (b). Single pixel AHS spectra for pure vegetation, soil and mixed vegetation-soil pixels (c). Automatic object-based crown detection algorithm applied to the hyperspectral imagery to identify pure crowns extraction (d).

Figure 4.3. PROSPECT-5+DART simulated image (a); High-resolution multispectral image acquired from the AHS sensor (b) Tree crown and soil spectral reflectance obtained from the multispectral image and the simulated image (c).

Figure 4.4. Relationships obtained at the crown level between the R_{515}/R_{570} index obtained from the airborne hyperspectral imagery and Cx+c measured in the field for *Pinus sylvestris* and *Pinus nigra*.

Figure 4.5. Relationships obtained at the crown level between the red edge index obtained from the airborne hyperspectral imagery and Ca+b content measured in the field for *Pinus sylvestris* and *Pinus nigra*.

Figure 4.6. Relationships obtained at the crown level between the TCARI/OSAVI index obtained from the airborne hyperspectral imagery and Ca+b measured in the field for *Pinus sylvestris* and *Pinus nigra*.

Figure 4.7. Validation results obtained for the estimation of Cx+c from the airborne hyperspectral imagery using R_{515}/R_{570} and red edge based on infinitive formulations ($R_{\infty 1}$ and $R_{\infty 2}$) (a) and the infinitive formulation ($R_{\infty 3}$) and DART(b).

Figure 4.8. Validation results obtained for the estimation of Ca+b from the airborne hyperspectral imagery using red edge based on infinitive formulations ($R_{\infty 1}$ and $R_{\infty 2}$) (a) and the infinitive formulation ($R_{\infty 3}$) DART(b).

Figure 4.9. Mapping results obtained on two samples of *P. sylvestris* and *P. nigra* forest acquired with thy hyperspectral imager AHS in a sample area with high concentration of chlorophyll and carotenoid pigments. Color Infrared image (a), Cx+c content was estimated from indices R_{515}/R_{570} and R_{700}/R_{750} using $R_{\infty 3}$ (b), Ca+b content was estimated from R_{700}/R_{750} using $R_{\infty 3}$ (c).

Figure 4.10. Mapping results obtained on two samples of *P. sylvestris* and *P. nigra* forest acquired with thy hyperspectral imager AHS in a sample area with low concentration of chlorophyll and carotenoid pigments. Color Infrared image (a), Cx+c content was estimated from indices R_{515}/R_{570} and R_{700}/R_{750} using $R_{\infty 3}$ (b), Ca+b content was estimated from R_{700}/R_{750} using $R_{\infty 3}$ (c).

List of tables

Summary

Recently, widespread forest mortality related to drought or temperature stress has been described for drought-prone forests throughout the world. Long-term exposure of water stress to a combination of high light levels and temperatures causes a depression of photosynthesis and photosystem II efficiency that is not easily reversed even for resistant Mediterranean pines. Several authors have demonstrated that declining physiological status is connected with decline in chlorophyll content and with decreasing rate of photosynthesis; whereas the ratio C a+b/C x+c shows a decreasing trend. This thesis evaluates different physiological vegetation indices (SVI) at the canopy level and methods for the estimation of chlorophyll (C a+b) and carotenes (C x+c) pigment content with high spatial resolution sensors and radiative transfer models in heterogeneous conifer canopies. The objective is the early detection of decline processes based on the analysis of the trees physiological status and mapping of the major pigments regulating photosynthesis efficiency. Relationships between spectral vegetation indices and pigment content have been widely analyzed at the leaf level in previous works. However, studies were lacking where these kind of relationships were explored at the canopy level and for heterogeneous forest canopies. The heterogeneous forest canopies are more structurally complex than other vegetation types, therefore previous relationships obtained at the leaf level or on homogeneous canopies might not be applicable in a general way. Consequently, modelling work at leaf and canopy scales is needed to enable an operational use of SVI to map stress levels in non-homogeneous canopies where structural variation plays the main role in the reflectance signature. New formulations of SVI related to Cx+c and xanthophylls cicle were formulated based on radiative transfer simulation and experiemtal data and demonstrated to be more robust at the canopy level. A new modelling method is presented in this thesis based on scaling-up methods to estimate Ca+b and Cx+c pigment concentration. The methodology has been tested in two conifer species: *Pinus sylvestris* and *Pinus nigra*. This study required extensive field measurements of biophysical paremeters of the canopy, leaf optical and biochemistry laboratory analysis, as well as analysis of highperspectral airborne imagery acquired by a sensor on board and unmanned aerial vehicle (UAV). Moreover, the use of radiative transfer models allowed the evaluation of the influence of different biophysical paramenters; at the leaf level, such us Ca+b and Cx+c as well as the relation between them,and at the canopy level, such as Leaf Area Index (LAI) or tree density.

Resumen

En los últimos años se han descrito procesos de mortalidad en distintos tipos de bosques en todo el mundo, siendo una de las causas más importantes el estrés hídrico y térmico. La exposición a largo plazo de estrés hídrico combinado con altos niveles de radiación y altas temperaturas provoca una depresión de la fotosíntesis y la eficiencia del fotosistema II, que no es fácilmente reversible incluso para especies vegetales resistentes a este tipo de ambientes como las coníferas mediterráneas. Varios autores han demostrado que el estado de estrés fisiológico está relacionado con la disminución en el contenido de clorofila y de la fotosintésis, mientras que la proporción de C a+b / Cx +c muestra una tendencia decreciente. Esta tesis evalúa diferentes índices de vegetación fisiológicos (SVI) a nivel de la cubierta y para la estimación del contenido de clorofila (C a + b) y carotenos (C x + c) con sensores de alta resolución espacial y modelos de transferencia radiativa en bosques de coníferas. El objetivo es la detección temprana de los procesos de decaimiento basados en el análisis del estado fisiológico de los árboles y la cartografía del contenido de los principales pigmentos que regulan la eficiencia de la fotosíntesis. Las relaciones entre los índices espectrales de vegetación y contenido de pigmentos han sido ampliamente analizadas a nivel de hoja en trabajo anteriores. Sin embargo, existe una carencia de conocimiento de este tipo de relaciones a nivel de cubierta, y más concretamente aplicado a doseles de vegetación heterogéneos como los bosques de coníferas. Los doseles en este tipo de masas son estructuralmente más complejos que otros tipos de vegetación, por lo tanto, las relaciones derivadas a nivel de hoja o de cubierta homogénea no se pueden aplicar de una manera generalizada. En consecuencia, la modelización a escala de la hoja y de cubierta es necesaria para permitir un uso operativo de SVI que permitan determinar los niveles de estrés en cubiertas no homogéneos, donde la variación estructural tiene gran efecto sobre la firma espectral de la cubierta. Este trabajo presenta nuevas formulaciones de SVI relacionados con Cx+c y ciclo de las xantofilas (VAZ) obtenidas a partir de la simulación con modelos de transferencia radiativa y datos experimentales, demostrando la fiabilidad de dichas formulaciones a nivel de cubierta. La metodología ha sido probada en dos especies de coníferas mediterráneas: *Pinus sylvestris* y *Pinus nigra*. Este estudio ha requerido mediciones de parámentros biofísicos en campo, análisis ópticos y bioquímicos foliares de laboratorio, así como el análisis de imágenes hiperespectrales adquiridas en plataformas tripuladas y de vehículos aéreos no tripulados (UAV).

Además, el uso de modelos de transferencia radiativa permitieron la evaluación de la influencia de diferentes parámetros biofísicos; a nivel de hoja, tales como Ca+b y Cx+c así como la relación entre ellos, y a nivel de dosel, tales como el índice de área foliar (LAI) o la densidad de árboles.

1. Background

Chapter 1

1.1. Forest die-off of the world: a linkage between biotic and abiotic stress and global warming.

Forests are biologically diverse systems, representing some of the richest biological areas on Earth. They offer a variety of habitats for plants, animals and micro-organisms. However, forest biodiversity is increasingly threatened as a result of deforestation, fragmentation, climate change and other stressors (CBD, 2012). Loss and degradation due to human encroachment, agricultural expansion for crop and rangelands, invasive species, over-harvesting and trade in natural resources, epidemic diseases, fires, and pollution still exceed the current impacts of climate change (Kaeslin et al., 2012).

Forests are one of the most important renewable resources. The best known forest product is the timber, from which sawn wood, panels, paper or simple fuel is derived. But a host of non-wood products such as cork, forest fruits and berries, mushrooms and truffles, honey, game meat and pelts, decorative foliage and Christmas trees, and medicinal plants are sometimes just as important to local people's livelihoods (Jones, 2006). Furthermore, forests are a central part of the carbon cycle, transforming carbon dioxide from the atmosphere into carbon stored in biomass (cellulose and lignin, both above and below ground) and oxygen; this cycle impacts on the climate. As such, forests are generally considered to help attenuate the build-up of carbon dioxide in the atmosphere and contribute towards efforts to mitigate climate change (Wamelink et al., 2009).

Forest ecosystems store approximately 45% of the carbon found in terrestrial ecosystems, but they are sensitive to climate-induced dieback (McDowell, 2008; Allen et al., 2010). Forest die-off constitutes a large uncertainty in projections of climate impacts on terrestrial ecosystems, climate–ecosystem interactions, and carbon-cycle feedbacks.

In the past decade, widespread forest mortality related to drought or temperature stress has been described for drought-prone forests throughout the world (Allen & Breshears, 2007); Allen, 2010; Breshears et al., 2005; McDowell et al., 2008). In temperate North America, some of these events have been linked to "global change-type droughts," defined as severe drought coupled with elevated summer temperatures

(Breshears et al., 2005; Logan et al., 2003; Shaw et al., 2005, Worrall et al., 2010). Such mortality events can radically transform regional land cover and effect biodiversity, fire risk, ecosystem function, land–atmosphere interactions, and ecosystem services (Dale et al., 2000; Breshears et al., 2002).

CO_2 sources have a positive feedback to climate warming (Lewis et al., 2011) Climate-mediated die-off of pine forests caused by insect outbreak in Canada led to estimated carbon emissions of 990 Mt CO_2 (CO_2 equivalent) over a 20-y period, equivalent to 5 y of Canada's annual transportation sector emissions (200 Mt CO_2) (Kurz et al., 2008). The response of forests to climate warming remains a large uncertainty in climate change impacts projections on terrestrial ecosystems, climate-ecosystem feedbacks, and climate policy (Kurz et al., 2008; Phillips et al., 2009).

In Europe, forest mortality is mainly concentrated in the Mediterranean region. Increased death among many woody species in Spain (Peñuelas et al., 2001; Martinez-Vilalta & Piñol, 2002; Sánchez-Salguero et al., 2012) had been caused due to dry and warm conditions in the 1990s and 2000s decades. There has been increased death of many mixed conifer and broadleaf species in Spain with up to 19% of some populations dying. Southernmost populations of pines growing in xeric sites may be more vulnerable to warming- induced drought stress than similar populations from growing in mesic sites (Jump et al., 2006; Linares et al., 2009). Recent episodes of growth decline associated to drought events have been reported for *Pinus sylvestris* L. in central Europe (Rebetez & Dobbertin, 2004; Bigler et al., 2006) and Spain (Martínez-Vilalta & Piñol, 2002; Navarro-Cerrillo et al., 2007; Sánchez Salguero et al., 2012). Moreover, mortality and growth decline of several conifers throughout the Iberian Peninsula have been the subject of considerable study (Camarero et al., 2004).

There have also been high levels of tree mortality further north due to drought and stress from insect pests, for example, there was a loss of 111,000 m^3 of timber from English oak (*Quercus robur* L.) in Poland due to moths and other pests. And an increased rate of mortality rate of oak, fir, spruce, beech and pine was found in France after the extreme heat wave and drought during the summer of 2003 (Breda et al., 2006; Landmann et al., 2006; Vennetier et al., 2007). A severe drought in 2000 killed many *Abies cephalonica* in mainland Greece (Tsopelas et al., 2004) and *Pinus brutia* Ten. (the

most drought tolerant of the Mediterranean pines) in eastern Greece (Körner et al., 2005).

Global change have a negative effect on the forest, stressing forests through higher mean annual temperatures, altered precipitation patterns and more frequent and extreme weather events, increasing irradiation rate levels and changing the net carbon balance of plants. Thus, forest decline is a synergistic process caused by the disruption of biotic and abiotic processes that trigger joint alteration in vegetation. In particular, in Mediterranean-type ecosystems most tree and shrub species are evergreen. As a consequence their photosynthetic tissues must be adapted to a wide range of environmental conditions. Among those, summer water stress has been considered to be the main factors in limiting the distribution of Mediterranean plants, since temperatures over 45°C have been measured in Pine forest in South Spain (Martínez-Vilalta & Piñol, 2002). Because many Mediterranean environments are associated with high summer temperatures, most of the ecophysiological research on this vegetation has been focused on the plant physiological effects of water stress and heat during summer (Feret et al., 2011).

1.2. Physiological indicators of forest decline.

These factors effects on the plants light reactions or enzymatic functions and increased respiration from reparative activities. Short, climate change conditions can results in acute damage, but chronic exposure usually results in cumulative effects on physiological process. Gradual decreases in photosynthesis, stomatal conductance, carbon fixation, water use efficiency, resistance to insect and cold resistance were found in most of trees which are very typical symptom of air pollution stress (McDowell et al., 2008)

A recent synthesis put forth two broad non–pathogen-mediated and nonexclusive physiological hypotheses that could underlie drought-induced (soil water depletion or high evaporative demand) forest mortality (Anderegg et al., 2012). The carbon starvation hypothesis posits that drought drives stomatal closure and/or other effects on photosynthesis, leading to a negative carbon balance that depletes carbohydrate reserves and ends in tissue-level carbohydrate starvation (McDowell et al., 2008). The hydraulic

failure hypothesis suggests that drought increases an individual tree's water stress to the point at which the water transport system that supplies leaves is impaired (McDowell et al., 2008). Thus, potential physiological indicators of forest decline such us pigment concentration, photosynthesis, respiration and transpiration rate holds great potential to shed light on the mechanisms and processes that occur as a result of drought stress.

Long-term exposure of water stress-resistant Mediterranean pines to a combination of high light levels and high temperatures causes a depression of photosynthesis and photosystem II efficiency (Faria et al., 1998) that is not easily reversed. The conversion of violaxanthin to antheraxanthin and zeaxanthin is strongly correlated with an increase in harmless non-radiative energy dissipation (qN) that lowers the photochemical efficiency of photosystem II (ΦPSII) and provides photo-protection from oxidative damage (Demmig-Adams & Adams, 1992). This decrease in photosynthetic rate induced by visible light is called photoinhibition and it represents an integration of photodamage, repair processes and down-regulation of photosynthesis as resulting from various protective mechanisms.

Studies carried out in Mediterranean ecosystems, where vegetation is typically subjected to a summer drought, have shown an inverse relationship between photosynthetic and photo-protective capacities in tree species—species with low net photosynthetic rates exhibited high carotenoid to chlorophyll ratios and xanthophyll de-epoxidation rates (Faria et al., 1998).

Carotenoids (Cx+c) and chlorophylls (Ca+b) are the main pigments of green leaves (Blackburn, 1998). Cx+c are usually represented by two (a- and b-) carotenes and five xanthophylls (lutein, zeaxanthin, violaxanthin, antheraxanthin and neoxanthin). Xanthophyll cycle consists in the interconversions of violaxanthin and zeaxanthin through the intermediate antheraxanthin in the presence of ascorbate and an acidic pH induced by the light promoted proton pump, whereas the epoxidation reactions occur in the dark (Dall'Osto et al., 2005). Carotenoids have several physiological functions associated with photosynthesis, including structural role in the organization of photosynthetic membranes, participation in light harvesting, energy transfer (Frank & Cogdell, 1996; Ritz et al., 2000), as well as , quenching of Chl excited states and photoprotection (Demmig-Adams, 1998). The quantity of several types of carotenoids is known to correlate with plant stress and photosynthetic capacity. For example, it has

been observed that the content of some carotenoids increases in high irradiance and high temperature environments (Kirchgebner et al., 2003) or at the onset of leaf senescence (Munné-Bosch & Peñuelas, 2003). Several authors (eg Batič et al., 1999; Hoshizaki, 1988; Matyssek et al., 1993) have been demonstrated that declining physiological state is connected with decline in chlorophyll content and with decreasing rate of photosynthesis, whereas the values of ratio Ca/Cb are increasing. On the other hand, the ratio C a+b/C x+c shows a decreasing trend.

1.3. Quantitative remote sensing of forest decline based on hyperspectral and thermal data.

Water deficits occur in plants when evaporative demand exceeds the supply of water in the soil (Slatyer, 1967). It has long been found that water stress may affect adversely both metabolic processes like photosynthesis (Hsiao et al., 1976), and vegetative growth processes. Short-term water deficits also induce stomatal closure, which reduces the transpiration rate, thus decreasing evaporative cooling and increasing leaf temperature. The increase in leaf and canopy temperatures was first suggested in the 1960s as a method of tracking water stress using thermal infrared thermometers (Fuchs & Tanner, 1966; Idso et al., 1978; Jackson, 1982; Jackson et al., 1977a, 1977b; Idso et al., 1981; Jackson et al., 1981; Tanner, 1963). More recently, Sepulcre-Cantó et al. (2006, 2007) demonstrated that high-resolution airborne thermal imagers flown over orchard crops detected small canopy temperature differences linked to water stress levels. Later, Berni et al. (2009) generated maps of tree canopy conductance (Gc) in orchards by applying a model based on canopy temperature estimated from high resolution airborne imagery, using as inputs net radiation and aerodynamic resistance as a function of wind speed and canopy structure.

Even though canopy temperature is considered reliable as a proxy for plant water status monitoring (Jackson, 1982), there are physiological and remote sensing operational issues that support the development of new water-stress sensitive indices based on the visible and near infrared spectral regions (Suárez et al., 2009, 2010). Two pre-visual indicators of water stress proposed in the literature are the Photochemical Reflectance Index (PRI) (Gamon et al., 1992), an index sensitive to the epoxidation state of the xanthophyll cycle pigments and to photosynthetic efficiency, serving as a proxy for water stress detection (Peguero-Pina et al., 2008; Suarez et al., 2008, 2009,

2010; Thenot et al., 2002), and the solar-induced chlorophyll fluorescence emission (Flexas et al., 1999, 2000; Moya et al., 2004) due to the link demonstrated between steady-state chlorophyll fluorescence and stomatal conductance.

Although PRI was initially proposed as an indicator of the de-epoxidation state of the xanthophyll pigments and related to photosynthesis, recent studies demonstrate the sensitivity of this index for vegetation stress detection (Peguero-Pina et al., 2008; Suárez et al., 2009, 2010, 2008; Thenot et al., 2002). Therefore, PRI could be used for water stress detection as an alternative to thermal measurements, enabling the use of high spatial resolution capabilities that are more difficult in the thermal region.

Leaf biochemical constituents, such as chlorophyll a+b (Ca+b), water (Cw) and dry matter (Cm), are physiological indicators used as a proxy of stress that can be estimated by remote sensing data in the 400-2500 nm spectral region. In particular, several studies demonstrate that estimating chlorophyll content in leaves is feasible using leaf reflectance and transmittance (Jacquemoud et al., 1996; Carter & Spiering, 2002; Sims & Gamon, 2002; Gitelson et al., 2003; le Maire et al., 2004). For this purpose, a large number of narrow band indices calculated from hyperspectral reflectance have been proposed with success in different crops (Haboudane et al., 2002; 2004; Zarco-Tejada et al., 2001, 2005). Recently, combined indices sensitive to Ca+b content have been developed with the Transformed Chlorophyll Absorption in Reflectance Index (TCARI, Haboudane et al., 2002), and the Optimized Soil-Adjusted Vegetation Index (OSAVI, Rondeaux et al., 1996), used to minimize soil and leaf area index (LAI) effects in closed crops (Haboudane et al., 2002), tree orchards (Zarco Tejada et al., 2004) and vineyards (Zarco-Tejada et al., 2005; Martin et al., 2007; Meggio et al., 2010).

Carotenoids (Cx+c), which include two carotenes and five xanthophylls, are also important photosynthetic pigments (Demmig-Adams & Adams, 1996). Carotenoids are physiologically relevant because of their role associated with photosynthesis, participation in light harvesting and energy transfer (Frank and Cogdell, 1996; Ritz et al., 2000), quenching and photoprotection (Thayer and Björkman, 1990; Young and Britton, 1990; Demmig-Adams, 1996) Nevertheless, less research has been conducted on carotenoid content estimation due to the difficulties associated with the overlapping absorption in the blue / green region by photosynthetic pigments such as Ca+b, Cx+c and anthocyanins (Anth). The overlapping absorption by chlorophyll and carotenoids in

the 400-700 nm region poses a problem when trying to retrieve both Ca+b and Cx+c concentration independently (Feret et al., 2011). In addition, some indices have been identified as sensitive to Cx+c; they generally work well at the leaf level but there are considerable effects caused by canopy structure and background when they are applied to reflectance imagery (Meggio et al., 2010). Furthermore, achieving progress on carotenoid content estimation has become even more difficult in vineyards because they are complex heterogeneous canopies, with large effects caused by shadows and soil components as a function of sun angle and row orientation.

The main spectral bands proposed for Cx+c estimation in the visible/NIR region are based on band ratios in the 700 nm region (678, 708 and 760 nm) and the green region (500 and 550 nm) (Chappelle et al., 1992; Merzlyak et al., 1999). In addition, some indices have been proposed using the 800 nm band combined with 470, 680, and 635 nm bands (Peñuelas et al., 1995; Blackburn, 1998). In particular, the work conducted by Chappelle et al. (1992) concluded that Cx+c showed a maximum absorption peak at 500 nm, proposing ratios such as R_{760}/R_{500} for Cx+c estimation. Other authors (Gamon et al., 1992; Gitelson et al., 2003, 2006; Garrity et al., 2011) proposed visible ratios. Specific leaf-level studies conducted by Gitelson et al. (2002) showed that Cx+c absorption was directly related to a spectral absorption at 520 nm. They proposed the Carotenoid Concentration Index as $(1/R_{515})-(1/R_{550})$ and $(1/R_{515})-(1/R_{700})$ (Gitelson et al., 2002).

However, these studies relied entirely on leaf-level work and required scaling up to the canopy level, assessing the effects on the proposed indices caused by structure and background due to mixed pixels. Pigment retrieval from canopy image reflectance can be carried out through two main methodologies: based on in-situ statistical relationships or using optical radiative transfer modeling. The first method studies the correlation between leaf or canopy reflectance and ground-measured pigment. This methodology allows the derivation of relationships corresponding to specific biophysical processes targeted for measurement. Therefore, no predictive capabilities could be inferred to other study studies or situations because locally-derived measurements are related to a limited range of biophysical parameters variation. Although, the main advantage of this methodology is closely related with ground truth, and therefore is very useful in order to analyze the specific relationships between narrow-band vegetation indices and biophysical parameters.

In the second methodology, the same relationships between leaf constituent and canopy reflectance are derived scaling-up the optical indices or through the inversion of the canopy reflectance obtained from radiative transfer modeling simulation. This methodologies permits direct prediction of the canopy biochemical parameter, although this estimation are limited to the biochemical parameters including into radiative transfer modeling. A complete review of this methodologies and a direct application on forest canopies is found on the study of Zarco-Tejada et al., (2001).

1.4. Radiative transfer modelling of forest canopies.

A radiative optical model simulates radiation transfer processes in certain media. In the case of vegetation covers, it computes the bidirectional or hemispherically integrated reflectances from individual leaves to entire soil-vegetation-atmosphere radiative systems (eg. Jacquemoud & Baret 1990; Vermote et al., 1997). Consequently, radiative transfer modeling takes into account physical processes describing the interaction of radiation with the diverse canopy components at foliage and canopy levels. The simulation of reflectance at the canopy level is the results of coupling different optical simulation models that takes into account the leaf optical biochemical properties and the structure composition of forest canopies.

The main biochemical properties included in radiative transfer models at the leaf level are the content of chlorophyll (Ca+b), *C*arotenoid (Cx+c), dry matter (Cm), water (Cw) and the leaf internal structure paramenter (N). Radiative transfer modeling methods had been mainly applied based on the *Leaf Incorporating Biochemistry Exhibiting Reflectance and Transmittance Yields* (LIBERTY) model (Dawson *et al.*, 1998) and the

PROSPECT model (Jacquemoud & Baret, 1990). LIBERTY was designed to model conifer (particularly pine) needles at the cellular scale, based on Melamed's radiative transfer theory of powders (Melamed, 1963). This model calculates the directional–hemispherical reflectance and transmittance by assuming the needle structure to be cell spheres separated by air gaps. With the PROSPECT model, scattering is described by the refractive index of leaf materials (n) and by a parameter characterizing the leaf mesophyll structure (N). In the original version, absorption was modeled using pigment concentration (Ca+b, Cw, Cm), and the corresponding specific absorption coefficients

Ka+b, Km and Kw. The latter version of PROSPECT model included a physically-based separate treatment of chlorophylls and carotenoids.
The LIBERTY and PROSPECT models were assessed by Zarco-Tejada *et al.* (2004) and Moorthy *et al.* (2008) suggesting that PROSPECT could be used to model needle optical properties. PROSPECT is a radiative model initially designed for broad leaves, although it was later adapted to needles (Malenovsky *et al*., 2006). In a recent paper, Di Vittorio (2009) enhanced the limitation of LIBERTY to resolve individual pigments and the gaps in the estimation of *in vivo* specific absorption coefficients and model biophysics.

At the canopy level, modeling simulation approach becomes more complex when we move from homogeneous to heterogeneous canopies. Infinite reflectance formulations had been widely used, being even simpler canopy model approximation. They simulate the reflectance without canopy structure or viewing geometry considerations and are based solely on leaf reflectance and transmittance (see Zarco-Tejada et al., 2001 for a review of infinite reflectance models). These formulations are valid for optically thick leaf material, with different assumptions for the multiple scattering. Lillestaeter (1982), Miller et al. (1992), Yamada and Fujimura, (1991) and Hapke (1993) discussed these infinite reflectance models, applied with success to forest sites for Ca+b estimation (Zarco-Tejada et al., 2001) and for equivalent water thickness estimation (Riaño et al., 2005). Other modelization approach, such us plane parallel RT models remain spatially continuous in their conception that is they generally assume an infinite, horizontally homogeneous vegetation cover, not really representative of the architectural properties of forest vegetation cover types. The architecture of the canopy is defined by LAI and leaf angle distribution function (LADF), and no geometrical effects other than the leaf inclinations are considered. The most common turbid model applied is the Scattering by Arbitrarily Inclined Leaves (SAIL model) (Verhoef, 1984). There is a wide range of hybrid models applied for forest canopies. For example, INFORM (Invertible Forest Reflectance Model; Schlerf &Atzberger, 2006; Atzberger, 2000) is a combination of the PROSPECT leaf model (Baret & Fourty, 1997), the SAILH radiative transfer model for homogeneous canopies (Verhoef, 1984; 1985) and the semiempirical forest model FLIM (Rosema et al., 1992).

Moving from one-dimensional to three-dimensional formulations, a wide range of optical models is designed to simulate the reflectance of heterogeneous canopies (Pinty et al., 2001). The geometrical optical models are primarily designed for non-dense canopies and simulate the reflectance of the canopy according to specific dimensions and shape, placed and distributed in different configurations. Although, forest canopies should required more 3-D complex approaches to simulate the radiation transfer regime in structurally heterogeneous scenes, including ray tracing techniques associated with inverse/direct Monte-Carlo (FLIGHT, SPRINT, Raytran), and discrete ordinate methods (DART), as well as hybrid, i.e., combining analytical and numerical solutions for random distributions of plant stands (GORT, SGORT, LIM and FRT). So far, FLIGHT (North, 1996) and SPRINT (Goel & Thompson, 2000) had been widely applied to simulate forest canopies (Zarco-Tejada et al., 2004; Verrelst et al., 2010). Although, one of the more advance simulation approaches is the Discrete Anisotropic Radiative Transfer model (DART) (Gastellu-Etchegorry et al., 1996) that can operate simulating reflectance or temperature, combining the ray tracing and the discrete ordinate methods. DART is designed to simulate different landscapes, comprising forest scenes with different tree types and scene components. DART uses a 3D matrix of cells containing the turbid material for simulating vegetation, and the opaque material for simulating surfaces such as ground, urban elements or trunks.

1.5. Aim and outline of the thesis.

The main objective of this research was primarily based on the quantification of biophysical parameters for detecting forest decline indicators in an early stage of stress based on hyperspectral and thermal data. The major challenge of this work was the assessment of the confounding structural parameters affecting remote sensing data and the selection of robust vegetation indices for the retrieval of biophysical parameters at the canopy level. To achieve these objectives optical modeling simulation were performed and related to biophysical experimental measurements and to hyperspectral and thermal data acquired on board of manage and unmanaged platforms. The general scope and methodological outline of the thesis is summarized on Fig.1.1.

The specific objectives were developed on three different chapters:

Chapter 2: The study provides new insights into the application of narrow-band vegetation indices and thermal data as previsual detection of forest decline processes.

The work was focused on the analysis of PRI as an indicator of stress on complex canopies, analyzing the effects on PRI formulations due to the structure. The study assessed imaged and model-simulated PRI obtained through radiative transfer simulation of conifer canopies, evaluating the sensitivity of PRI formulations to EPS while minimizing canopy structural effects.

Chapter 3: The study provides an assessment of the estimation of carotenoid content in a complex conifer forest using high spatial and spectral resolution imagery and 3D canopy modeling methods. A combined observation and modeling-based approach was applied to assess the influence of leaf and canopy parameters on various narrow-band vegetation indices proposed to estimate carotenoid content.

Chapter 4: The study aims to analyze the retrieval of both Ca+b and Cx+c content on forest canopies using scaling-up approaches based on the model simulation of narrow band vegetation indices. The study involved the comparison analysis of using complex 3D canopy radiative transfer model (DART) coupled with the leaf-model PROSPECT from using three different infinitive models for the retrieval of pigment content at the crown level.

In the final section (**Chapter 5**), the main findings of this thesis are synthesized including a general discussion that links the three main researches developed in this work.

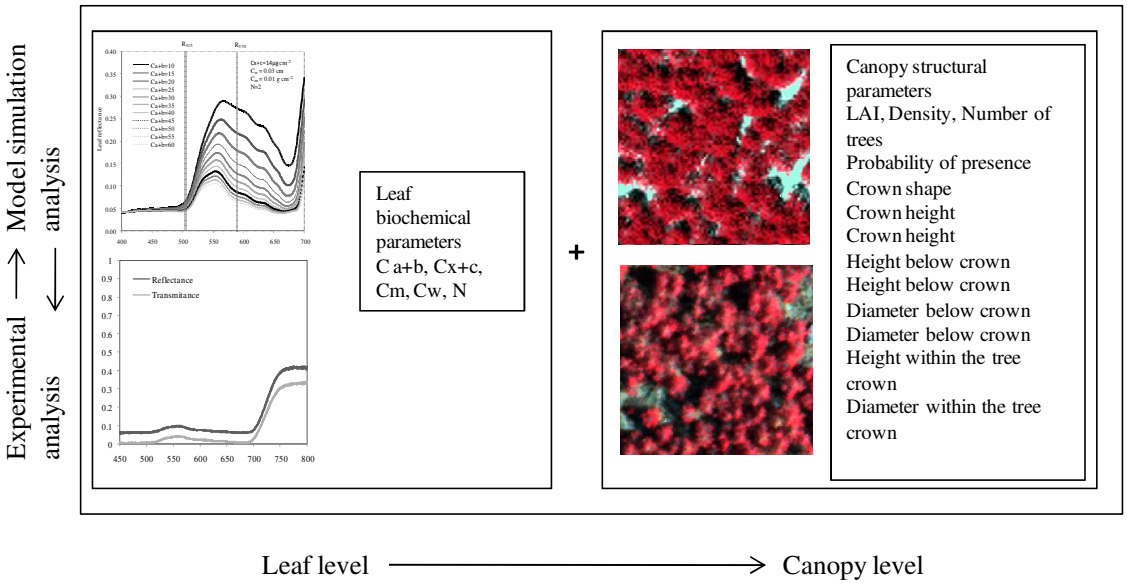

General aim of the thesis:
Assesment of forest decline at the canopy level based on hyperspectral and thermal data.

Specific objectives:

Analysis of structural effects on leaf vegetation indices formulations and thermal data.
Chapter 2: Assessing structural effects on PRI for stress detection in conifer forests.
Chapter 3: Carotenoid content estimation in a heterogeneous conifer forest using narrow-band indices and PROSPECT + DART simulations.

Pigment retrieval at canopy level based on scaling-up methods.
Chapter 4: Scaling-up with narrow-band optical Indices for chlorophyll and carotenoid content estimation in conifer forest under decline with Hyperspectral data and radiative transfer model.

Figure 1.1. General aim of the thesis and methodological outline.

1.5. Study area.

The experimental area is located in Sierra de Filabres (Almeria province, southeastern Spain) (37° 13' 27" N, 2° 32' 54" W), the driest region in Western Europe. The elevation of the study area ranges from 1540 to 2000 m.a.s.l.. Climatic trends in eastern Andalusia, southern Spain, during the second half of the 20th century were characterized by a high drop of spring rain (De Luis et al., 2008). Such increase in

spring aridity was particularly noticeable in mountains from SE Spain (Fernández-Cancio et al., 2011). Concurrently, a dieback process was detected in 2002 in Sierra de los Filabres (Andalusia, SE Spain) affecting at least 10,000 ha of Pinus afforestations that showed massive defoliation, spreading to the neighboring range in Sierra de Baza (Navarro-Cerrillo et al., 2007; Sánchez-Salguero et al., 2010). The lack of visual symptoms of forest pathogens and pests, and its coincidence with previous extreme droughts in the mid 1990s, suggested that the decline might be linked to drought stress (Fernández-Cancio et al., 2011).

In the study area, the mean annual rainfall (1950- 2009 period) ranged between 320 mm and 400 mm and the estimated mean annual temperature was 11°C, reaching a maximum of 32ºC during summer and a minimum of -8ºC during winter. These values correspond to a Mediterranean semi-arid climate. Parent material is composed of siliceous rock with quartz micaschists, forming eutric cambisol-regosol soils.

The vegetation analyzed consists of a 40-year-old mixed pine afforestation of Pinus nigra Arnold and *Pinus sylvestris* L. (Table 1.1 and 1.2).

Table 11. Structural parameters of *Pinus nigra* and *Pinus sylvestris* forest in the training areas. Mean values of age, height, basimetric area (BA) and min and max values of density.

Main species (Units)	Age (years)	Height (m)	Density (trees ha^{-1})	BA ($m^2 ha^{-1}$)
Pinus sylvestris L.	35	7.99	1100-1895 (Mean: 1475	26.55
Pinus nigra Arnold	40	8.60	950-2263 (Mean:1594)	27.33

Table 1.2. Mean values and standard deviation of structural parameters calculated from the twelve trees measured in each study area for *Pinus sylvestris* (SS1, SS2, SS3) *and Pinus nigra* (SN1, SN2, SN3). Mean values of defoliation (%), basimetric area (BA), perimeter, height, stem height, trunk longitude, crown diameter and leaf area index (LAI).

Study area	BA (m^2 ha^{-1})	Perimeter (cm)	Height (m)	Stem height (m)	Trunk long. (m)	Crown diameter (m)	LAI
SS1	27.67	49.61	8.71	2.16	0.47	3.13	2.25
	(±3.78)	*(± 5.42)*	*(± 0.93)*	*(± 1.72)*	*(± 0.02)*	*(± 0.74)*	*(± 0.02)*
SS2	22.00	48.33	7.97	2.17	0.64	3.12	2.36
	(±7)	*(± 4.47)*	*(±0.49)*	*(± 0.147)*	*(± 0.01)*	*(± 0.41)*	*(± 0.46)*
SS3	30.00	41.72	7.30	1.76	0.19	2.82	1.69
	(±4)	*(± 7.08)*	*(± 0.55)*	*(± 1.07)*	*(± 0.42)*	*(± 0.55)*	*(± 0.19)*
SN1	32.33	47.20	8.95	2.61	1.71	4.14	1.90
	(± 1.52)	*(± 8.76)*	*(± 0.14)*	*(± 0.00)*	*(± 0.52)*	*(± 0.68)*	*(±0.01)*
SN2	25	38.98	10.17	3.98	1.84	3.23	1.92
	(± 4.35)	*(± 3.91)*	*(± 1.25)*	*(± 0.46)*	*(± 0.00)*	*(± 0.63)*	*(±0.19)*
SN3	24.66	28.22	6.70	1.56	0.55	3.29	2.28
	(± 6.80)	*(± 2.71)*	*(± 0.97)*	*(± 1.27)*	*(± 0.23)*	*(± 0.45)*	*(±0.45)*

References

Allen, C.D. & Breshears, D.D. (2007). Climate-induced forest dieback as an emergent global phenomenon, *Eos Trans AGU*, 88, 47–54.

Allen, C.D., Macalady, A.K., Chenchouni, H., Bachelet, D., McDowell, N., Vennetie, M., Kitzberger, T., Rigling, A., Breshears, D.D., Hogg, E.H, González, P., Fensham, R., Zhang, Z., Castro, J., Demidova, N., Lim, J.H., Allard, G., Running, S.W., Semerci, A. & Cobb, N. (2010). A global overview of drought and heat-induced tree mortality reveals emerging climate change risks for forests. *Forest Ecology and Management*, 259, 660-684.

Anderegg, W.R.L., Berry, J.A., Smith, D.D., Sperry, J.S., Anderegg, L.D.L. & Field, C.B. (2012). The roles of hydraulic and carbon stress in a widespread climate-induced forest die-off. *Proc. Natl. Acad. Sci. U.S.A.*, 109(1), 233-237.

Atzberger, C., (2000). Development of an invertible forest reflectance model: The INFOR model. In: Buchroithner (ed.): *A decade of transeuropean remote sensing cooperation*, 39-44. Dresden, Germany

Baret F. & Fourty T. (1997). Estimation of leaf water content and specific leaf weight from reflectance and transmittance measurements. *Agronomie*, *17*, 455-464.

Batič, F.; Kalan, P.; Kraigher, H.; Šircelj, H.; Simončič, P.; Vidergar-Gorjup, N.; & Turk, B. (1999). Bioindication of different stresses in forest decline studies in Slovenia. Water. *Air and Soil Pollution*, 116, 377-382.

Berni, J.A.J., Zarco-Tejada, P.J., Sepulcre-Cantó, G., Fereres, E. & Villalobos, F.J., (2009). Mapping canopy conductance and CWSI in olive orchards using high resolution thermal remote sensing imagery. *Remote Sensing of Environment*, 113, 2380-2388.

Bigler, C., Bräker O.U., Bugmann, H., Dobbertin, M. & Rigling, A. (2006). Drought as an inciting mortality factor in Scots pine stands of the Valais, Switzerland**,** 9 *Ecosystems*, 330-343.

Blackburn, G.A. (1998). Quantifying chlorophylls and carotenoids at leaf and canopy scales: An evaluation of some hyperspectral approaches. *Remote Sensing of Environment*, 66, 273-285.

Breda, N., Huc, R., Granier, A., Dreyer, E. (2006). Temperate forest trees and stands under severe drought: a review of ecophysiological responses, adaptation processes and long-term consequences. *Annals of Forest Science*, 63, 625–644.

Breshears, D.D., & Allen, C.D. (2002). The importance of rapid, disturbance-induced losses in carbon management and sequestration. *Global Ecology and Biogeography Letters*, 11, 1-15.

Breshears, D.D., Cobb N.S., Rich, P.M., Price, K.P., Allen, C.D., Balice, R.G., Romme, W.H., Kastens, J.H., Floyd, M.L., Belnap, J., Anderson, J.J., Myers, O.B., & Meyer, C.W. (2005). Regional vegetation die-off in response to global-change type drought. *Proceedings of the National Academy of Sciences of United States of America*, 102(42), 15144–15148.

Camarero, J.J., Lloret, F., Corcuera, L., Peñuelas, J., & Gil-Pelegrín, E. (2004). Cambio global y decaimiento del bosque. In Valladares, F. (Ed.), *Ecología del bosque mediterráneo en un mundo cambiante* (pp. 397-423). Ministerio de Medio Ambiente, Madrid.

Carter, G. A., & Spiering, B. A. (2002). Optical properties of intact leaves for estimating chlorophyll content. *Journal of Environmental Quality*, 31, 1424-1432.

CBD (2012). Forest Biodiversity. Convention on Biological Diversity, http://www.cbd.int/forest/.

Chappelle, E. W., Kim, M. S., & McMurtrey, J. E., III (1992). Ratio analysis of reflectance spectra (RARS): An algorithm for the remote estimation of the concentrations of chlorophyll a, chlorophyll b, and carotenoids in soybean leaves. *Remote Sensing of Environment*, 39, 239-247.

Dale, V.H., Joyce, L.A., McNulty, S., Neilson, R.P., Ayres, M.P., Flannigan, M.D., Hanson, P.J., Irland, L.C., Lugo, A.E., Peterson, C.J., Simberloff, D., Swanson, F.J.,

Stocks, B.J., & Wotton, M. (2001). Climate change and forest disturbance. *BioScience*, 51, 723-734.

Dall'Osto, L., Caffarri, S., & Bassi, R. (2005). A mechanism of nonphotochemical energy dissipation, independent from Psbs, revealed by a conformational change in the antenna protein CP26. *Plant Cell*, 17, 1217-1232.

Demmig-Adams B. & Adams W. W. (1996). The role of xanthophyll cycle carotenoids in the protection of photosynthesis. *Trends in Plant Science*, 1, 21-26.

Demmig-Adams, B., & Adams, W. W. III (1992). Photoprotection and other responses of plants to high light stress. *Annual Review of Plant Physiology and Plant Molecular Biology*, 43, 599-626.

di Vittorio, A. V. (2009). Enhancing a leaf radiative transfer model to estimate concentrations and in-vivo specific absorption coefficients of total carotenoids and chlorophylls a and b from single-needle reflectance and transmittance. *Remote Sensing of Environment*, *113*, 1948-1966.

Faria, T., Silvério, D., Breia, E., Cabral, R., Abadia, A., Abadia, J., Pereira, J.S., & Chaves, M.M. (1998). Differences in the response of carbon assimilation to summer stress (water deficits, high light and temperature) in four Mediterranean tree species. *Physiologia Plantarum*, 102, 419-428.

Feret, J. B., François, C., Asner, G.P., Gitelson, A.A., Martin, R.E., Bidel, L.P.R., Ustin, S.L., le Maire, G., & Jacquemoud, S. (2008). PROSPECT-4 and 5: Advances in the leaf optical properties model separating photosynthetic pigments. *Remote Sensing of Environment*, 112, 3030-3043.

Fernández Cancio, A., Navarro Cerrillo, R.M., Sánchez Salguero, R., Fernández Fernández, R., & Manrique Menéndez, E. (2011). Phytoclimatic suitability of Scots pine plantations (*Pinus sylvestris* L.) at Sierra de los Filabres (Almería). *Ecosistemas*, 20 (1),124-144.

Flexas, J., Briantais, J.-M., Cerovic, Z., Medrano, H., Moya, I. (2000). Steady-state and maximum chlorophyll fluorescence responses to water stress in grapevine leaves: a new remote sensing system. Remote Sens. Environ. 73, 283–297.

Flexas, J., Escalona, J.M., & Medrano H. (1999). Water stress induces different levels of photosynthesis and electron transport rate regulations in grapevines. *Plant, Cell and Environment*, 22, 39–48.

Frank, H., & Cogdell, R. (1996). Carotenoids in photosynthesis. *Photochemistry and Photobiology*, 63, 257–264.

Fuchs, M., & Tanner, C.B. (1966). Infrared Thermometry of Vegetation. *Agronomy Journal*, 58, 597–601.

Gamon, J.A., Peñuelas, J., & Field, C.B. (1992). A narrow-wave band spectral index that tracks diurnal changes in photosynthetic efficiency. *Remote Sensing of Environment*, 41, 35-44.

Garrity, S.R., Eitel, J.U.H., & Vierling, L.A. (2011). Disentangling the relationships between plant pigments and the photochemical reflectance index reveals a new approach for remote estimation of carotenoid content. *Remote Sensing of Environment*, 115, 628-635.

Gastellu-Etchegorry J.P., Demarez V., Pinel V., & Zagolski F., (1996). Modelling radiative transfer in heterogeneous 3-D vegetation canopies. *Remote Sensing of Environment*, *58*, 131-156.

Gitelson, A.A., Gritz, U., & Merzlyak, M.N. (2003). Relationships between leaf chlorophyll content and spectral reflectance and algorithms for non-destructive chlorophyll assessment in higher plant leaves. *Journal of Plant Physiology*, 160, 271-282.

Gitelson, A.A., Keydan, G.P., & Merzlyak, M.N. (2006). Three-band model for noninvasive estimation of chlorophyll, carotenoids, and anthocyanin content in higher plant leaves. *Geophysical Research Letters*, 33, L11402.

Gitelson, A.A., Zur, Y., Chivkunova, O.B., & Merzlyak, M.N. (2002). Assessing carotenoid content in plant leaves with reflectance spectroscopy. *Journal of Photochemistry and Photobiology B-Biology*, 75, 272-281.

Goel, N., & Thompson, R. (2000). A snapshot of Canopy Reflectance Models and a Universal Model for the Radiation Regime. *Remote Sensing Reviews*, *18*, 197-225

Haboudane, D., Miller, J. R., Pattey, E., Zarco-Tejada, P. J., & Strachan, I. (2004). Hyperspectral vegetation indices and novel algorithms for predicting green LAI of crop canopies: modeling and validation in the context of precision agriculture. *Remote Sensing of Environment,* 90, 337-352.

Haboudane, D., Miller, J. R., Tremblay, N., Zarco-Tejada, P. J., & Dextraze, L. (2002). Integrated narrow-band vegetation indices for prediction of crop chlorophyll content for application to precision agriculture. *Remote Sensing of Environment*, 81, 416-426.

Hapke, B., (1993). *Theory of reflectance and emittance spectroscopy (Topics in Remote Sensing 3)*. Cambridge University Press, Cambridge England and New York, NY, USA.

Hoshizaki, T.; Rock, B.N.; & Wong, S.K.S. (1988). Pigment analysis and spectral assessment of spruce trees undergoing forest decline in the NE United States and Germany. *GeoJournal*, 17, 173-178.

Hsiao, T.C., Acevedo, E., Fereres, E., & Henderson D.W. (1976). Stress metabolism: Water stress, growth and osmotic adjustment. *Philosophical Transactions of the Royal Society of London. B: Biological Sciences*, 273, 479-500.

Idso, S.B.; Jackson, R.D.; Reginato, R.J. (1977). Remote sensing of crop yields. *Science*, 196, 19–25.

Idso, S.B.; Jackson, R.D.; & Reginato, R.J. (1978). Remote sensing for agricultural water management and crop yield prediction. *Agricultural Water Management*, 1. 299-310.

Jackson, R.D. (1982). Canopy temperature and crop water stress. *Adv. Irrig.*, 1, 43–85.

Jackson, R.D.; Idso, D.B.; Reginato, R.J.; and Pinter, P.J., Jr. (1981). Canopy temperature as a crop water stress indicator, *Water Resources Reseach*, 17, 1133-1138.

Jackson, R.D.; Idso, S. B.; Reginato, R. J.; & Ehrler, W.L. (1977b). Crop temperature reveals stress. *Crop Soils*, 29, 10-13.

Jackson, R.D.; Reginato, R.J.; & Idso, S.B. (1977a). Wheat canopy temperature: a practical tool for evaluating water requirements. *Water Resources Reseach*, 13,651-656.

Jacquemoud S. & Baret F. (1990). PROSPECT: a model of leaf optical properties spectra. *Remote Sensing of Environment*, 34, 75-91.

Jacquemoud S.; Ustin S.L.; Verdebout J.; Schmuck G.; Andreoli G.; & Hosgood B. (1996). Estimating leaf biochemistry using the PROSPECT leaf optical properties model. *Remote Sensing of Environment*, 56,194-202.

Jones, W. (2006). *LIFE and European forests*. Luxembourg: Office for Official Publications of the European Communities.

Jump, A.S.; Hunt, J.M.; Martinez-Izquierdo, J.A.; & Peñuelas, J. (2006). Natural selection and climate change: temperature-linked spatial and temporal trends in gene frequency in *Fagus sylvatica*. *Molecular Ecology*, 15, 3469-3480.

Kaeslin, E.; Redmond, I.; & Dudley, N. (Eds.) (2012). *Wildlife in a changing climate.* FAO Forestry Paper, 167, Rome: Food And Agriculture Organization of the United Nations.

Kirchgebner, H.-D.; Reichert, K.; Hauff, K.; Steinbrcher, R.; Schnitzler, J.-P.; Pfündel E.E. (2003). Light and temperature, but not UV radiation, affect chlorophylls and carotenoids in Norway spruce needles (*Picea abies* (L.) Karst.). *Plant, Cell & Environment*, 26, 1169-1179.

Körner, C.; Sarris, D. & Christodoulakis, D. 2005. Long-term increase in climatic dryness in the East-Mediterranean as evidenced for the island of Samos. *Regional Environmental Change Journal*, 5, 27-36.

Kurz, W.A.; Dymond, C.C.; Stinson G.; Rampley, G.J.; Neilson, E.T.; Carroll, A.L.; Ebata, T.; & Safranyik, L. (2008). Mountain pine beetle and forest carbon feedback to climate change. *Nature*, 452, 987-990.

Landmann, G.; & Dreyer, E. (Eds.) (2006). Impacts of drought and heat on forest. Synthesis of available knowledge, with emphasis on the 2003 event in Europe. *Annals of Forest Science*, 3 (6), 567-652.

Lewis, S.L.; Brando, P.M.; Phillips, O.L.; van der Heijden, G.M.; & Nepstad, D. (2011). The 2010 Amazon drought. *Science*, 331,554.

Lillestaeter, O. (1982). Spectral reflectance of partly transmitting leaves: Laboratory measurements and mathematical modelling. *Remote Sensing of Environment,* 12, 247-254.

Linares, J.C.; Camarero, J.J.; & Carreira, J.A. (2009). Interacting effects of climate and forest-cover changes on mortality and growth of the southernmost European fir forests. *Global Ecology and Biogeography*, 18, 485-497.

Logan, J.A.; Régnière, J.; & Powell, J. (2003). Assessing the impacts of global warming on forest pest dynamics. *Frontiers in Ecology and the Environment*, 1,130-137.

de Luis, M., González-Hidalgo, J. C., Longares, L. A., & Štepánek, P. (2008). Regímenes estacionales de precipitación en la vertiente Mediterránea de la Península Ibérica. In Sigró Rodriguez, J., Brunet India, M. & Aguilar Afons, E. (Eds.), *Cambio Climático Regional y sus Impactos* (Serie A, nº 6., pp. 81-90). Tarragona: Publicaciones de la Asociación Española de Climatología (AEC).

le Maire, G.; François, C.; & Dufrêne, E. (2004). Towards universal broad leaf chlorophyll indices using PROSPECT simulated database and hyperspectral reflectance measurements. *Remote Sensing of Environment*, 89, 1-28.

Malenovský Z., Albrechtová J., Lhotáková Z., Zurita-Milla R., Clevers J. G. P. W., Schaepman M. E., & Cudlín P. (2006). Applicability of the PROSPECT model for Norway spruce needles. *International Journal of Remote Sensing*, *24*, 5315-5340.

Martín, P.; Zarco-Tejada, P.J.; González, M.R.; Berjón, A. (2007). Using hyperspectral remote sensing to map grape quality in Tempranillo vineyards affected by iron deficiency chlorosis. *Vitis*, 46, 7-14.

Martínez-Vilalta, J. & Piñol, J. (2002). Drought-induced mortality and hydraulic architecture in pine populations of the NE Iberian Peninsula. *Forest Ecology and Management*, 161, 247-256.

Matyssek, R.; Keller, T., & Koike, T. (1993). Branch growth and leaf gas-exchange of *Populus tremula* exposed to low ozone concentrations throughout 2 growing seasons. *Environmental Pollution*, 79, 1-7.

McDowell, N.; Pockman, W.T.; Allen, C.D.; Breshears, D.D.; Cobb, N.; Kolb,T.; Plaut, J.; Sperry, J.; West, A; Williams, D.G.; & Yepez, E.A. (2008). Mechanisms of plant survival and mortality during drought: why do some plants survive while others succumb to drought?. *New Phytologist*, 178, 719-739.

Meggio, F.; Zarco-Tejada, P.J.; Núñez, L.C.; Sepulcre-Cantó, G.; González, M.R.; & Martin, P. (2010). Grape quality assessment in vineyards affected by iron deficiency chlorosis using narrow-band physiological remote sensing indices. *Remote Sensing of Environment*, 114, 1968-1986.

Melamed N.T. (1963), Optical properties of powders. Part I. Optical absorption coefficients and the absolute value of the diffuse reflectance. Part II. Properties of luminescent powders, Applied Optics, 34(3):560-570.

Merzlyak, M.N.; Gitelson, A. A.; Chivkunova, O.B.; & Rakitin, V.Y. (1999). Non-destructive optical detection of leaf senescence and fruit ripening. *Physiologia Plantarum*, 106, 135- 141.

Miller, J.R.; Steven, M.D.; & Demetriades-Shah, T.H. (1992). Reflection of layered bean leaves over different soil backgrounds Measured and simulated spectra. *International Journal of Remote Sensing*, 13, 3273-3286.

Moorthy I., Miller J. R., & Noland T. L. (2008). Estimating chlorophyll concentration in conifer needles with hyperspectral data: An assessment at the needle and canopy level. Remote Sensing of Environment, 112, 2824-2838.

Moya, I.; Camenen, L.; Evain, S.; Goulas, Y.; Cerovic, Z. G.; Latouche, G.; Flexas, J.; & Ounis A. (2004). A new instrument for passive remote sensing 1. Measurements of sunlight-induced chlorophyll fluorescence. *Remote Sensing of Environment*, 91, 186–197.

Munné-Bosch, S. & Peñuelas, J. (2003). Photo and antioxidative protection and a role for salicylic acid during drought and recovery in field-grown *Phillyrea angustifolia* plants. *Planta*, 217, 758-766.

Navarro-Cerrillo, R.M.; Varo, M.A.; Lanjeri, S.; & Hernández Clemente, R. (2007). Cartografía de defoliación en los pinares de pino silvestre (*Pinus sylvestris* L.) y pino salgareño (*Pinus nigra* Arn.) en la Sierra de los Filabres. *Ecosistemas*, 16,163-171.

North, P. R. J. (1996). Three-dimensional forest light interaction model using a Monte Carlo method. *IEEE Transactions on Geoscience and Remote Sensing*, *34*, 946-956.

Peguero-Pina, J. J.; Morales, F.; Flexas, J.; Gil-Pelegrín, E.; & Moya, I. (2008). Photochemistry, remotely sensed physiological reflectance index and de-epoxidation state of the xanthophyll cycle in *Quercus coccifera* under intense drought. *Oecologia*, 156, 1-11.

Peñuelas, J.; Baret, F.; & Filella, I. (1995). Semi-empirical indices to assess carotenoids/ chlorophyll a ratio from leaf spectral reflectance. *Photosynthetica*, 31, 221-230.

Peñuelas, J.; Lloret, F.; & Montoya, R. (2001). Severe drought effects on Mediterranean woody flora in Spain. *Forest Science*, 47, 214-218.

Phillips, O.L.; Aragão, L.E.O.C.; Lewis, S.L.; Fisher, J.B.; Lloyd, J.; López-González, G.; Malhi, Y.; Monteagudo, A.; Peacock, J.; Quesada, C.A.; van der Heijden, G.; Almeida, S.; Amaral, I.; Arroyo, L.; Aymard, G.; Baker, T.R.; Bánki, O.; Blanc, L.; Bonal, D.; Brando, P.; Chave, J.; Alves de Oliveira, A.C.; Dávila Cardozo, N.; Czimczik, C.I.; Feldpausch, T.R.; Freitas, M.A.; Gloor, E.; Higuchi, N.; Jiménez, E.; Lloyd, G.; Meir, P.; Mendoza, C.; Morel, A.; Neill, D.A.; Nepstad, D.; Patiño, S.; Peñuela, M.C.; Prieto, A.; Ramírez, F.; Schwarz, M.; Silva, J.; Silveira, M.; Thomas,

A.S.; ter Steege, H.; Stropp, J.; Vásquez, R.; Zelazowski, P.; Alvarez Dávila, E.; Andelman, S.; Andrade, A.; Chao, K-J.; Erwin, T.; Di Fiore, A.; Honorio E.C.; Keeling, H.; Killeen, T.J.; Laurance, W.F.; Peña Cruz, A.; Pitman, N.C.A.; Núñez Vargas, P.; Ramírez-Angulo, H.; Rudas, A.; Salamão, R; Silva, N.; Terborgh, J.; & Torres-Lezama, A. (2009). Drought sensitivity of the Amazon rainforest. *Science*, 323, 1344-1347.

Pinty, B., Gobron, N., Widlowski, J. L., Gerstl, S. A. W., Verstraete, M. M., Antunes, M., Bacour, C., Gascon, F., Gastellu, J.P., Goel, N., Jacquemoud, S., North, P. R. J., Qin, W., & Thompson, R. (2001). The Radiation Transfer Model Intercomparison (RAMI) exercise. *Journal of Geophysical Research*, *106*, 11,937- 11,956.

Rebetez, M. & Dobbertin, M. (2004). Climate change may already threaten Scots pine stands in the Swiss Alps. *Theoretical and Applied Climatology*, 79, 1-9.

Riaño, D., Vaughan, P., Chuvieco, E., Zarco-Tejada, P. J., & Ustin, S. L. (2005). Estimation of fuel moisture content by inversion of radiative transfer models to simulate equivalent water thickness and dry matter content: analysis at leaf and canopy level. *IEEE Transaction on Geoscience and Remote Sensing*, *43*, 819–826

Ritz, T.; Damjanovic, A.; Schulten, K.; Zhang, J-P; & Koyama, Y. (2000). Efficient light harvesting through carotenoids. *Photosynthesis Research*, 66: 125-144.

Rondeaux, G.; Steven, M.; & Baret, F. (1996). Optimization of Soil-adjusted vegetation indices. *Remote Sensing of Environment*, 55, 95-107.

Rosema, A., Verhoef, W., Noorbergen, H., & Borgesius, J.J. (1992) A new forest light interaction model in support of forest monitoring, *Remote Sensing of Environment 42*,23-41.

Sánchez-Salguero, R.; Navarro-Cerrillo, R.M.; Camarero Martínez, J.J.; Fernández Cancio, A. (2010). Drought-induced growth decline of Aleppo and maritime pine forests in south-eastern Spain. *Forest Systems,* 19 (3), 458-470.

Sánchez-Salguero, R.; Navarro-Cerrillo, R.M.; Camarero, J.J.; & Fernández-Cancio, A. (2012). *Selective drought-induced decline of pine species in southeastern Spain*. Climatic change. DOI 10.1007/s10584-011-0372-6.

Schlerf, M., & Atzberger, C. (2006). Inversion of a forest reflectance model to estimate structural canopy variables from hyperspectral remote sensing data. *Remote Sensing of Environment*, *100*, 281- 294.

Sepulcre-Cantó, G.; Zarco-Tejada, P.J.; Jiménez-Muñoz, J.C.; Sobrino, J.A.; de Miguel, E.; & Villalobos, F.J. (2006). Detection of Water Stress in an Olive Orchard with Thermal Remote Sensing Imagery. *Agricultural and Forest Meteorology*, 136, 31-44.

Sepulcre-Cantó, G.; Zarco-Tejada, P.J.; Jiménez-Muñoz, J.C.; Sobrino, J.A.; Soriano, M.A.; Fereres, E.; & Vega, V. (2007). Monitoring Yield and Fruit Quality parameters in Open-Canopy Tree Crops under Water Stress. Implications for ASTER. *Remote Sensing of Environment* 107, 455-470.

Shaw, J.D.; Steed, B.E.; & DeBlander, L.T. (2005). Forest inventory and analysis (FIA) annual inventory answers the question: What is happening to pinyon-juniper woodlands?. *Journal of Forestry*, 103: 280-285.

Sims, D. A., & Gamon, J. A. (2002). Relationships between leaf pigment content and spectral reflectance across a wide range of species, leaf structures and developmental stages. *Remote Sensing of Environment*, 81, 337-354.

Slatyer, R. O. (1967). *Plant-water relationships* (Last edited on 2002/02/27). London and New York. Academic Press.Vol.2.

Suárez, L.; Zarco-Tejada, P.J.; Berni, J.A.J.; González-Dugo, V.; & Fereres, E. (2009). Modelling PRI for Water Stress Detection using Radiative Transfer Models. *Remote Sensing of Environment*, 113, 730-744.

Suárez, L., Zarco-Tejada, P.J., González-Dugo, V., Berni, J.A.J., Sagardoy, R., Morales, F., Fereres, E. (2010). Detecting water stress effects on fruit quality in orchards with time-series PRI airborne imagery. *Remote Sensing of Environment*, 114, 286-298.

Suárez, L.; Zarco-Tejada, P.J.; Sepulcre-Cantó, G.; Pérez-Priego, O.; Miller, J.R.; Jiménez-Muñoz, J.C.; & Sobrino, J., (2008). Assessing Canopy PRI for Water Stress detection with Diurnal Airborne Imagery. *Remote Sensing of Environment*, 112, 560-565.

Tanner, C. B. (1963). Plant temperatures. *Agronomy Journal*, 55, 210-211.

Thayer, S.S. & Björkman, O. (1990). Leaf xanthophyll content and composition in sun and shade determined by HPLC. *Photosynthesis Research*, 23, 331-343.

Thenot, F.; Méthy, M.; & Winkel, T. (2002). The Photochemical Reflectance Index (PRI) as a water-stress index. *International Journal of Remote Sensing*, 23(23), 5135-5139.

Tsopelas, P.; Angelopoulos, A.; Economou, A.; & Soulioti, N. (2004). Mistletoe (*Viscum album*) in the fir forest of Mount Parnis, Greece. *Forest Ecology and Management*, 202, 59-65.

Vennetier, M.; Vila, B.; Liang, E.Y.; Guibal, F.; Thabeet, A.; Gadbin-Henry, C. (2007). Impact of climate change on pine forest productivity and on the shift of a bioclimatic limit in a Mediterranean area. *Options Mediterraneennes*, Serie A, n8 75, CIHEAM/IAMB, Bari, Italy, 189-197.

Verhoef, W. (1984). Light scattering by leaf layers with application to canopy reflectance modeling: the SAIL model. *Remote Sensing of. Environment*, *16*, 125-141.

Verhoef, W. (1985). Earth Observation Modelling Based on Layer Scattering Matrices. *Remote Sensing of Environment*, *17*, 165-178

Vermote, E. F., Tanré, D., Deuzé, J.L., Herman, M., Morcrette, J.J. (1997). Second Simulation of the Satellite Signal in the Solar Spectrum, 6S : An Overview, IEEE Transactions On *Geoscience and Remote Sensing, 35* , 675-686 .

Verrelst, J., Schaepman, M. E., Malenovský, Z., & Clevers J. G. P. W. (2010). Effects of woody elements on simulated canopy reflectance: Implications for forest chlorophyll content retrieval. *Remote Sensing of Environment*, *114*, 647-656.

Wamelink, G.W.W.; Wieggers, H.J.J.; Reinds, G.J.; Kros, J.; Mol-Dijkstra, J.P.; van Oijen, M.; & de Vries W. (2009). Modelling impacts of changes in carbon dioxide concentration, climate and nitrogen deposition on carbon sequestration by European forests and forest soils. *Forest Ecology and Management*, 258, 1794-1805

Worrall, J.J.; Marchetti, S.B.; Egeland, L.; Mask, R.A.; Eager, T.; & Howell, B. (2010). Effects and etiology of sudden aspen decline in southwestern Colorad, USA. *Forest Ecology and Management*, 260, 638-648.

Yamada, N. & Fujimura, S. (1991). Non destructive measurement of chlorophyll pigment content in plant leaves from three-color reflectance and transmittance. *Applied Optics*, 30, 3964–3973.

Young, A. & Britton, G. (1990). Carotenoids and stress. In Alscher, R. G. & Cumming, J. R. (Eds.), *Stress responses in plants: adaptation and acclimation mechanisms* (pp. 87-112). New York: Wiley- Liss. Inc.

Zarco-Tejada, P.J.; Berjón, A.; López-Lozano, R.; Miller, J.R.; Martín, P.; Cachorro, V.; González, M.R.; & Frutos, A. (2005). Assessing Vineyard Condition with Hyperspectral Indices: Leaf and Canopy Reflectance Simulation in a Row-Structured Discontinuous Canopy. *Remote Sensing of Environment*, 99, 271-287.

Zarco-Tejada, P.J., Miller J. R., Harron, J., Hu, B., Noland, T. L., Goel, N., Mohammed, G. H. & Sampson P. H. (2004). Needle chlorophyll content estimation through model inversion using hyperspectral data from boreal conifer forest canopies. *Remote Sensing of Environment*, *89*, 189-199.

Zarco-Tejada, P. J.; Miller, J. R.; Mohammed, G.H.; Noland, T. L.; & Sampson, P.H. (2001). Scaling-up and model inversion methods with narrow-band optical indices for chlorophyll content estimation in closed forest canopies with hyperspectral data. *IEEE Transactions on Geoscience and Remote Sensing*, 39, 1491-1507.

2. Assessing structural effects on PRI for stress detection in conifer forests.

Chapter 2

Assessing structural effects on PRI for stress detection in conifer forests.

Abstract

The retrieval of indicators of vegetation stress from remote sensing imagery is an important issue for the accurate assessment of forest decline. The Photochemical Reflectance Index (PRI) has been demonstrated as a physiological index sensitive to the epoxidation state of the xanthophyll cycle pigments and to photosynthetic efficiency, serving as a proxy for short-term changes in photosynthetic activity, stress condition, and pigment absorption, but highly affected by illumination conditions, viewing geometry and canopy structure. In this study, a diurnal airborne campaign was conducted over *Pinus sylvestris* and *Pinus nigra* forest areas with the Airborne Hyperspectral Scanner (AHS) to evaluate the effects of canopy structure on PRI when used as an indicator of stress in a conifer forest. The AHS airborne sensor was flown at two times (8:00 GMT and 12:00 GMT) over forest areas under varying field measured stress levels, acquiring 2 m spatial resolution imagery in 80 spectral bands in the 0.43-12.5 μm spectral range. Five formulations of PRI (based on R_{531} as a xanthophyll-sensitive spectral band) were calculated using different reference wavelengths, such as PRI_{570} (reference band $R_{REF}=R_{570}$), and the PRI modifications PRI_{m1} ($R_{REF}=R_{512}$), PRI_{m2} ($R_{REF}=R_{600}$), PRI_{m3} ($R_{REF}=R_{670}$), and PRI_{m4} ($R_{REF}=R_{570}$, R_{670}), along with other structural indices such as NDVI, SR, OSAVI, MSAVI and MTVI2. In addition, thermal bands were used for the retrieval of the land surface temperature. A radiative transfer modeling method was conducted using the LIBERTY and INFORM models to assess the structural effects on the PRI formulations proposed, studying the sensitivity of PRIm indices to detect stress levels while minimizing the effects caused by the conifer architecture. The PRI indices were related to stomatal conductance, xanthophyll epoxidation state (EPS) and crown temperature. The modeling analysis showed that the coefficient of variation (CV) for PRI was 50%, whereas the CV for PRI_{m1} (band R_{512} as a reference) was only 20%. Simulation and experimental results demonstrated that PRI_{m1} ($R_{REF}=R_{512}$) was less sensitive than PRI ($R_{REF}=R_{570}$) to changes in Leaf Area Index (LAI) and tree densities. PRI_{512} was demonstrated to be sensitive to EPS at both leaf ($r^2=0.59$) and canopy level ($r^2=0.40$), yielding superior performance than PRI_{570} ($r^2=0.21$) at the canopy level. In addition, PRI_{512} was significantly

related to water stress indicators such as stomatal conductance (Gs; r^2=0.45) and water potential (Ψ; r^2=0.48), yielding better results than PRI_{570} (Gs, r^2=0.21; Ψ, r^2=0.21) due to the structural effects found on the PRI_{570} index at the canopy level.

Keywords: forest decline, water stress, photosynthetic pigments, Airborne Hyperspectral Scanner, photochemical-related indices.

2.1. Introduction

Intercepted The Photochemical Reflectance Index (PRI) is a physiological reflectance index sensitive to the epoxidation state of the xanthophyll cycle pigments and to photosynthetic efficiency (Gamon et al., 1992). PRI was proposed by Gamon et al. (1992) as a normalized difference of 530 nm and a reference band at 550 nm, related to photosynthetic processes and affected by xanthophyll pigment absorption. Several studies report good results using 550 (or 551) nm as a reference wavelength (Peñuelas et al., 1994 and Middleton et al., 2009). Based on research on leaves exposed to short-term changes in illumination, several studies (Peñuelas et al., 1995; Gamon et al., 1993; and Gamon et al., 1997) found that 570 nm appeared to be a better reference wavelength. Since then, PRI has been applied by using 570 nm as a standard reference at leaf and canopy levels (Sims and Gamon, 2002; Suárez et al., 2010). For example, the accumulation of de epoxidated (DEPS) forms of xanthophyll cycle pigments was found by Peguero-Pina and co-workers in a silver fir stand growing under Mn deficiency (Peguero-Pina et al., 2007) and *Quercus coccifera* growing under intense drought (Peguero-Pina et al., 2008), assessing the stress effects on leaf PRI. Later, Filella et al. (2009) found significant correlation between PRI and DEPS across seasons and treatments for Pinus sylvestris and *Quercus ilex*. PRI was also related to carotenoid/chlorophyll ratio and b-carotene/chlorophyll ratio. It was only under brief variations in illumination conditions that PRI was correlated with DEPS, but was not related to other leaf pigments such as other carotenoids (Car) and chlorophyll a+b (Cab). Recent work (Suárez et al., 2009) demonstrated that PRI is a pre visual water stress indicator in crops, but suggested that

radiative transfer models were required to account for Cab and LAI effects for estimating the theoretical canopy PRI to help separating between stress levels. Nevertheless, such work relied on results obtained from tree crowns when targeting pure vegetation, thus causing smaller structural effects on PRI than forest canopy architectures. In addition, assessing plant physiological condition based on PRI at canopy scale is a difficult approach due to the different factors affecting this index, such as viewing and illumination geometry effects, crown architecture and shadow/sunlit fraction (Barton and North, 2001; Hall et al., 2008; Hilker et al., 2008; Middleton et al., 2009; Suárez et al., 2008).

At the leaf level, additional PRI formulations have been proposed using varying reference wavelengths (Filella et al., 1996; Gamon et al., 1992; Inoue et al., 2008; Peñuelas et al., 1994). Many studies adopted 570 nm, largely based on the observation that it provided a good reference wavelength for leaf-level studies (Gamon et al., 1993; Peñuelas et al., 1995; Gamon et al., 1997). At canopy scale, Gamon et al. (1992) showed how reflectance at several wavebands (from 539 to 670 nm) in combination with 531 nm worked rather well, and that 550 nm was the best overall reference wavelength based on a combination of statistical tests (regression, principle components analysis). This wavelength seemed to best correct for "greenness" (i.e., canopy structure) effects. Other studies showed similar good results with 551 nm as a reference (the nearest MODIS band) (Middleton et al., 2009). Most authors adopted 570 nm as a reference, although the sensitivity of this index to structural and illumination effects were demonstrated (Suárez et al., 2008).

Forest decline is expressed through multiple effects due to an array of interacting biotic and abiotic factors. Assessing stress condition of a forest in decline using PRI is a complex problem because of the different alterations of the tree at the canopy- and stand-level (e.g., changes in Leaf Area Index (LAI), Fraction of Photosynthetically Active Radiation (FPAR) and Leaf Angle Distribution (LAD), vegetation cover or stand density); at the leaf level, with alterations in photosynthetic activity, pigment content, and internal leaf structure; and at the cell level, with changes in water content, among others (Melzack et al., 1985). In the past, conifer forests in decline were assessed by changes in vegetation indices related to canopy structure, such as LAI (Schlerf et al., 2005; Schlerf and Atzberger, 2006), and chlorophyll concentration (Zarco-Tejada et al., 2004; Moorthy et al., 2008; Zhang et al., 2008). However, when canopy chlorophyll concentration or total leaf area is affected by water stress, damage to the plant has already occurred, and plant status is compromised. The detection of stress in its early phase is normally defined as pre-visual and takes place before there are structural (visual) effects or consequences of the stress; this is critical information required for the assessment of forest decline. These processes related to water stress have affected important areas in Spain and other European countries (Allen et al., 2010; Martínez-Vilalta et al., 2008; Navarro-Cerrillo et al., 2007; Rebetez and Dobbertin, 2004). Such studies demonstrate that drought plays an important role in Mediterranean forest decline, especially in species sensitive to water stress like Pinus sylvestris (Martínez-Vilalta et al., 2008; Poyatos et al., 2008). Research has shown that in an early stage of stress, before damage has occurred, photosynthesis declines. Under these conditions, the absorbed light exceeds the

photosynthetic demand, and plants react with mechanisms for dissipating this excess energy non-destructively (Björkman and Demmig-Adams, 1994). One mechanism is linked to xanthophyll cycle activation, where pigment violaxanthin is converted into antheraxanthin and zeaxanthin via de-epoxidase reactions (Yamamoto, 1979). Several manuscripts have revealed a close correlationship between xanthophyll pigment conversions and excess energy dissipation in the leaf pigments associated with photosystem II (PSII) (Demmig-Adams and Adams, 1996). Another stress indicator suggested in several studies (proposed by Jackson et al., 1977) is the temperature of the canopy as an indicator of tree transpiration. Thermal remote sensing of water stress has been successfully applied to tree crop canopies based on high resolution thermal remote sensing imagery (Berni et al., 2009), airborne thermal imagery (Sepulcre-Cantó et al., 2007) and satellite thermal information in combination with 3D radiative transfer models to understand the effects of scene thermal components on large ASTER pixels (Sepulcre-Cantó et al., 2009).

However, very few references have shown feasible remote sensing methods for successfully linking remote sensing indices and physiological variables by focusing on the pre-visual detection of forest decline before damage is visible. At canopy scale, most of this research has dealt primarily with photosynthetic light use efficiency and carbon dioxide using satellite images such as the Moderate Resolution Imaging Spectroradiometer data (MODIS) (Drolet et al., 2005; Garbulsky et al., 2008; Hilker et al., 2009) or EO-1 Hyperion data (Asner et al., 2005). Nevertheless, few of these studies are focused on PRI and other spectral indices validated with in situ

measurements of EPS in heterogeneous forest ecosystems. Questions need to be answered regarding PRI interpretation on forest canopies where crown mixture, shadows and tree architecture play a critical role in physiological remote sensing indices. The present study provides new insights into the understanding of PRI as an indicator of stress on complex canopies, analyzing the effects on PRI formulations due to the structure. The study assesses imaged PRI and model-simulated PRI obtained through radiative transfer simulation of conifer canopies, evaluating the sensitivity of PRI formulations to EPS while minimizing canopy structural effects.

2.2. Material and Methods

2.2.1. Field data collection

Field sampling campaigns were conducted concurrently with airborne overflights during the last week of July 2008 (Fig. 2.1). Two sets of measurements were collected at 8:00 and 12:00 (GMT). The monitored trees consisted of 36 *Pinus nigra* and 36 *Pinus sylvestris*, located in three study areas (12 trees per study areas) (Fig. 2.1). Table 2.1 shows the mean values and the standard deviation of xanthophyll epoxidation state (EPS), water potential (ψ) and stomatal conductance (Gs) calculated for each study area at 12:00 GMT. To test the null hypothesis that EPS, water potential, and stomatal conductance were not significantly different among study areas, a one-way ANOVA analysis was conducted using a significance level of 0.05.

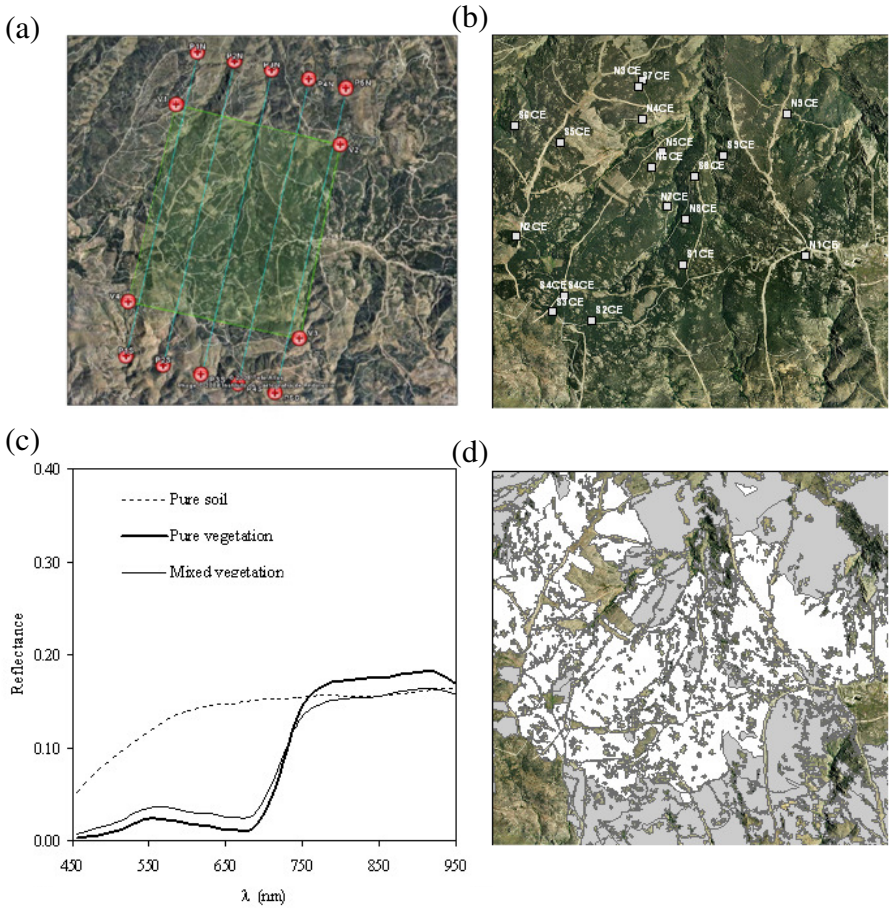

Figure 2.1. AHS airborne footprint (a). Overview of the area acquired with the AHS instrument (b). Single pixel AHS spectra for pure vegetation, soil and mixed vegetation-soil pixels (c). Distribution of *Pinus sylvestris* (white) and *Pinus nigra* (grey) on the study area (d).

A Tukey's post-hoc analysis was performed to evaluate differences between study areas. In the case of water potential a Kruskal-Wallis (KW) test was applied because the data were not normally distributed. The variables measured showed significant differences in the physiological status for each study area ($p<0.05$).

Table 2.1. Mean values and standard deviation of xanthophyll epoxidation state (EPS), water potential (Ψ) (Mpa) and stomatal conductance (Gs) (mmol H_2O $m^{-2}s^{-1}$) calculated for each study area for *Pinus sylvestris* and *Pinus nigra.* Measurements obtained at 12:00 GMT.

Study area *Pinus sylvestris*	EPS	Ψ	Gs
SS1 (Not stressed)	0.85±0.08*	-0.53±0.03*	50.91±9.44*
SS2 (Moderate stress)	0.75±0.11*	-0.63±0.02*	43.99±9.04*
SS3 (Stressed)	0.58±0.14*	-0.77±0.06*	36.24±6.44*
*p < 0.05			
Study area *Pinus nigra*	EPS	Ψ	Gs
SN1 (Not stressed)	0.85±0.05*	-0.40±0.01*	64.86±9.35*
SN2 (Moderate stress)	0.80±0.11*	-0.43±0.01*	57.64±9.62*
SN3 (Stressed)	0.70±0.10*	-0.50±0.01*	44.636±9.84*
*p < 0.05			

The measurements were conducted on trees of similar height located in low slope areas (<10%), therefore with a similar sun/shade fraction. The trees are largely the same age since they were part of a reforestation program undertaken by the Spanish government in 1980.

Physiological parameters measured from the selected trees were total concentration of chlorophyll (chlorophyll a (chla) and chlorophyll b (chlb)), needle water content and dry mass, stomatal conductance (using a portable gas exchange system CIRAS-1 instrument, PP Systems, Hitchin Herts, UK) and crown temperature (using an infrared thermometer, Optris LS, DE). These data were averaged from four measurements per tree during each period at the time of the AHS imagery acquisition (8:00 and 12:00, GMT).

Field Gas exchange measurements were performed in attached leaves at controlled CO2 external concentration (Ca = 350 ppm) and ambient relative humidity. Stomatal conductance (Gs) was estimated using gas exchange data and the total needle area exposed obtained from photos taken for each measurement. Predawn (Ψpd, 4:00 GTM) and midday (Ψm, 12:00 GTM) xylem water potential (pressure chamber, SKPM 1400, Skye Instruments, UK) (Scholander et al., 1965) were also measured. LAI was estimated with a PCA (Plant Canopy Analyzer, LAI-2000, LI-COR, Lincoln, NE, USA).

2.2.2. Leaf-level measurements

Leaf-level measurements were collected on a total of 15 needles per tree, five needles per needle age (current-year, n; young, n+1; and mature, n+3), with a total of 540 needles measured per species. The needles were collected from the top of the crown by selecting branches of illuminated areas. Two sets of needles were collected from the same shoots at the time of the AHS flights, 8:00 and 12:00 (GMT). One set was placed under cold storage in coolers, and the other set was frozen in liquid nitrogen in the field. Both storage conditions were in darkness, and the needles were harvested and immediately frozen in the field. The first set was transported directly to the laboratory and used to measure leaf spectral reflectance and transmittance, and water content. The second set was kept under -80ºC and used for pigment analysis by destructive methods.

Needle pigments were extracted as reported by Abadía and Abadía (1993). Pigment extracts were obtained from a mixed sample of 5 cm of needle material, 1 linear cm per needle. The area was calculated by assuming the needle to be a half cylinder and the diameter to be the measured width of

each needle. Needle diameter was measured with a digital caliper precision instrument. Pigment content was obtained based on this area. Five consecutive centimeters were also cut for structural measurements (thickness and width), water content and dry mass. The needles were ground in a mortar on ice with liquid nitrogen and diluted in acetone up to 5 ml (in the presence of Na ascorbate). Then, the extracts were filtered through a 0.45-μm filter to separate the pigment extracts from the Na ascorbate. The spectrophotometric and High-Performance Liquid Chromatography (HPLC) determinations were carried out simultaneously on the same extracts, 20 μl were injected into the HPLC and 1 ml was inserted into the spectrophotometer. The extractions and measurements were undertaken concurrently to avoid pigment degradation. Absorption at 470, 644.8 and 661.6 nm was measured with the spectrophotometer to derive chlorophyll *a* and *b*, and total carotenoid concentrations (Abadía and Abadía, 1993) and pigment extracts were analyzed using an isocratic HPLC method (Larbi *et al.*, 2004). Samples were injected into a 100×8 mm Waters Novapak C18 radial compression column (4 μm particle size) with a 20 μl loop, and mobile phases were pumped by a Waters M45 high pressure pump at a flow of 1.7 ml/min. The EPS ratio between the pigment concentration was calculated as (V+0.5A)/(V+A+Z) (Thayer & Björkman, 1990), where V is violaxanthin, A is antheraxanthin and Z is zeaxanthin.

Optical measurements were taken on needles from a total of 42 trees, 21 trees per species. Needle reflectance and transmittance were measured with a Li-Cor 1800-12 integrating sphere (Li-Cor, Lincoln, NE, USA) coupled to a fiber optic spectrometer (Ocean Optics model USB2000 spectrometer, Ocean Optics, Dunedin, FL, USA), using the method described in Moorthy *et al.* (2008) and Zarco-Tejada *et al.* (2004). Needle reflectance and

transmittance measurements of *Pinus nigra* (Fig. 2.2a, b) and *Pinus sylvestris* (Fig. 2.2c, d) showed variations in the visible spectral region due to stress levels affecting both chlorophyll and xanthophyll pigments. Needle spectral reflectance was also measured with a UniSpec Spectral Analysis System (PP Systems, Herts, UK), following a similar procedure to that described by Richardson and Berlyn (2002). The Unispec measurements were conducted in the field minutes before the needles were collected.

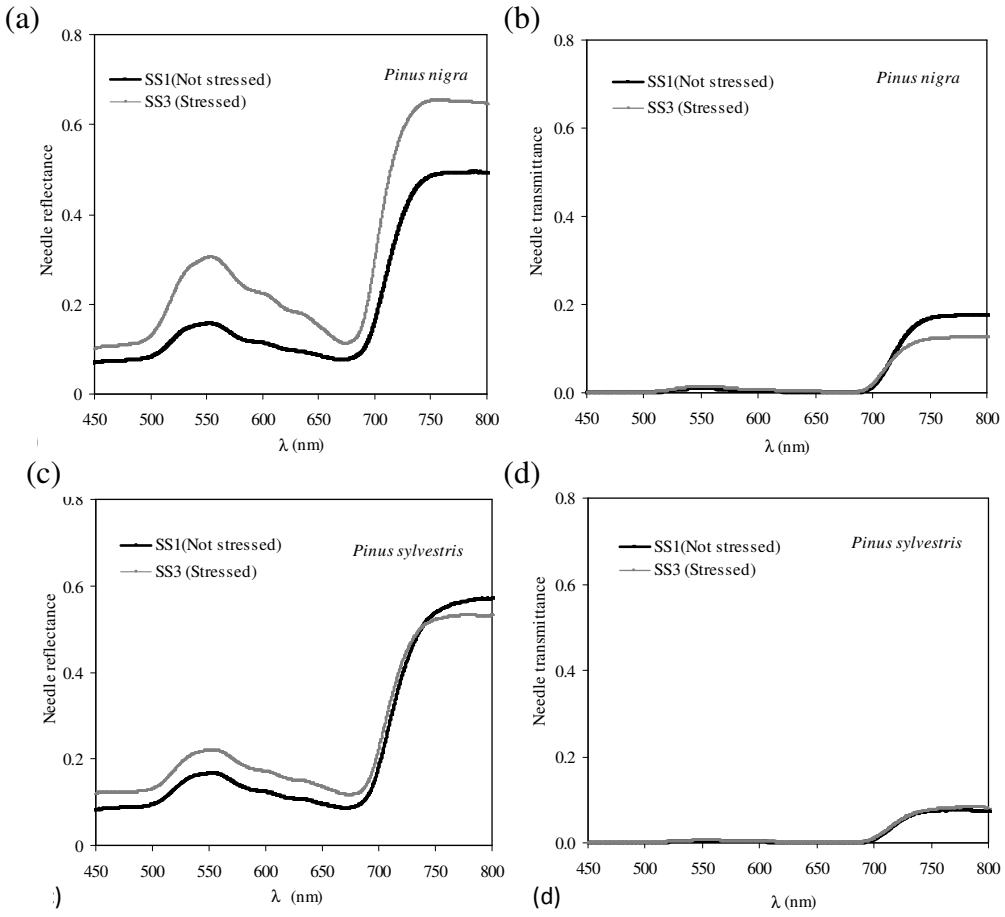

Figure 2.2. Needle reflectance and transmittance measurements collected with a Li-Cor 1800-12 integrating sphere corresponding to *Pinus nigra* (a, b) and *Pinus sylvestris* (c, d) from stressed and non-stressed study areas.

2.2.3. Airborne image acquisitions.

The airborne campaign was conducted by the Spanish Aerospace Institute (INTA) with the Airborne Hyperspectral Scanner AHS (Sensytech Inc., currently Argon St. Inc., Ann Arbor, MI, USA) during the last week of July 2008. The airborne data acquisition was carried out at 8:00 GMT and 12:00 GMT, acquiring 2 m spatial resolution imagery in 38 bands in the 0.43-12.5 μm spectral range. The Field of View (FOV) and Instantaneous Field of View (IFOV) of the AHS sensor were 90º and 2.5 mrad respectively, and plots were located in the central region of the scene in order to avoid edge effects. *At-sensor* radiance processing and atmospheric correction were performed at the INTA facilities. Atmospheric correction was conducted with ATCOR4 based on the MODTRAN radiative transfer model (Berk *et al.*, 1998; 2000) using aerosol optical depth at 550 nm collected with a Micro-Tops II sun photometer (Solar Light, Philadelphia, PA, USA). Land surface temperature retrieval from thermal remote sensing data was obtained with the two-channel algorithm proposed by Sobrino *et al.* (2002; 2006), taking into account emissivity and water vapor effects. The emissivity value applied for vegetation was 0.98. A full description of land surface temperature retrieval from thermal imagery via AHS can be found in Sepulcre-Cantó *et al.* (2006) and Sobrino *et al*. (2006) . The mean air temperature during the flight was 20.9ºC (±0.05) at 8:00 GMT and 24.5ºC (±0.11) at 12:00 GMT. The temperature data were collected by the meteorological station at Calar Alto Astronomical Observatory, located within the study area.

Vegetation indices were calculated to track changes in canopy structure and pigment concentration as a function of the stress condition. The AHS spectra (Fig. 2.1c) were extracted from the imagery at windows of 3x3 pixels. Pure vegetation pixels were located by selecting the pixels with NDVI higher than 0.6 on 3x3 windows. Fig. 2.3 shows one region of interest extracted for affected and non-affected areas of *Pinus nigra* and *Pinus sylvestris.* The airborne reflectance extracted for each tree, and comparing the spectra for stressed and non-stressed study areas (SS1 and SS3) of pure crowns and mixed pixels are shown in Fig. 2.3a and 2.3b, respectively.

Spectra extracted from the imagery were related to the field data using pure vegetation pixels (NDVI higher than 0.6). The analysis aimed at assessing the relationships between EPS, G and Ψ and the different PRI formulations calculated to minimize the structural effects on PRI. The index PRI was reformulated as derived from R_{531} (adapted to AHS using band R_{540} as in Suárez *et al.*, 2008) using reference bands R_{512} (PRI_{m1}), R_{600} (PRI_{m2}), R_{670} (PRI_{m3}), and R_{670} and R_{570} (PRI_{m4}) (Table 2.2). The PRI formulations proposed in this study (Table 2.2) were based on the results obtained in previous work (Gamon *et al*., 1993; Rouse *et al*., 1974; Jordan, 1969) and on the spectral trend of the reflectance at the 500-600 nm region. Fig. 2.4a shows the needle spectral reflectance of *Pinus sylvestris* measured with a Unispec spectroradiometer for two stress levels at 12:00 GMT. As shown in Fig. 2.4b both regions at 500-520 nm and 570-590 nm could be used as a reference band. Fig. 2.4b also shows the bandwidth corresponding to AHS airborne sensor used to calculate PRI_{570} and PRI_{512}.

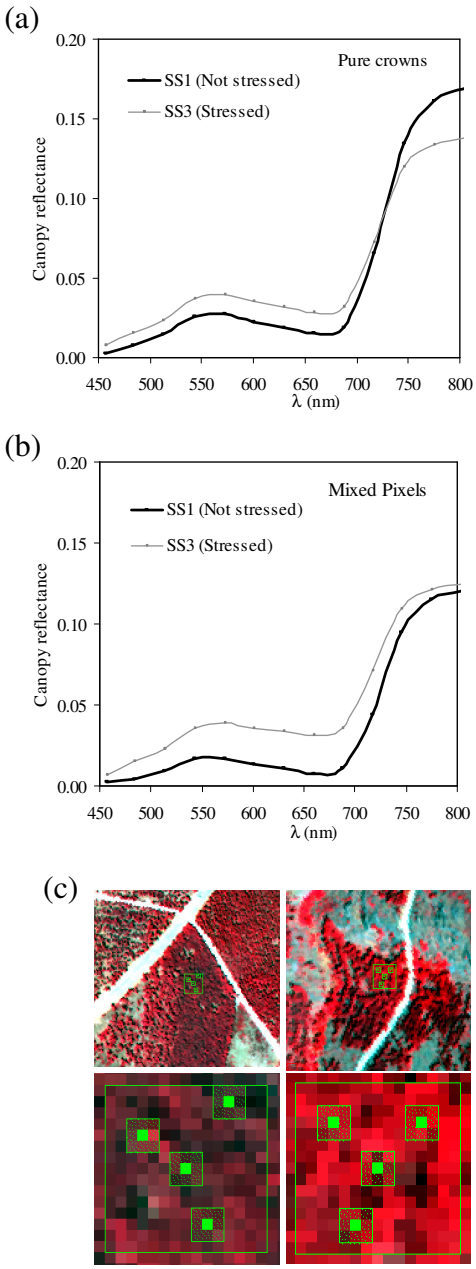

Figure 2.3. AHS spectra for *Pinus sylvestris* of (a) pure tree crowns and (b) mixed pixels comprising pure crown, soil and shadow. (c) Example of stressed and non-stressed study areas for *Pinus sylvestris*.

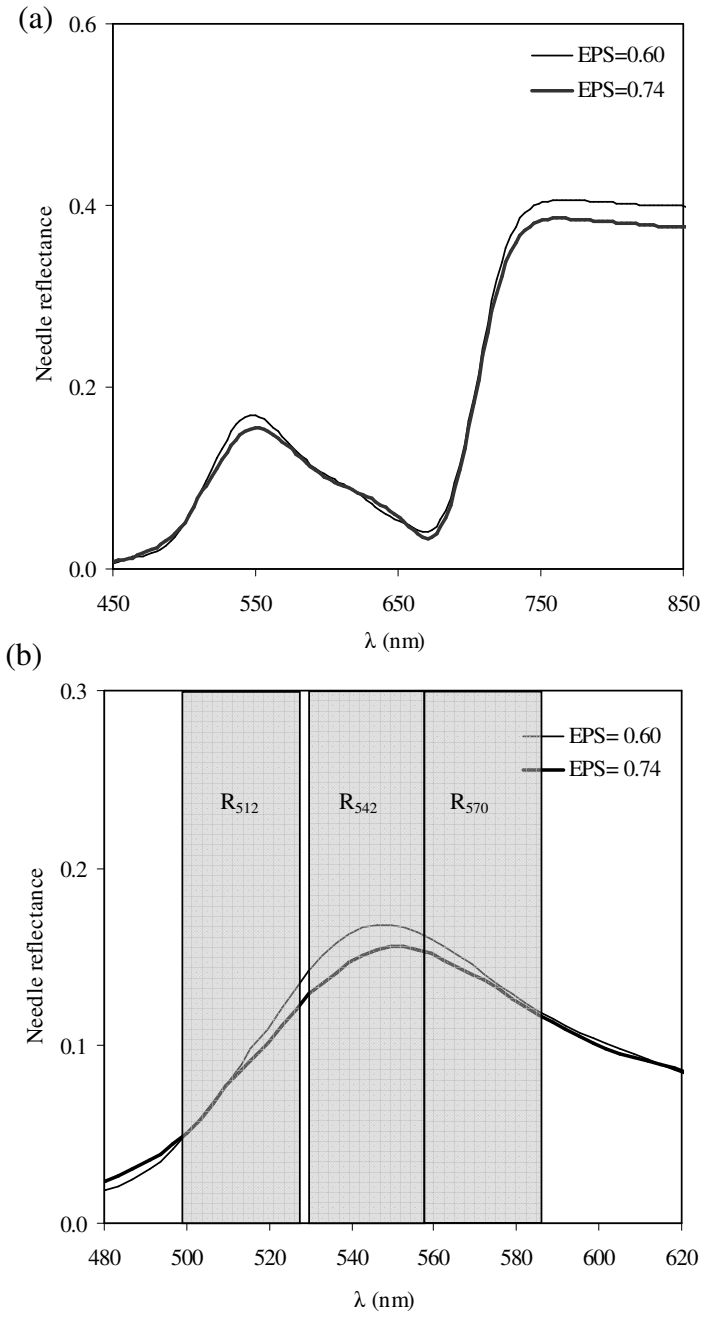

Figure 2.4. (a) Spectral reflectance of needles of *Pinus sylvestris* with different epoxidation state of the xanthophylls (EPS) values. (b) Zoom of the region of absorption of the xanthophylls cycle and center wavelength and bandwidth for the AHS bands used to calculate PRI (R_{512}, R_{542}, R_{571}). Measurements obtained at 12:00 GMT.

The indices were also normalized by structure-sensitive effects using indices such as NDVI (Rouse *et al.*, 1974), SR (Jordan, 1969; Rouse *et al.*, 1974), MTVI2 (Haboudane *et al.*, 2004), OSAVI (Rondeaux *et al.*, 1996) and MSAVI (Haboudane *et al.*, 2004). Indices were adapted to the AHS bandset using the closest bands available.

Table 2.2. Photochemical reflectance index formulations and structural vegetation indices used in this study and indices calculated from the AHS bandset.

	Equation	Reference
PRI_{570}	$(R_{570}-R_{531})/(R_{570}+R_{531})$	Gamon *et al.* (1993)
PRI_{m1}	$(R_{512}-R_{531})/(R_{512}+R_{531})$	This study
PRI_{m2}	$(R_{600}-R_{531})/(R_{600}+R_{531})$	Gamon *et al.* (1993)
PRI_{m3}	$(R_{670}-R_{531})/(R_{670}+R_{531})$	Gamon *et al.* (1993)
PRI_{m4}	$(R_{570}-R_{531}-R_{670})/(R_{571}+R_{531}+R_{670})$	This study
NDVI	$(R_{NIR} - R_{red})/(R_{NIR} + R_{red})$	Rouse *et al.* (1974)
SR	(R_{NIR}/R_{red})	Jordan (1969); Rouse *et al.* (1974)
OSAVI	$(1 + 0.16)* (R_{800} - R_{670})/(R_{800} + R_{670} + 0.16)$	Rondeaux *et al.* (1996)
MSAVI	$\frac{1}{2}\left[2*R_{800}+1-\sqrt{(2*R_{800}+1)^2-8*(R_{800}-R_{670})}\right]$	Qi *et al.* (1994)
$MTVI_2$	$\frac{1.5*[1.2*(R_{800}-R_{550})-2.5*(R_{670}-R_{550})]}{\sqrt{(2*R_{800}+1)^2-(6*R_{800}-5*\sqrt{R_{670}})-0.5}}$	Haboudane *et al.* (2004)

2.2.4. Model simulation with LIBERTY and INFORM

Radiative transfer modeling methods were applied with the *Leaf Incorporating Biochemistry Exhibiting Reflectance and Transmittance Yields* (LIBERTY) model (Dawson *et al.*, 1998) linked to the *Invertible Forest Reflectance Model* (INFORM) (Atzberger, 2000). LIBERTY was designed to model conifer (particularly pine) needles at the cellular scale, based on Melamed's radiative transfer theory of powders (Melamed, 1963). This model calculates reflectance and transmittance by assuming the needle structure to be cell spheres separated by air gaps. The LIBERTY and PROSPECT models were assessed by Zarco-Tejada *et al.* (2004) and Moorthy *et al.* (2008) suggesting that PROSPECT could be used to model needle optical properties. PROSPECT is a radiative model initially designed for broad leaves, although it was later adapted to needles (Malenovsky *et al*., 2006). In a recent paper, Di Vittorio (2009) enhanced the limitation of LIBERTY to resolve individual pigments and the gaps in the estimation of *in vivo* specific absorption coefficients and model biophysics. At canopy level, INFORM simulates the *bi-directional* reflectance of forest stands between 400 and 2500 nm, being a combination of the *Forest Light Interaction Model* (FLIM) (Rosema *et al.*, 1992) and *Scattering by Arbitrarily Inclined Leaves* (SAILH) (Verhoef, 1984, 1985), coupled with LIBERTY for this study. Neither FLIM nor INFORM incorporates a correction to account for the fact that, in coniferous forests, needles are densely clumped into shoots. Such correction has been suggested by Nilson and Ross (1997) and Smolander and Stenberg (2003). However, INFORM is an innovative hybrid model with crown transparency, infinite crown reflectance and understory reflectance simulated using physically based sub-models. Hybrid models are combinations of geometrical and turbid medium models, therfore with

INFORM tree crowns are not considered opaque but rather treated as a turbid medium. This factor plays an important role in conifer Mediterranean forests characterized by heterogeneous structures, thin leafy canopies and mutually shaded crowns.

A total of 125 simulations were performed with the LIBERTY+INFORM coupled model, varying LAI (1-3), tree density (800-2800 trees/ha), and chlorophyll concentration (100-500 mg/m^2). The simulated spectral reflectance dataset was used to calculate the vegetation indices under analysis: PRI_{570}, modified PRI formulations, and PRI indices normalized by the NDVI, SR, OSAVI, MSAVI and MTVI2 structural indices (Table 2.2). Model simulations were conducted for each PRI formulation to assess the effects of the reference band on PRI. The purpose of the simulation analysis was to assess the effects of the variability found in a pine forest on the simulated PRI formulations as a function of i) LAI; ii) fractional cover; and iii) Cab concentration. Model assessments and comparison against ground-measured EPS both at leaf and canopy levels were conducted.

2.3. Results

2.3.3. Model simulations

Model simulations conducted with LIBERTY for *Pinus nigra* needles using the PROSPECT chlorophyll absorption coefficient (k_{ab}) revealed good agreement when compared with needle spectra measured with the integrating sphere (Fig. 2.5). In contrast, LIBERTY simulations conducted with the original chlorophyll absorption coefficient (Dawson *et al*., 1998) reported a significant failure to match the needle reflectance measured in the 500-700 nm region (Fig. 2.5a and 2.5b).

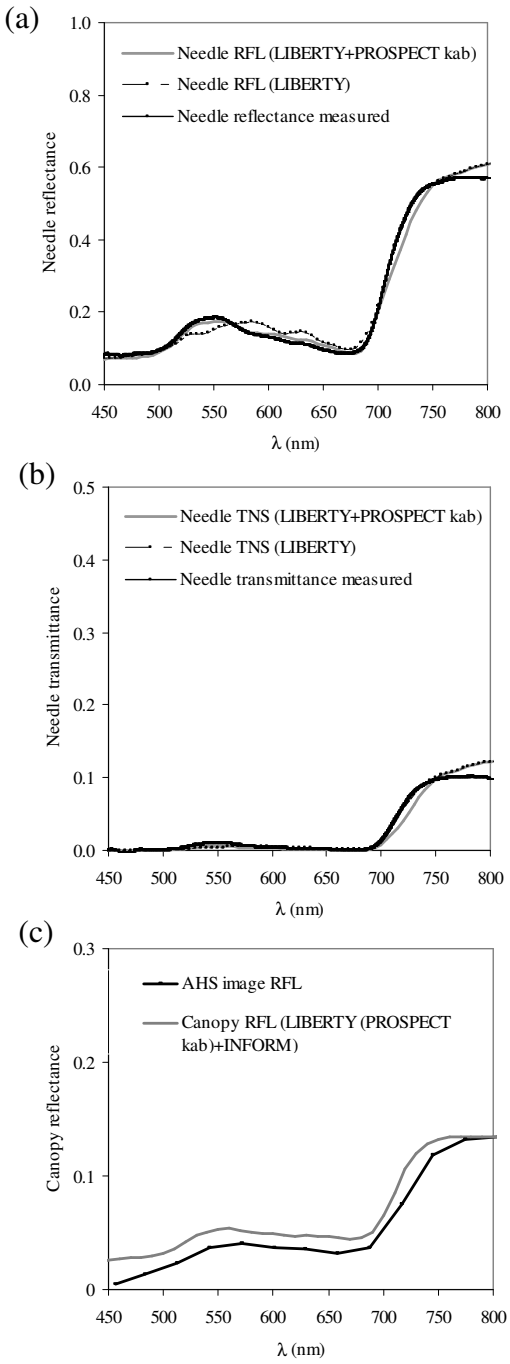

Figure 2.5. Needle reflectance (RFL) (a) and transmittance (TNS) (b) measured with the integrating sphere, simulated with LIBERTY and simulated with LIBERTY using the absorption coefficient of PROSPECT. Crown reflectance spectra obtained from the AHS image and simulated with LIBERTY+INFORM (c).

Input parameters and ranges used for the coupled LIBERTY+INFORM model (Table 2.3) were estimated by the inversion of 128 needle spectra measured in the laboratory with the integrating sphere for both species. At the canopy level, the coupled model was assessed against the reflectance extracted from the AHS data for study areas from both species. Fig. 2.5c shows good agreement between the reflectance spectra obtained from the AHS image and those simulated with the LIBERTY+INFORM coupled model for one of the study areas.

Table 2.3. Nominal values and range of parameters used for leaf and canopy modeling with LIBERTY and INFORM for *Pinus nigra.*

Leaf optical and structural parameters	Units	Values
Hemispherical reflectance and transmittance of green leaves	nm	Measured
Average internal cell diameter (D)	μm	65
Intercellular Air Space Determinant (*xu*)	/	0.06
NeedleThickness	/	4.09
Linear (Baseline) Absorption	/	0.0006
Albino Leaf Absorption	/	1.25
Leaf Chl a+b content	mg/m^2	100 - 500
Leaf Equivalent Water	g/m^2	100
Lignin / Cellulose Content	g/m^2	40
Protein Content	g/m^2	1
Canopy structural parameters		
LAI	m^2/m^2	1 - 3
nº trees/ha	/	800 - 2800
Crown height	m	7.9
Crown diameter	m	3.7
Background and viewing geometry		
Solar zenith and azimuth	Degrees	190.68
Instrument solar zenith and azimuth	Degrees	17.7
Soil reflectance	mm	Measured

The LIBERTY+INFORM coupled model was used to assess the effects of canopy architecture on PRI and on the proposed PRI formulations (Table

2.2). A comparison between the coefficient of variation (CV) for each PRI reference band was conducted to assess the PRI formulation showing less variation as a function of LAI, tree density and chlorophyll content. Fig. 2.6 shows the mean, the CV, and the standard deviation of simulated spectral reflectance for a range of LAI and tree densities. The simulations were conducted for LAI values of 1 to 3, and tree densities in the range 800 - 2800 trees/ha. The remaining inputs were set to the mean nominal values (Table 2.3). The CV obtained from each reference band (R_{512}, R_{570}, R_{600} and R_{670}) was 4.35%, 5.28%, 5.02% and 13.52%, respectively. Although the differences among the CV of the reference bands were no greater than 15%, R_{512} had the lowest value (Fig. 2.6).

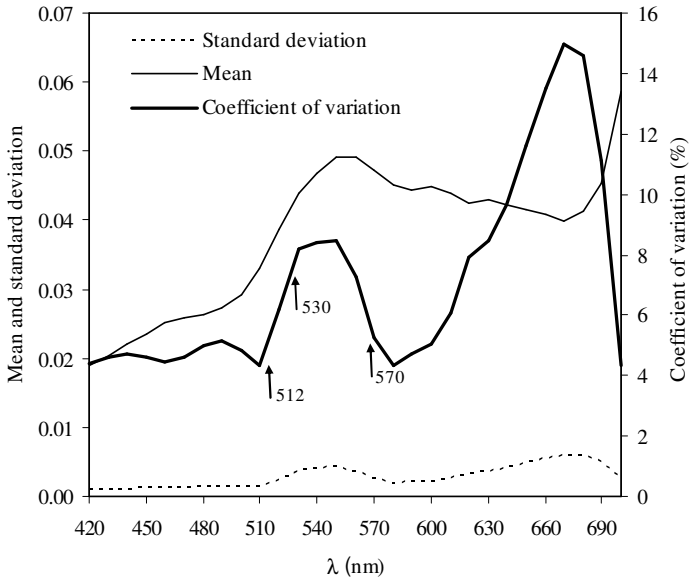

Figure 2.6. Mean, coefficient of variation (CV), and standard deviation of spectral reflectance for LAI ranges (1-3) and tree densities (800-2800 trees/ha) simulated with the coupled LIBERTY+INFORM model.

However, such differences increased when calculating the CV for PRI formulations, yielding CV=48.98% for PRI_{570} and CV=22.05% for PRI_{512}, demonstrating that PRI_{570} had a higher variation than other PRI formulations such as PRI_{512}. These theoretical results suggest that PRI_{512} is less sensitive to changes in LAI and tree densities than PRI_{570}. The effect of chlorophyll concentration was also studied by simulating a range of chlorophyll (100-500 mg/m^2), in addition to the variation in LAI (1-3) and tree density (800-2800 trees/ha).

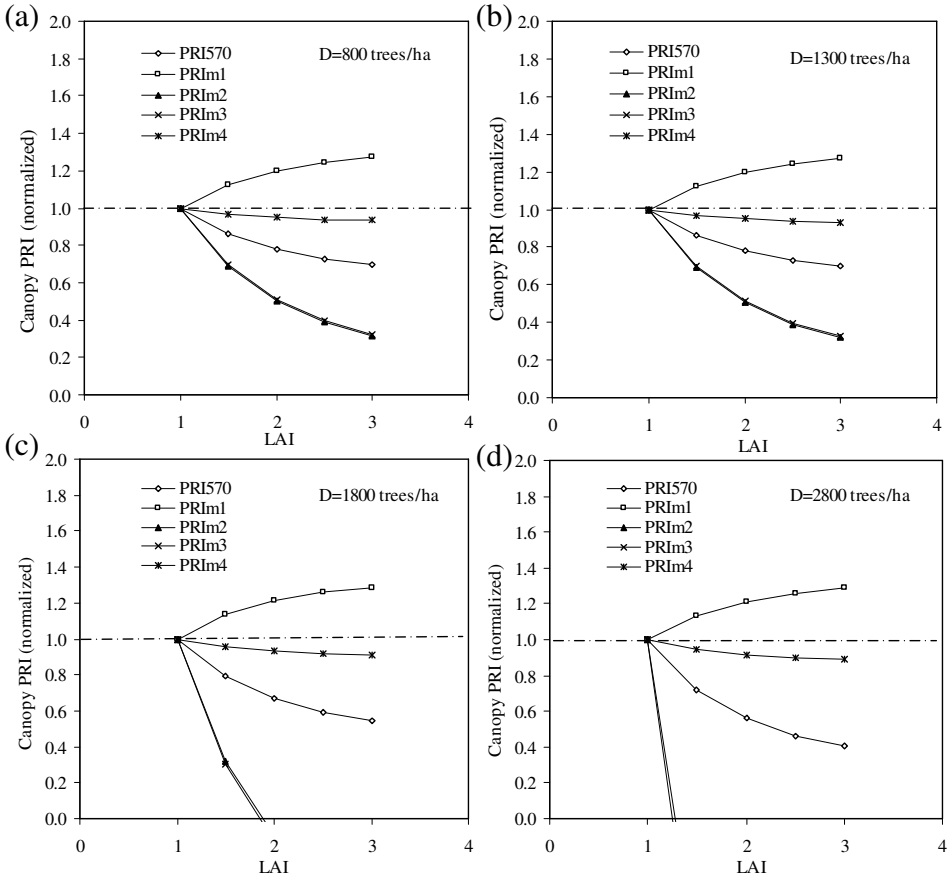

Figure 2.7. Model simulations conducted with INFORM for PRI_{570} and modified PRI formulations. Results obtained by simulating the plot reflectance with different densities (D) and LAI values. Results normalized for LAI=1. Tree densities (D) used were a) 800, b) 1300, c) 1800, d) 2800 trees/ha.

In this case, the CV for PRI_{570} decreased slightly (CV=30.48%), while PRI_{512} remained almost invariant (CV=23.01%). These results suggest that PRI_{512} is less sensitive to structural parameters and chlorophyll variations than PRI_{570}.

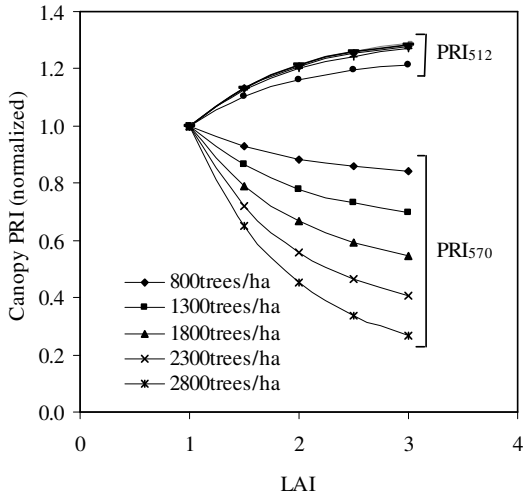

Figure 2.8. Model simulations conducted with INFORM for PRI_{570} and PRI_{512}. Results obtained by simulating the plot reflectance with different densities (D) and LAI values. Results normalized to LAI=1.

The structural effects on PRI formulations are shown as normalized for LAI=1 (Fig. 2.7), showing the variation in PRI_{570} and PRI_m for a range of LAI and tree densities (Fig. 2.7 a, b, c and d). The variation in PRI_{m1} and PRI_{m4} was less significant than that of the rest of the PRI formulations (PRI_{570}, PRI_{m2}, PRI_{m3}). Such differences were even greater when tree density or LAI increased. The patterns tracked by PRI_{570} versus PRI_{m1} as simulated for a range of LAI and tree density values (Fig. 2.8) demonstrates the lower sensitivity of PRI_{m1} to canopy structural changes than PRI_{570}. These results demonstrate the smaller effect caused by the tree density on PRI_{512} as compared to PRI_{570}.

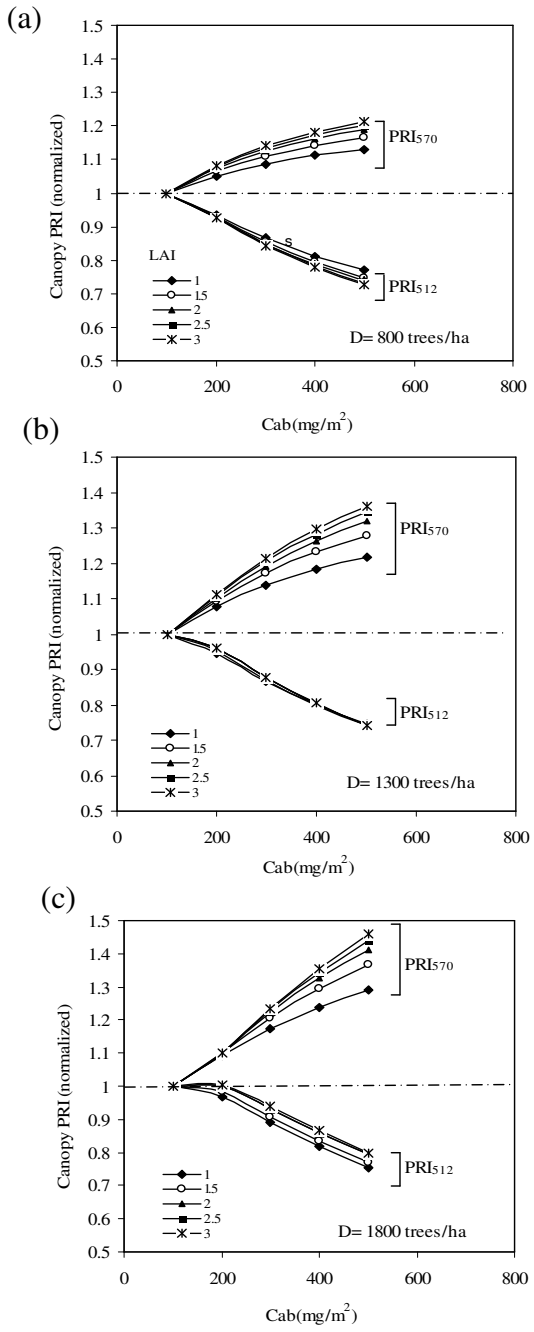

Figure 2.9. Model simulations conducted with INFORM for canopy PRI_{570} and PRI_{512} for different values of chlorophyll (Cab). Results obtained by simulating the plot reflectance with different values of LAI for a) 800 trees/ha, b) 1300 trees/ha, c) 1800 trees/ha.

The structural effects on PRI formulations are shown as normalized for LAI=1 (Fig. 2.7), showing the variation in PRI_{570} and PRI_m for a range of LAI and tree densities (Fig. 2.7 a, b, c and d). The variation in PRI_{m1} and PRI_{m4} was less significant than that of the rest of the PRI formulations (PRI_{570}, PRI_{m2}, PRI_{m3}). Such differences were even greater when tree density or LAI increased. The patterns tracked by PRI_{570} versus PRI_{m1} as simulated for a range of LAI and tree density values (Fig. 2.8) demonstrates the lower sensitivity of PRI_{m1} to canopy structural changes than PRI_{570}. These results demonstrate the smaller effect caused by the tree density on PRI_{512} as compared to PRI_{570}.

Model simulations for canopy PRI_{570} and PRI_m indices were also conducted with LIBERTY+INFORM for assessing index variation as a function of chlorophyll concentration (Fig. 2.9). Simulations performed for increasing tree densities (Fig. 2.9a (800 trees/ha); 2.9b (1300 trees/ha); 2.9c (1800 trees/ha)) as a function of LAI and Cab demonstrate that PRI_{570} and PRI_{m1} are affected by Cab.

2.3.3. Experimental result: PRI measurements at the needle level

The assessment to study the relationship between PRI_{570} and the epoxidation state of the xanthophylls pigments (EPS) was conducted on the diurnal dataset acquired at the leaf level. The comparison between EPS at 8:00 and 12:00 GMT for *Pinus sylvestris* (Fig. 2.10a) and *Pinus nigra* (Fig. 2.10b) for each study area demonstrates the differences found on EPS as a function of the stress level. There were significant differences in EPS between study areas for both species at 12:00 GMT. Values were not significantly different at 8:00 GMT for *P. sylvestris* and *P. nigra*. However, both species displayed

a similar pattern, as diurnal differences in EPS increased on the areas with higher stress.

Based on midday measurements, EPS showed a consistent pattern of decline on needle PRI_{570} and needle PRI_{512} data at 10 and 30nm bandwidths for both *Pinus sylvestris* (Fig. 2.11) and *Pinus nigra* sites (Fig. 2.12). Results demonstrated a similar sensitivity of both PRI_{570} and PRI_{512} to EPS, yielding coefficients of determination of r^2=0.61 for PRI_{570} (Fig. 2.11a) and r^2=0.59 for PRI_{512} (Fig. 2.11b) for *Pinus sylvestris,* and r^2=0.62 for PRI_{570} (Fig. 2.12a) and r^2=0.61 for PRI_{512} (Fig. 2.12b) for *Pinus nigra*. A higher concentration of the photosynthetic active pigment violaxanthin over the whole xanthophyll pool corresponds with higher values of EPS, and consequently smaller stress levels, thus showing lower PRI values. Similar results were found at the leaf level in *Abies alba* (Peguero-Pina *et al.*, 2007) and *Pinus sylvestris* (Filella *et al.*, 2009) needles, and in *Quercus coccifera* (Peguero-Pina *et al.*, 2008) and *Prunus persica* (Suárez *et al.*, 2010) leaves.

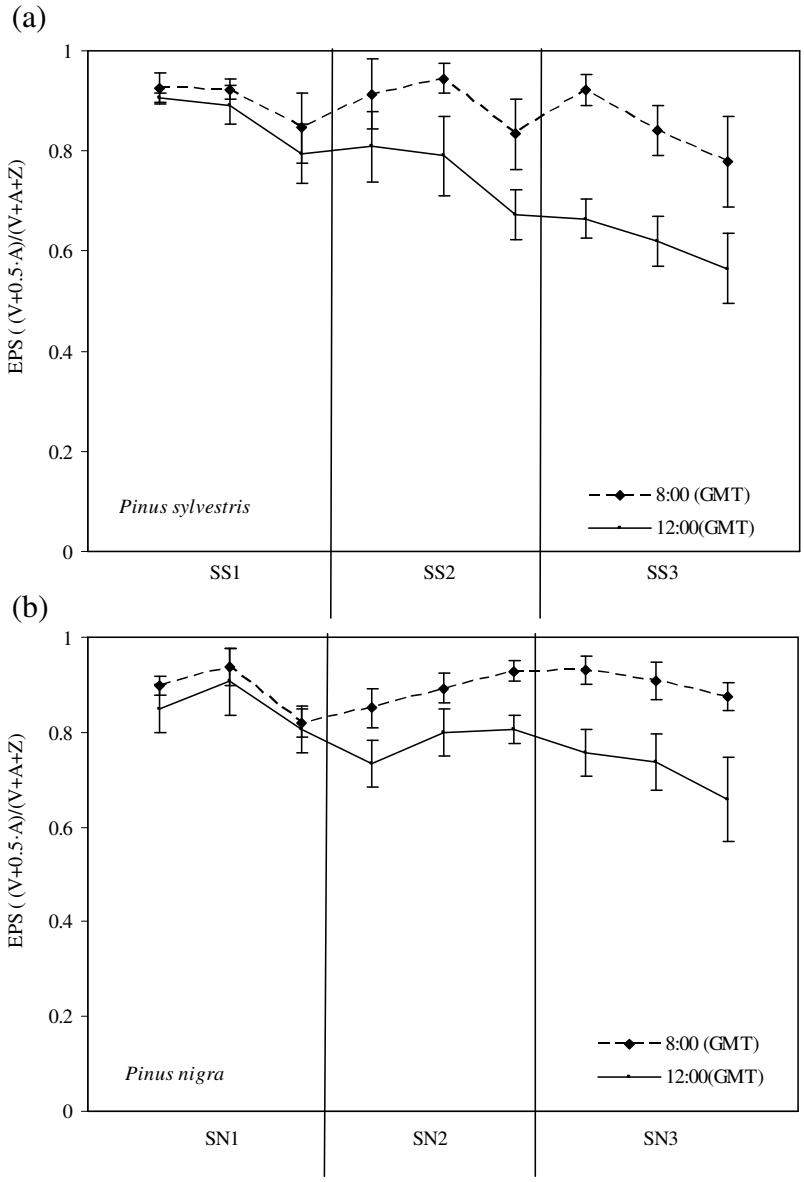

Figure 2.10. Comparison between the epoxidation state of the xanthophylls pigments at 8:00 and 12:00 GMT measured at each study areas (SS1, SS2, SS3) for *Pinus sylvestris* (a) and (SN1, SN2, SN3) for *Pinus nigra* (b). The value on each plot is the mean EPS of the four trees measured per plot and the corresponding standard deviation.

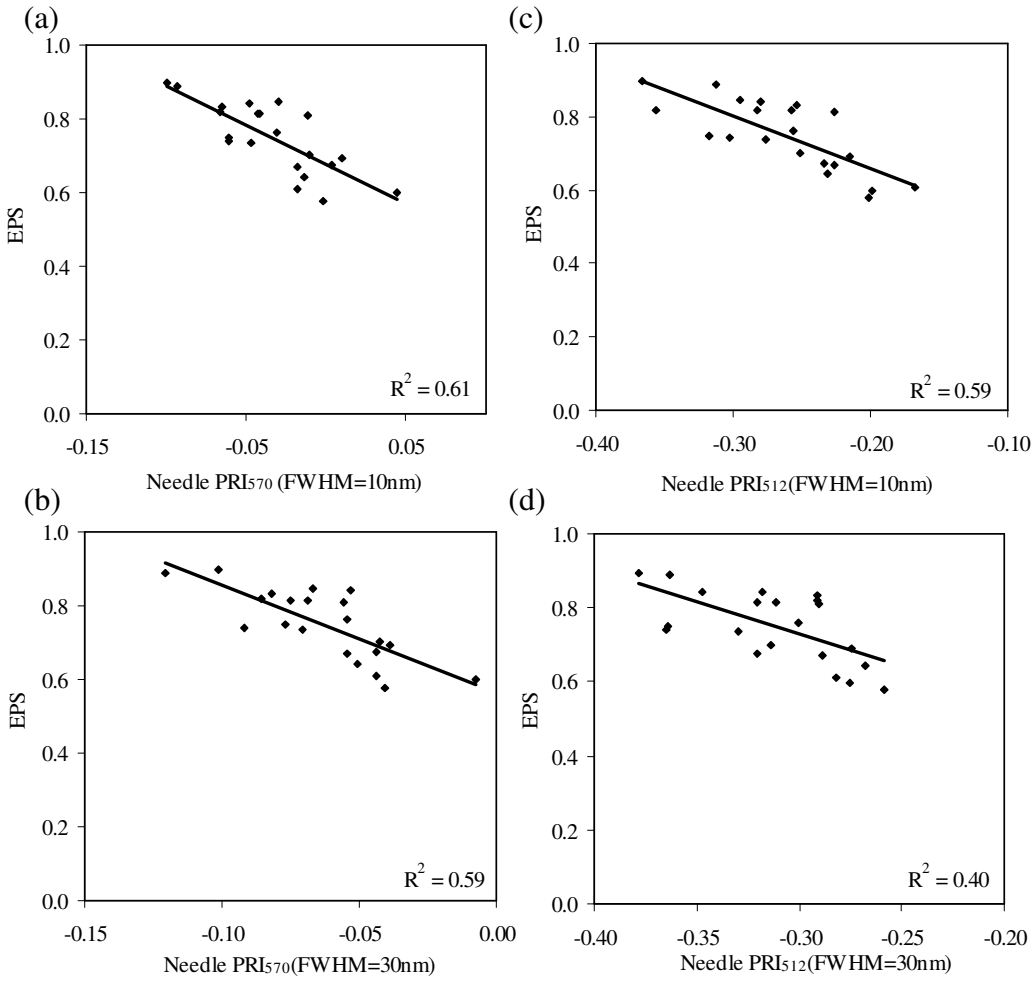

Figure 2.11. Relationships obtained between the epoxidation state of the xanthophylls pigments EPS= (V+0.5*A)/(V+A+Z) and PRI_{570} for FWHM of 10nm (a) and 30nm (c), and PRI_{512} with FWHM of 10nm (b) and 30nm (d). Needle measurements obtained at 12:00 GMT from crowns with different levels of stress on *Pinus sylvestris*.

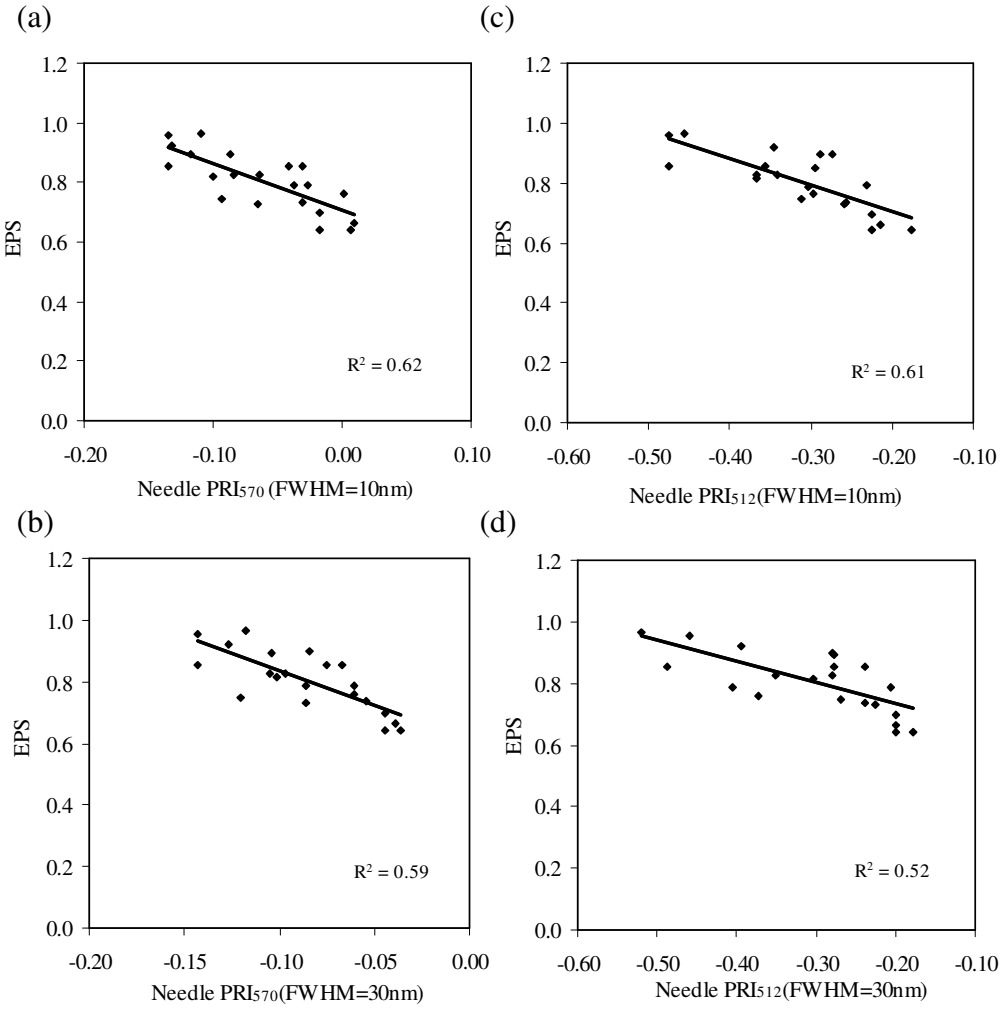

Figure 2.12. Relationships obtained between the epoxidation state of the xanthophylls pigments EPS= (V+0.5*A)/(V+A+Z) and PRI_{570} for FWHM of 10nm (a) and 30nm (c), and PRI_{512} with FWHM of 10nm (b) and 30nm (d). Needle measurements obtained at 12:00 GMT from crowns with different levels of stress on *Pinus nigra.*

The PRI formulations were then calculated for a FWHM of 30nm, simulating the airborne AHS sensor bandwidth. Results showed significant relationships between EPS and indices PRI_{570} and PRI_{512} for *P. sylvestris* and *P. nigra* (Fig. 2.11 and 2.12). The coefficients of determination obtained for both species were similar, r^2=0.59 for PRI_{570} (Fig. 2.11c) and r^2=0.40 for PRI_{512} (Fig. 2.11d) for *Pinus sylvestris,* and r^2=0.59 for PRI_{570} (Fig. 2.12c)

and r^2=0.57 for PRI_{512} (Fig. 2.12d) for *Pinus nigra*. The comparison of the relationships obtained with a FWHM of 10 and 30 nm (Fig. 2.11 and 2.12) shows that the instrument FWHM affects the relationships between PRI and EPS, as expected. Nevertheless, results obtained at 30nm FWHM yielded significant relationships between EPS and both PRI_{570} and needle PRI_{512}. Consistent relationships were also obtained when aggregating the needle spectra at the plot level using the FWHM of the airborne AHS sensor (later used to acquire the imagery). Results of these relationships are shown in Fig. 2.13, yielding coefficients of determination of r^2=0.89 for EPS vs PRI_{570} (Fig. 2.13a) and r^2=0.73 for EPS vs PRI_{512} (Fig. 2.13b).

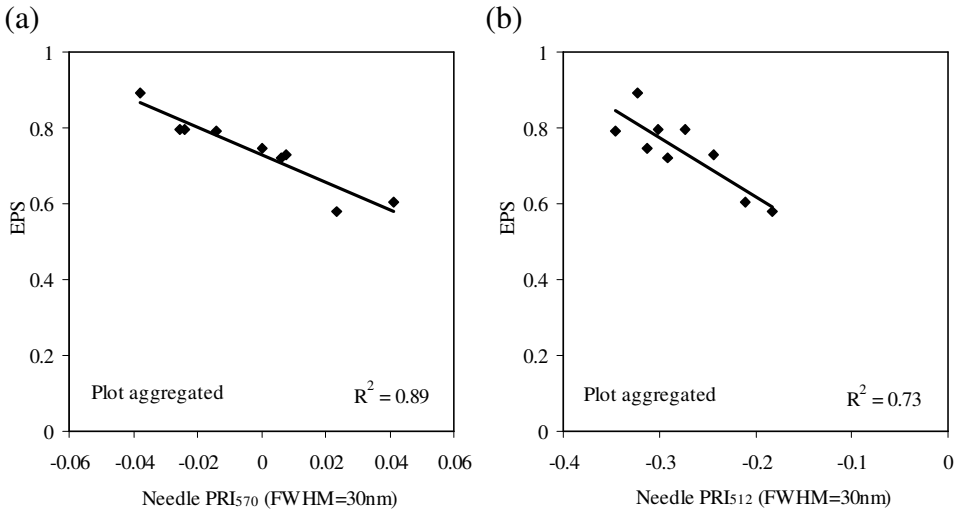

Figure 2.13. Leaf-level relationships obtained between the epoxidation state of the xanthophylls pigments EPS= (V+0.5*A)/(V+A+Z) and PRI_{570} (a) and PRI_{512} (b) both with FWHM of 30nm. Needle measurements obtained at 12:00 GMT at the plot level with different levels of stress on *Pinus sylvestris*.

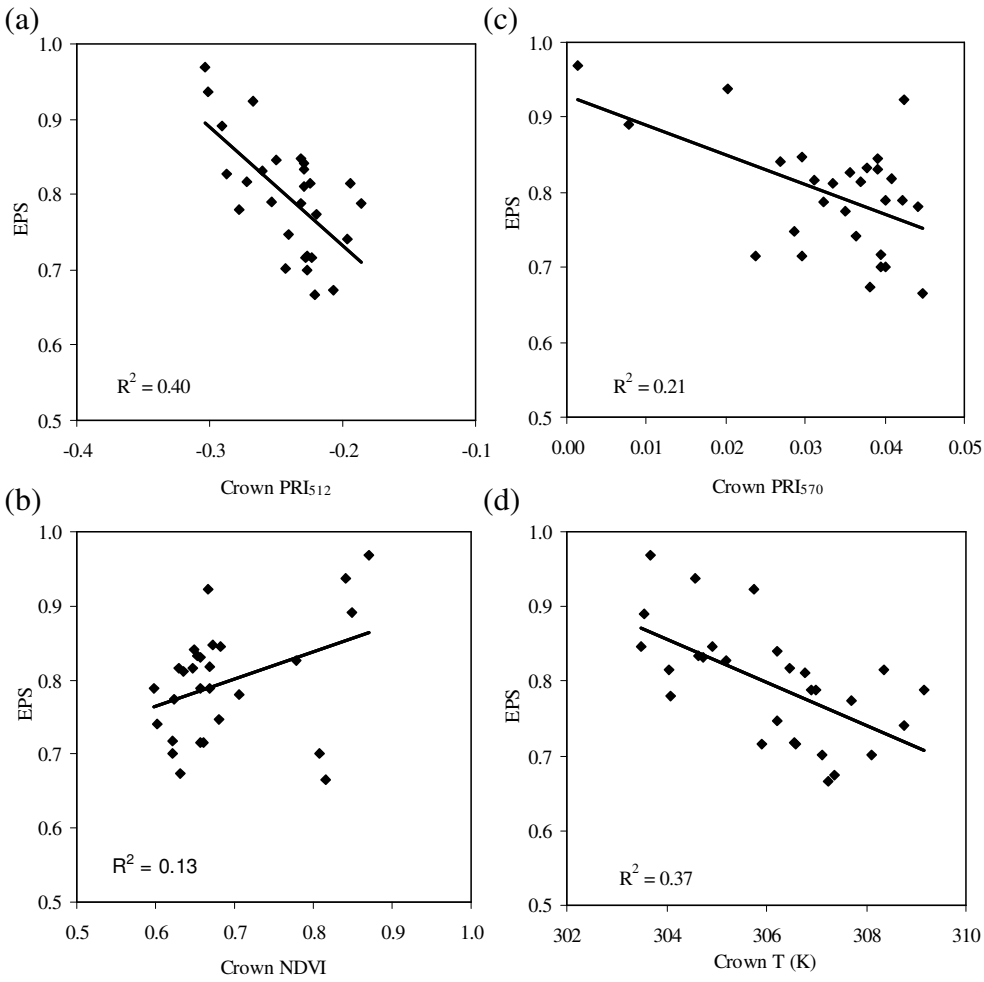

Figure 2.14. Crown-level relationships obtained between the epoxidation state of the xanthophylls EPS (V+0.5*A)/(V+A+Z) and vegetation indices: PRI_{512} (a), NDVI (b), PRI_{570} (c) and T(d). Needle measurements obtained at 12:00 GMT from crowns with different levels of stress on *Pinus sylvestris* and NDVI>0.6. PRI_{570}, PRI_{512} and T obtained from the AHS airborne sensor.

2.3.3. Experimental result: PRI formulations at the canopy level

The study conducted to assess the relationships between field-measured EPS and crown-level PRI indices was conducted by selecting pixels with NDVI higher than 0.6 from windows of 3x3 pixels with center on the targeted crown. Vegetation indices assessed were PRI_{570}, and modified PRI

formulations (PRI_{m1}, PRI_{m2}, PRI_{m3}, PRI_{m4}), as well as the normalized modified PRI_{m1} indices over structural vegetation indices NDVI, SR, OSAVI, MSAVI and $MTVI_2$. Results showed that the airborne-level PRI indices were sensitive to EPS but, as expected were also highly affected by structural parameters. The relationships between EPS and indices PRI_{570}, PRI_{512}, NDVI and T are shown in Fig. 2.14. The index PRI_{512} shows higher relationships with EPS (r^2=0.40) than PRI_{570} (r^2=0.21) (Fig. 2.14a and b), demonstrating with the EPS vs NDVI relationship that structural effects due to stress were not the major driver (Fig. 2.14c) (r^2=0.13). Significant relationships were also found between T and EPS, although with lower coefficient of determination (r^2=0.37) (Fig. 2.14d). These results show that the relationship between PRI_{512} and EPS was stronger than with PRI_{570}. In agreement with the modeling results obtained, results show that PRI_{570} might be more affected by structural effects than PRI_{512}. According to the modeling results presented in Fig. 2.7, the PRI_{512} index seems less affected by structural effects than the PRI_{570} index for high tree densities (Fig. 2.7c, 2.7d) and slightly less or equally affected for low tree densities (Fig. 2.7a, 2.7b). Moreover, the normalized results (Fig. 2.8) show less LAI effects on PRI_{512} as compared to PRI_{570}. Besides the mentioned structural effects, clear differences can be seen between both indices under varying chlorophyll content (Fig. 2.9) where the pigment effects were smaller for PRI_{512}. In the field study, structural effects on the indices were further restricted by selecting pixels with NDVI>0.6, therefore targeting pure vegetation pixels and limiting the variation of the canopy structure. Under these conditions, the experimental results suggested a greater robustness of PRI_{512} for both canopy structure (tree density and LAI) and chlorophyll content variation.

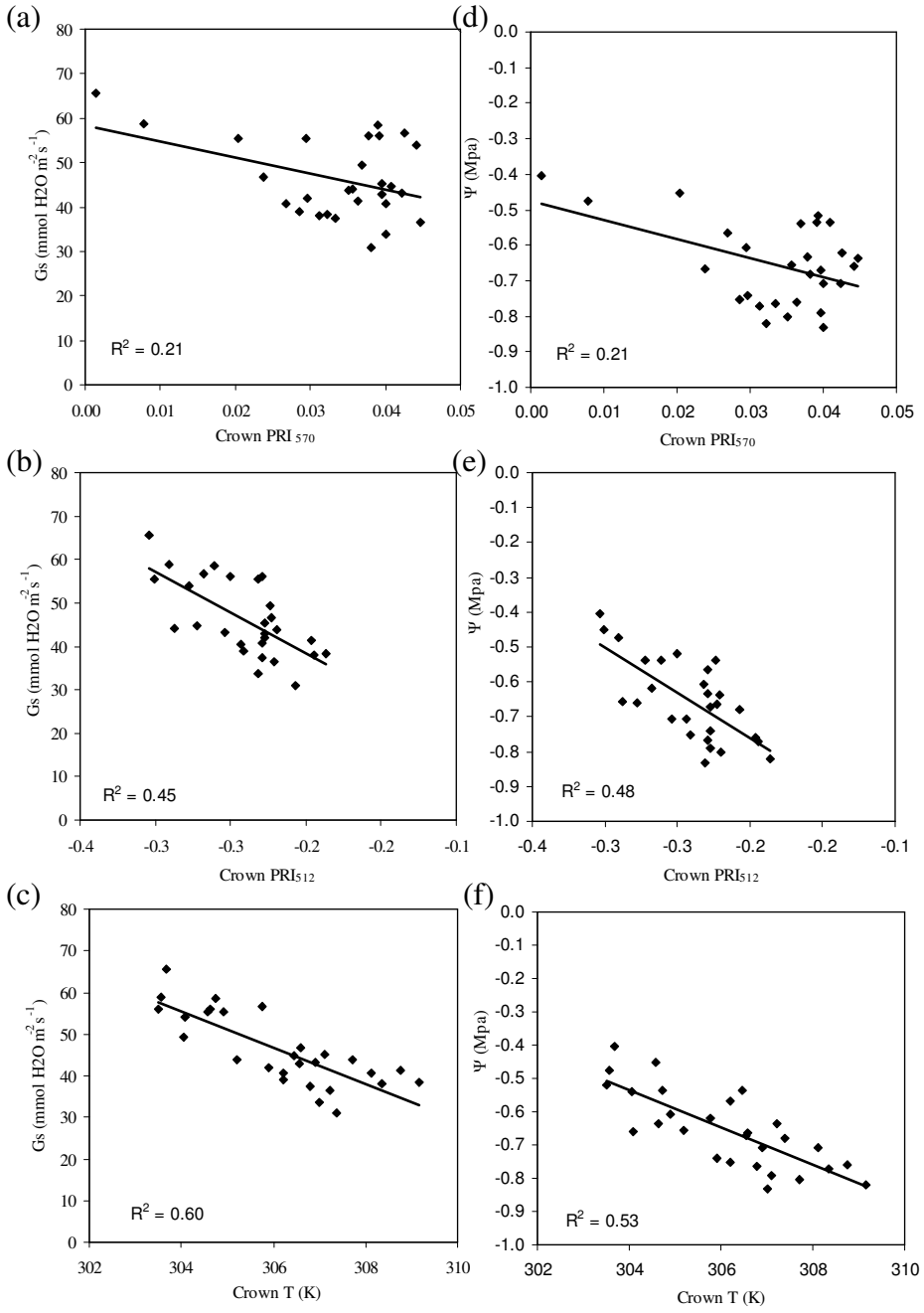

Figure 2.15. Crown-level relationships obtained for *Pinus sylvestris* between the stomatal conductance (Gs) and PRI_{570} (a), PRI_{512} (b) and temperature (T) (c). Crown-level relationships between midday water potential (Ψ) and PRI_{570} (d), PRI_{512} (e) and temperature (T) (f) of trees with NDVI>0.6.

Crown-level relationships also showed significant coefficients of determination between PRI_{512} and field-measured indicators of water stress such as Gs, (r^2=0.45) and Ψ, (r^2=0.48) (Fig. 2.15). In comparison, PRI_{570} yielded a coefficient of determination of r^2=0.21 (Gs) and r^2=0.21 (Ψ). These results demonstrate that PRI_{512} might be used as an indicator of water stress in conifer forest, and demonstrate the consistency with previously presented modeling results. Furthermore, these results are in agreement with the canopy results between EPS and PRI_{512}, which shows a superior performance for PRI_{512}. Other index modifications for PRI, such as PRI_{m2}, PRI_{m3} and PRI_{m4}, were shown to be very sensitive to structural parameters (data not included). The study conducted to assess the effects of normalizing PRI by structural vegetation indices such as NDVI, SR, OSAVI and MSAVI indicated little improvement (data not included).

PRI_{570}, PRI_{m1} and NDVI were applied at the image level to map stress over the study areas. Fig. 2.16 shows the three *Pinus nigra* study areas (SN1, SN2, SN3) and two zoomed images of each central plot at 1x1 and 3x3 resolution (pixel based) and at object level. A visual analysis reveals that the study areas with different stress levels showed similar NDVI and PRI_{570} values, but different PRI_{512} values (Fig. 2.16). To quantify these differences the mean and the standard deviation for each index were calculated for the four trees displayed in the zoom images (Fig. 2.16), for a total of twelve trees for each species. While the mean values for NDVI and PRI_{570} were similar among the study areas, PRI_{512} showed different ranges for each stress level (Fig. 2.17a). A similar comparison was conducted for *Pinus sylvestris* (Fig. 2.17b). Simulation and experimental results were consistent with the mapping results obtained for PRI_{512}, showing its ability for accurately mapping stress at both pixel and object levels in conifer forests.

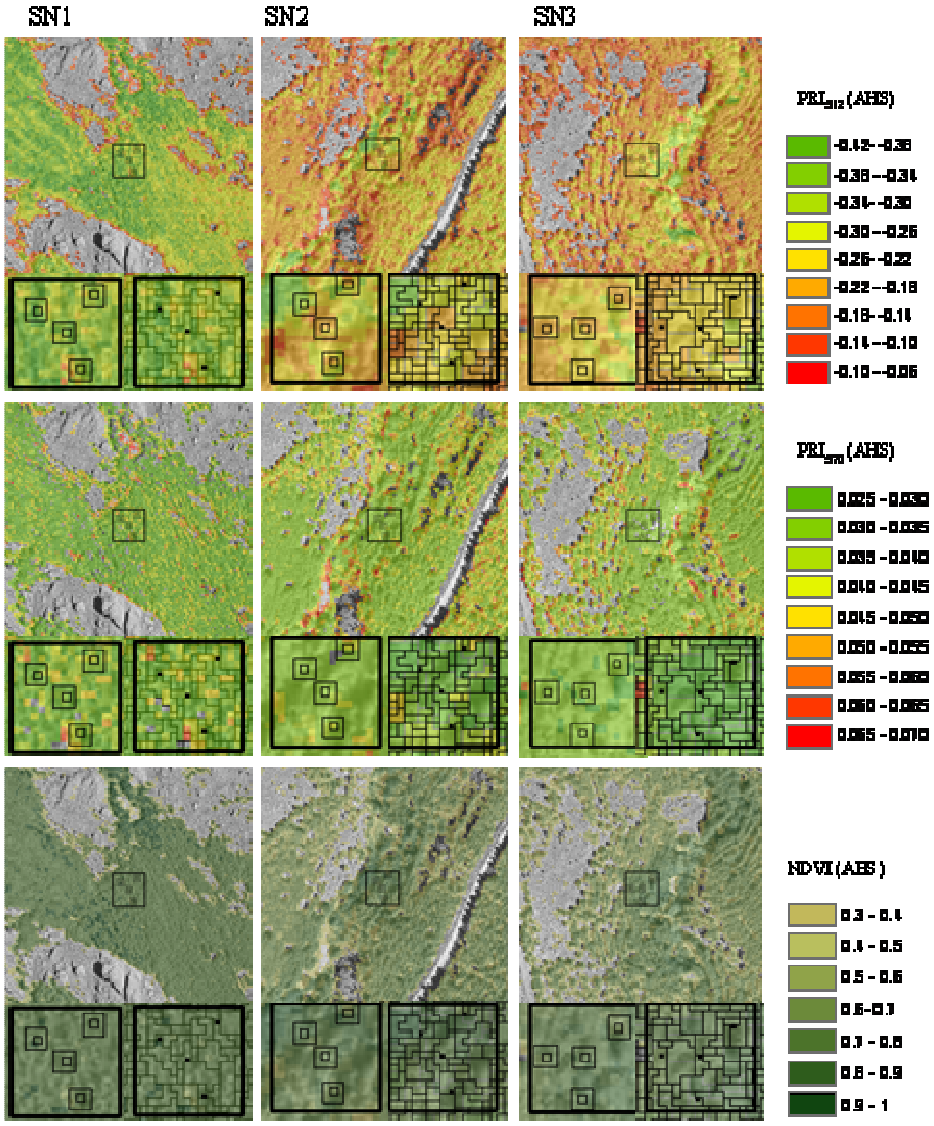

Figure 2.16. PRI_{512}, PRI_{570} and NDVI obtained from the AHS airborne sensor from three study areas of *Pinus nigra* with different levels of stress: SN1, SN2 and SN3. At the bottom of each image, two zoom images of a central plot, one pixel-based displaying 1x1 and 3x3 resolutions and the other at object level.

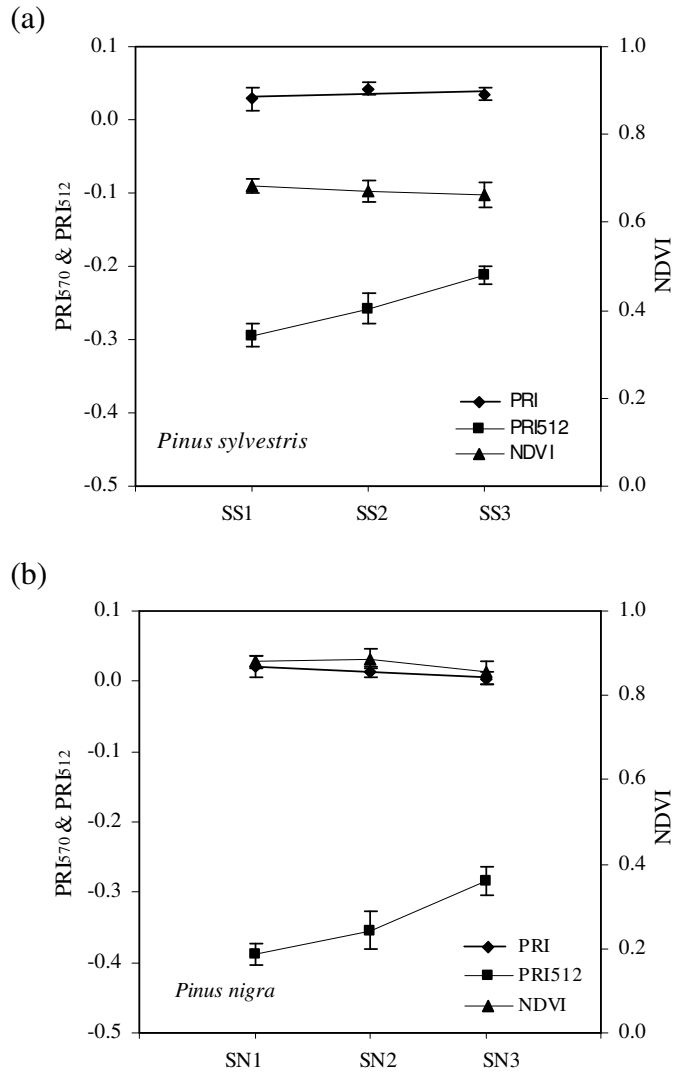

Figure 2.17. Mean values and standard deviation obtained from the AHS image of PRI_{570}, PRI_{512} and NDVI. Values calculated from twelve trees located in the study areas SN1, SN2 and SN3 of *Pinus nigra* (a) and SS1, SS2 and SS3 of *Pinus sylvestris* (b).

2.4. Conclusions

Radiative transfer simulation methods were applied using INFORM as a canopy reflectance model linked with a modified LIBERTY leaf model in order to assess the effects of canopy structure on different formulations of PRI. The simulations were conducted by computing canopy reflectance spectra with different values of LAI, tree density and chlorophyll content, assessing the effects of these biochemical and structural inputs on the proposed PRI formulations. The study demonstrated the sensitivity of PRI and modified PRI indices to canopy structural parameters and, therefore, the need for assessing robust PRI formulations with less structural effects. The simulation results demonstrate that PRI_{512} is less sensitive to changes in LAI values, tree densities and chlorophyll content than PRI_{570}.

In addition to the simulation work conducted, PRI indices were also tested using experimental data collected from the study sites at 8:00 and 12:00 GMT. Significant differences for both species were found in EPS measured at 12:00 GMT as a function of the stress levels, showing that EPS declined consistently with PRI_{570} and PRI_{512}. At the leaf level, both PRI_{570} and PRI_{512} were sensitive to EPS measured by destructive sampling. Nevertheless, the study conducted at the canopy level revealed that PRI_{512} was better correlated with EPS and physiological indicators, such as water potential and stomatal conductance, than PRI_{570}. The better performance obtained for PRI_{512} over PRI_{570} at the canopy level in the experimental study confirms the modeling results which showed the lower sensitivity of PRI_{512} to structural effects in conifer canopies as compared to PRI_{570}. Other formulations such as PRI_{m2}, PRI_{m3} and PRI_{m4} were highly sensitive to structural parameters and therefore not optimum for stress detection in these canopies. The sensitivity

of the PRI indices to structural parameters is critical in conifer forests, where the heterogeneity allows greater influence due to the ground layer and shadows.

This work demonstrates the link between PRI_{512} and PRI_{570} with EPS in *P. sylvestris* and *P. nigra* at the leaf level, and it suggests the superior performance at the canopy level for PRI_{512} versus PRI_{570} when mapping previsual stress levels in conifer forests.

References

Abadía, A. & Abadía, J. (1993). Iron and plant pigments. In L. L. Barton & B. C. Hemming (Eds.), *Iron Chelation in Plants and Soil Microorganisms* (pp. 327-344). Academic: San Diego.

Asner, G. P., Carlson, K. M., & Martin, R. E. (2005). Substrate age and precipitation effects on Hawaiian forest canopies from spaceborne imaging spectroscopy. *Remote Sensing of Environment*, *98*, 457-467.

Allen C. D., Macalady A. K., Chenchouni H., Bachelet D., McDowell N., Vennetier M., Kitzberger T., Rigling A., Breshears D. D., Hogg E. H., Gonzalez P., Fensham R., Zhang Z., Castro J., Demidova N., Lim J. H., Allard G., Running S.W., Semerci A. & Cobb N. (2009). A global overview of drought and heat-induced tree mortality reveals emerging climate change risks for forests. *Forest Ecology and Management*, *259*, 660-684.

Atzberger, C. (2000). Development of an invertible forest reflectance model: The INFOR-Model. In: Buchroithner (Ed.), *A Decade of Trans-European Remote Sensing Cooperation.* Proceedings of the 20th EARSeL Symposium, Dresden, Germany*,* 14-16 June 2000, pp. 39-44.

Barton, C. V. M. & North, P. R. J. (2001). Remote sensing of canopy light use efficiency using the Photochemical Reflectance Index. Model and analysis. *Remote Sensing of Environment*, *78*, 264-273.

Berk, A., Anderson, G. P., Acharya, P. K., Chetwynd, J. H., Bernstein, L. S., Shettle, E. P., Matthew, M. W., and Adler-Golden, S. M. (2000). *MODTRAN4 User's Manual*, Air Force Research Laboratory, Hanscom MA.

Berk A., Bernstein L. S., Anderson G. P., Acharya P. K., Robertson D. C., Chetwynd J. H. & Adler-Golden S. M. (1998). MODTRAN cloud and multiple scattering upgrades with application to AVIRIS. *Remote Sensing of Environment*, *65*, 367-375.

Berni, J. A. J., Zarco-Tejada, P. J., Sepulcre-Cantó, G., Fereres, E., & Villalobos, F. J. (2009). Mapping stomatal conductance and CWSI in olive orchards using high resolution thermal remote sensing imagery. *Remote Sensing of Environment*, *113*, 2380-2388.

Björkman, O. & Demmig-Adams, B. (1994). Regulation of photosynthetic light energy capture, conversion, and dissipation in leaves of higher plants. In: Schulze DE & MM Caldwell (Eds.), *Ecophysiology of Photosynthesis* (pp. 17-45). Springer-Verlag, Berlin, Germany.

Dawson, T. P., Curran P. J. & Plummer S. E. (1998). LIBERTY - Modelling the Effects of Leaf Biochemical Concentration on Reflectance Spectra. *Remote Sensing of Environment, 65*, 50-60.

Demmig-Adams B. & Adams W. W. (1996). The role of xanthophyll cycle carotenoids in the protection of photosynthesis. *Trends in Plant Science*, *1*, 21-26.

Di Vittorio A. V. (2009). Enhancing a leaf radiative transfer model to estimate concentrations and *in vivo* specific absorption coefficients of total carotenoids and chlorophylls *a* and *b* from single-needle reflectance and transmittance.
Remote Sensing of Environment, *113,* 1948-1966.

Drolet, G. G., Huemmrich, K. F., Hall, F. G., Middleton, E. M., Black, T. A., Barr, A. G. & Margolis, H. A. (2005). A MODIS-derived Photochemical Reflectance Index to detect inter-annual variations in the photosynthetic light-use efficiency of a boreal deciduous forest. *Remote Sensing of Environment*, *98*, 212-224.

Ferretti M. (1994). *Especies forestales mediterráneas. Guía para la evaluación de las copas*. CEE-UN/ECE. Bruselas, Ginebra.

Filella, I., Amaro, T., Araus, J. L., & Peñuelas, J. (1996). Relationship between photosynthetic radiation-use efficiency of barley canopies and the photochemical reflectance index (PRI). *Physiologia Plantarum*, *96*, 211-216.

Filella, I., Porcar-Castell, A., Munné-Bosch, S., Bäck, J. M., Garbulsky F. & Peñuelas, J. (2009). PRI assessment of long-term changes in carotenoids/chlorophyll ratio and short-term changes in de-epoxidation state of the xanthophyll cycle. *Remote Sensing of Environment*, *30*, 4443-4455.

Gamon, J. A., Filella, I., and Peñuelas, J. (1993). The dynamic 531nm reflectance signal: A survey of twenty angiosperm species. In: Yamamoto, H.Y. and Smith, C.M., Editors, 1993. Photosynthetic responses to the environment. *American Society of Plant Physiologists*, Rockville, MD, pp. 172-177.

Gamon, J. A., Serrano, L. and Surfus, J. S. (1997). The photochemical reflectance index: an optical indicator of photosynthetic radiation use efficiency across species, functional types and nutrient levels. *Oecologia 112*, 492-501.

Gamon, J. A., Peñuelas, J., & Field, C. B. (1992). A narrow-waveband spectral index that tracks diurnal changes in photosynthetic efficiency. *Remote Sensing of Environment*, *41*, 35-44.

Garbulsky, M. F., Peñuelas, J., Papale, D., & Filella, I. (2008). Remote estimation of carbon dioxide uptake by a Mediterranean forest. *Global Change Biology*, *14*, 2860-2867.

Haboudane D., Miller J. R., Pattey E., Zarco-Tejada P. J. & Strachan I. B. (2004). Hyperspectral vegetation indices and novel algorithms for predicting green LAI of crop canopies: Modeling and validation in the context of precision agriculture. *Remote Sensing of Environment, 90,* 337-352.

Hall, F. G., Hilker, T., Coops, N. C., Lyapustin, A., Huemmrich, K. F., Middleton, E. M., Margolis, H. A., Drolet, G. G., & Black, T. A. (2008). Multi-angle remote sensing of forest light use efficiency by observing PRI variation with canopy shadow fraction. *Remote Sensing of Environment*, *112*, 3201-3211.

Heikkilä, J., Nevalainen S. & Tokola T. (2002). Estimating defoliation in boreal coniferous forests by combining Landsat TM, aerial photographs and field data. *Forest Ecology and Management*, *158*, 9-23.

Hilker T., Coops N. C., Hall F. G., Black T. A., Wulder M. A., Nesic Z. & Krishnan P. (2008). Separating physiologically and directionally induced changes in PRI using BRDF models. *Remote Sensing of Environment, 112*, 2777-2788.

Hilker T., Lyapustin A., Hall F. G., Wang Y., Coops N. C., Drolet G., & Black T. A. (2009). An assessment of photosynthetic light use efficiency from space: Modeling the atmospheric and directional impacts on PRI reflectance. *Remote Sensing of Environment*, *113*, 2463-2475.

Inoue, Y., Peñuelas, J., Miyata A., & Mano, M. (2008). Normalized difference spectral indices for estimating photosynthetic efficiency and capacity at a canopy scale derived from hyperspectral and CO_2 flux measurements in rice. *Remote Sensing of Environment, 112,* 156-172.

Jackson, R. D., Reginato, R. J., & Idso, S. B. (1977). Wheat canopy temperature: A practical tool for evaluating water requirements. *Water Resources Research, 13*, 651-656.

Jordan, C. F. (1969). Derivation of leaf area index from quality of light on the forest floor. *Ecology*, *50*, 663-666.

Larbi, A., Abadía, A., Morales, F., & Abadía, J. (2004). Fe resupply to Fe-deficient sugar beet plants leads to rapid changes in the violaxanthin cycle and other photosynthetic characteristics without significant *de novo* chlorophyll synthesis. *Photosynthesis Research*, *79*, 59-69.

Martínez-Vilalta J., López B. C., Adell N., Badiella L. & Ninyerola M. (2008). Twentieth century increase of Scots pine radial growth in NE Spain shows strong climate interactions. *Global Change Biology, **14,*** 2868-2881.

Malenovsky Z., Albrechtova J., Lhotakova Z., Zurita-Milla R., Clevers G. P. W., Schaepman M. E., & Cudlín P. (2006). Applicability of the PROSPECT model for Norway spruce needles. *International Journal of Remote Sensing,* **27**, 5315-5340.

Melamed N. T. (1963). Optical properties of powders. Part I. Optical absorption coefficients and the absolute value of the diffuse reflectance. Part II. Properties of luminescent powders, *Applied Optics*, *34*, 560-570.

Melzack, R. N., Bravdo B. & Riov J. (1985). The effect of water stress on photosynthesis and related parameters in *Pinus halepensis*. *Physiologia Plantarum, 64*, 295-300.

Middleton E.M., Cheng Y.B., Hilker T., Black T.A., Krishnan P., Coops N.C. & Huemmrich K.F. (2009). Linking foliage spectral responses to canopy level ecosystem photosynthetic light use efficiency at a Douglas-fir forest in Canada. *Canadian Journal of Remote Sensing, 35,* 166-188.

Moorthy I., Miller J. R., & Noland T. L. (2008). Estimating chlorophyll concentration in conifer needles with hyperspectral data: An assessment at the needle and canopy level. *Remote Sensing of Environment*, *112*, 2824-2838.

Navarro-Cerrillo, R. M., Varo, M. A., Lanjeri, S., & Hernández-Clemente, R. (2007). Cartografía de defoliación en los pinares de pino silvestre (*Pinus sylvestris* L.) y pino salgareño (*Pinus nigra* Arnold) en la Sierra de los Filabres. *Ecosistemas*, 16, 163-171.

Nilson, T. & Ross, J. (1997). Modeling radiative transfer through forest canopies: Implications for canopy photosynthesis and remote sensing. In: H. L. Gholz, K. Nakane, and H. Shimoda (Eds.), *The Use of Remote Sensing in the Modeling of Forest Productivity* (pp. 23-60). Kluwer, Dordrecht.

Peguero-Pina, J. J., Camarero, J. J., Abadía, A., Martín, E., González-Cascón, R., Morales, F., & Gil-Pelegrín. (2007). Physiological performance of silver-fir (*Abies alba* Mill.) populations under contrasting climates near the south-western distribution limit of the species. *Flora, 202,* 226-236.

Peguero-Pina, J. J., Morales, F., Flexas, J., Gil-Pelegrín, E., & Moya, I. (2008). Photochemistry, remotely sensed physiological reflectance index and de-epoxidation state of the xanthophyll cycle in *Quercus coccifera* under intense drought. *Oecologia*, *156*, 1-11.

Peñuelas, J., Filella, I., and Gamon, J. A. (1995). Assessment of photosynthetic radiation use eficiency with spectral reflectance. *New Phytologist*, *131*, 291- 296.

Peñuelas, J., J. A. Gamon, A. L. Fredeen, Merino J. & Field C. B. (1994). Reflectance indices associated with physiological changes in nitrogen- and water-limited sunflower leaves. *Remote Sensing of Environment*, *48*, 135-146.

Poyatos R.; Llorens P.; Piñol J. & Rubio C. (2008). Response of Scots pine (*Pinus sylvestris* L.) and pubescent oak (*Quercus pubescens* Willd.) to soil and atmospheric water deficits under Mediterranean mountain climate. *Annals of Forest Science*, *65*, 306.

Qi, J., Chehbouni A., Huete A. R., Kerr Y. H. (1994). Modified Soil Adjusted Vegetation Index (MSAVI). *Remote Sensing of Environment, 48,* 119-126.

Rebetez M. & Dobbertin M. (2004). Climate change may already threaten Scots pine stands in the Swiss Alps. *Theoretical and Applied Climatology, 79*, 1-9.

Richardson, A. D. & Berlyn, P. (2002). Changes in foliar spectral reflectance and chlorophyll fluorescence of four temperate species following branch cutting. *Tree Physiology, 22,* 499-506.

Rondeaux, G., Steven, M., & Baret, F. (1996). Optimization of soil-adjusted vegetation indices. *Remote Sensing of Environment*, *55,* 95-107.

Rouse, J. W., Haas, R. H., Schell, J. A., Deering, D. W. & Harlan, J. C. (1974). Monitoring the Vernal Advancement and Retrogradation (Greenwave Effect) of Natural Vegetation. Type III Final Report, NASA Goddard Space Flight Center, Greenbelt, Maryland, 20771, USA, 371 pp.

Rosema A., W. Verhoef, H. Noorbergen & Borgesius J. J. (1992). A new forest light interaction model in support of forest monitoring. *Remote Sensing of Environment, 42,* 23-41.

Schlerf, M., Atzberger, C. G. & Hill, J. (2005). Remote sensing of forest biophysical variables using HyMap imaging spectrometer data. *Remote Sensing of Environment*, *95,* 177-194.

Schlerf, M. & Atzberger, C. G. (2006). Inversion of a forest reflectance model to estimate structural canopy variables from hyperspectral remote sensing. *Remote Sensing of Environment*, *100*, 281-294.

Scholander, P. F.; Hammel, H. T.; Bradstreet, E. D.; Hemmingsen, E.A. (1965). Sap pressure in vascular plants. *Science,148,* 339-346.

Sepulcre-Cantó, G., Zarco-Tejada, P. J., Jiménez-Muñoz, J. C., Sobrino, J. A., de Miguel, E., & Villalobos, F. J. (2006). Detection of Water Stress in an Olive Orchard with Thermal Remote Sensing Imagery. *Agricultural and Forest Meteorology, 136,* 31-44.

Sepulcre-Cantó, G., Zarco-Tejada, P. J., Jiménez-Muñoz, J. C., Sobrino, J. A., Soriano, M. A., Fereres, E., Vega, V., & Pastor, M. (2007). Monitoring yield and fruit quality parameters in open-canopy tree crops under water stress. Implications for ASTER. *Remote Sensing of Environment*, *107*, 455-470.

Sepulcre-Cantó, G., Zarco-Tejada, P. J., Sobrino, J. A., Berni, J. A. J., Jiménez Muñoz, J. C., & Gastellu-Etchegorry, J. P. (2009). Detecting water status in open canopies with thermal ASTER imagery and DART radiative transfer simulation. *Agricultural and Forest Meteorology*, *149*, 962-975.

Sims, D. A. & Gamon, J. A. (2002). Relationships between leaf pigment content and spectral reflectance across a wide range of species, leaf structures and developmental stages. *Remote Sensing of Environment*, *81*, 337-354.

Smolander S. & Stenberg P. (2003). A method to account for shoot scale clumping in coniferous canopy reflectance models. *Remote Sensing of Environment*, *88*, 363-373.

Sobrino, J. A., Jiménez-Muñoz, J. C., Labed-Nachbrand, J. & Nerry F. (2002). Surface emissivity retrieval from Digital Airborne Imaging Spectrometer data. *Journal of Geophysical Research*, 107, (D23), 4729, doi: 10.1029/2002JD002197.

Sobrino, J. A., Jiménez-Muñoz, J. C., Zarco-Tejada, P. J., Sepulcre-Cantó, G. & de Miguel, E. (2006). Land Surface Temperature derived from Airborne Hyperspectral Scanner Thermal Infrared data. *Remote Sensing Environment*, *102*, 99–115.

Suárez, L., Zarco-Tejada, P. J., Sepulcre-Cantó, G., Pérez-Priego, O., Miller, J. R., Jiménez-Muñoz, J. C., Sobrino, J. (2008). Assessing Canopy PRI For Water Stress Detection With Diurnal Airborne Imagery. *Remote Sensing of Environment*, *112*, 560-575.

Suárez, L., Zarco-Tejada, P. J., Berni, J. A. J., González-Dugo, V., Fereres, E. (2009). Modelling PRI for Water Stress Detection using Radiative Transfer Models. *Remote Sensing of Environment*, *113,* 730-744.

Suárez, L., Zarco-Tejada, P. J., González-Dugo, V., Berni, J. A. J., Sagardoy, R., Morales, F., Fereres, E. (2010). Detecting water stress effects on fruit quality in orchards with time-series PRI airborne imagery. *Remote Sensing of Environment, 114,* 286-298.

Thayer, S. S. & Björkman, O. (1990). Leaf xanthophyll content and composition in sun
and shade determined by HPLC. *Photosynthesis Research*, *23*, 331-343.

UN/ECE, (1994). Manual on Methods and Criteria for Harmonised Sampling, Assessment, Monitoring and Analysis of the Effects of Air Pollution on Forests. *Third ed. Programme Co-ordinating Centres*, Hamburg and Prague.
Verhoef, W. (1984). Light scattering by leaf layers with application to canopy reflectance modeling: The SAIL model. *Remote Sensing of Environment, 16*, 125-141.

Verhoef, W. (1985). Earth observation modeling based on layer scattering matrices. *Remote Sensing of Environment, 17,* 165-178.

Yamamoto, Y. (1979). Biochemistry of the violaxanthin cycle in higher plants, *Pure & Applied Chemistry, 51*, 639-648.

Zarco-Tejada, P. J., Miller, J. R., Harron, J., Hu, B., Noland, T. L., Goel, N., Mohammed G. H. & Sampson, P. H. (2004). Needle chlorophyll content estimation through model inversion using hyperspectral data from boreal conifer forest canopies. *Remote Sensing of Environment, 89*, 189-199.

Zhang, Y., Chen, J. M., Miller, J. R., & Noland, T. L. (2008). Retrieving chlorophyll content of conifer needles from hyperspectral measurements. *Canadian Journal of Remote Sensing, 34,* 296-310.

3. Carotenoid content estimation in a heterogeneous conifer forest using narrow-band indices and PROSPECT+DART simulations.

Chapter 2

Carotenoid content estimation in a heterogeneous conifer forest using narrow-band indices and PROSPECT + DART simulations.

Abstract

The present study explored the use of narrow-band indices formulated in the visible spectral region at leaf and canopy levels to estimate carotenoid content. The research area was a pine forest affected by decline processes. Spectral reflectance and pigment content including chlorophyll a and b (Ca+b), carotenoid (Cx+c) and xanthophyll cycle pigments (VAZ) were measured in needles for two consecutive years. The study was conducted using radiative transfer modeling methods and high-resolution airborne imagery acquired at 10 nm FWHM bandwidth. Airborne data consisted of high spatial resolution imagery acquired with a narrow-band multispectral camera on board an unmanned aerial vehicle (UAV). The imagery had 50 cm resolution and six spectral bands in the 500-800 nm range, enabling the identification of pure crowns to obtain the reflectance of individual trees. The indices evaluated were traditional formulations and new simple ratios developed by combining bands sensitive to Cx+c absorption in the 500-600 nm region. The PROSPECT-5 model was coupled with the Discrete Anisotropic Radiative Transfer (DART) model to explore the performance of Cx+c -sensitive vegetation indices at leaf and canopy levels. The sensitivity of these indices to structural effects was assessed to study the potential scaling-up of Cx+c -related vegetation indices on heterogeneous canopies. Coefficients of determination between Cx+c content and narrow-band vegetation indices revealed that traditional indices were highly related with Cx+c content at leaf level (r^2>0.90; P<0.001 for the CRI index ($1/R_{515}$)-($1/R_{550}$)) but highly affected by structural parameters at crown level (r^2>0.44; P<0.001). A new simple-ratio vegetation index proposed in this study (R_{515}/R_{570}) was found to be significantly related with Cx+c content both at leaf (r^2>0.72; P<0.001) and canopy levels (r^2>0.71; P<0.001). Remote sensing cameras on board UAV platforms can provide very high multispectral and hyperspectral imagery for mapping biochemical constituents in heterogeneous forest canopies. This study demonstrates the feasibility of mapping carotenoid content to assess the physiological condition of forests.

Keywords: narrow-band indices, carotenoids, R_{515}/R_{570}, radiative transfer, airborne remote sensing, UAV, heterogeneous conifer forest.

3.1. Introduction

Carotenoid and chlorophyll pigment content provide valuable information about the physiological status of plants (Demmig-Adams & Adams, 1992). Chlorophylls - C_a and C_b - are essential pigments to absorb the energy of light and convert it to store chemical energy (Carter, 1994; Lichtenhaler, 1998). Total carotenoid pigments ($Cx+c$) (xanthophylls and carotenes) are usually represented by two (α- and β-) carotenes and five xanthophylls (lutein, zeaxanthin, violaxanthin, antheraxanthin and neoxanthin) (Demmig-Adams & Adams, 1992). Carotenoids have several physiological functions associated with photosynthesis, including a structural role in the organization of photosynthetic membranes, participation in light harvesting and energy transfer (Frank & Cogdell, 1996; Ritz et al., 2000), as well as quenching of $Ca+b$ excited state and photoprotection (Demmig-Adams & Adams, 1996; Thayer & Björkman, 1990, Young & Britton, 1990). Carotenoid content is known to be correlated with plant stress and photosynthetic capacity. For example, it has been observed that some carotenoids increase under high irradiance levels and high temperature environments (Kirchgebner et al., 2003) or at the onset of leaf senescence (Munné-Bosch & Peñuelas, 2003; Peñuelas et al., 1994). Some xanthophylls have been found to be involved in the non-photochemical quenching of chlorophyll fluorescence (CF), an important photoprotective process (Demmig-Adams & Adams, 1992). The xanthophylls involved in this process dissipate excess energy. This is commonly referred to as the *xanthophyll cycle* (Young et al., 1997).

The photoprotection system plays a critical role in plants adapted to the Mediterranean climate (Faria et al., 1996; Hernández-Clemente et al., 2011)

because many Mediterranean environments are associated with high summer temperatures, high irradiation levels and drought. Thus, leaf pigment content has considerable importance as a physiological indicator of plant growth and stress in the Mediterranean forest.

Recent studies have focused on retrieving leaf pigment content from remote sensing data (Malenovsky et al., 2007; Meggio et al., 2008; Wu et al., 2008; Zarco-Tejada et al., 2004). Nevertheless, the overlapping absorption exhibited by chlorophyll and carotenoids in the visible region makes it difficult to retrieve *Ca+b* and *Cx+c* content independently (Feret et al., 2011). Several studies have successfully estimated *Ca+b* for chlorosis detection in vegetation using visible ratios (Datt, 1998), visible/NIR ratios (Gitelson et al., 2003, 2006; Haboudane et al., 2002), red edge reflectance-ratio indices (Carter & Spiering, 2002; Gitelson et al., 2003; le Maire et al., 2004; Richardson & Berlyn , 2002; Sims & Gamon, 2002), spectral and derivative red edge indices (Miller et al., 1990) and *scaling-up* and model inversion methods with narrow bands in forest canopies (Zarco-Tejada et al., 2001).

Most methods have focused on retrieving *Ca+b* content (Main et al., 2011), but only a few studies have focused on estimating *Cx+c* (Gitelson et al., 2002). In fact, research conducted at canopy level using high-resolution narrow-band imagery is very limited or nonexistent. Candidate *Cx+c* optical indices have been grouped into two main categories based on the spectral region used: visible ratios (Gamon et al., 1992; Garrity et al., 2011; Gitelson et al., 2003, 2006; Hernández-Clemente et al., 2011) and visible/NIR ratios (Blackburn 1998; Chappelle et al., 1992; Datt, 1998; Merzlyak et al., 1999;

Peñuelas et al., 1995). Gitelson et al. (2002) developed indices within the visible region and showed that carotenoid absorption was related to a prominent spectral peak located at 520 nm spectra corresponding to senescing and mature leaves. The same authors showed that the sensitivity of reciprocal reflectance to *Cx+c* content was maximal in a spectral range around 510 nm, proposing the *Carotenoid Content Index* as $(1/R_{515})$-$(1/R_{550})$ and $(1/R_{515})$-$(1/R_{700})$ (Gitelson et al., 2002). The 550 and 700 nm reflectance bands were used in their study to minimize the effect of chlorophylls in this spectral range. In other studies, the *Photochemical Reflectance Index* (PRI) (Gamon et al., 1992), originally developed to estimate changes in the xanthophyll cycle pigments, has been successfully related to the *Cx+c*/*Ca+b* ratio at leaf level (Garity et al., 2011; Sims & Gamon, 2002). In particular, Garity et al. (2011) found significant relationships between the $PRI \cdot [(R_{760}/R_{700})^{-1}]$ and the *Cx+c*/*Ca+b* ratio.

The main spectral bands proposed for *Cx+c* estimation in the visible/NIR region are the following: i) combinations of bands around the 700 nm region (678, 708 and 760 nm) and bands in the green region (500, 550 nm) (Chappelle et al., 1992; Merzlyak et al., 1999); and ii) combinations of R_{800} with visible bands (470, 680, 635 nm) (Blackburn, 1998; Peñuelas et al., 1995). Chappelle et al. (1992) analyzed different ratios of leaf reflectance spectra to identify bands corresponding to the absorption of *Ca+b* and *Cx+c*. They found that the *Cx+c* fraction had a maximum absorption peak at 500 nm and proposed the R_{760}/R_{500} ratio as a quantitative measure of this pigment at leaf level. Successful *scaling-up* of such results to the canopy level required additional studies focused on the effects of the structure and background on the indices proposed for *Cx+c* and *Ca+b* estimation, such as

the R_{750}/R_{710} index (Zarco-Tejada *et al.,* 2001). Recent studies have demonstrated that hyperspectral indices for *Ca+b* estimation in leaves cannot be readily applied to imagery due to the large structural effects present in heterogeneous canopies (Wu et al., 2008; Zarco-Tejada et al., 2004). In particular, Malenovsky et al. (2007) proposed a new optical index defined as the *Area under curve Normalized to Maximal Band depth* between 650 and 725 nm (ANMB 650-725) to estimate the chlorophyll concentration of a Norway spruce crown.

These *scaling-up* studies are even more important in forest canopies because *bidirectional* and background effects increase in conifer forests under sparse and open conditions (Zarco-Tejada et al., 2004). While some studies have used the inversion of physically-based models (Malenovsky et al., 2008), others have used simple statistical relationships with a variety of optical spectral indices or combined empirical relationships coupled with radiative transfer simulation models (Broge & Leblanc, 2001; Gastellu-Etchegorry & Bruniquel-Pinel, 2001). With the development of PROSPECT-5 (Féret et al., 2008; Jacquemoud & Baret, 1990), it is possible to explore the validation of carotenoid content retrieval at leaf level in a wide number of species (Féret et al., 2011). At canopy level, models such as the 3-dimensional *Discrete Anisotropic Radiative Transfer* (DART) model (Gastellu-Etchegorry et al., 1996, 2004) can be used to model complex structures and canopy architectures to simulate coniferous canopies.

The simulation of forest canopy reflectance is used as well to perform sensitivity analyses of canopy structure, viewing geometry and background effects. An example is the assessment of physiological indices such as the

PRI, which was found to be highly affected by background and structural variables (Suárez et al., 2008, 2009; Hernández-Clemente et al., 2011). Meggio et al. (2010) showed that *Cx+c* -related vegetation indices such as the Gitelson-*Cx+c* index and the Gitelson-anthocyanin index were highly affected by canopy structure and soil background. In addition, Malenovsky et al. (2008) analyzed the effect of woody elements introduced into DART and performed a sensitivity analysis of two spectral vegetation indices, the *Normalized Difference Vegetation Index* (NDVI) and the *Angular Vegetation Index* (AVI). Despite the efforts made to analyze *Ca+b* -related vegetation indices, further research should focus on understanding structural effects on *Cx+c* -related vegetation indices at canopy level.

The aim of the present study was to assess the estimation of carotenoid content in a complex conifer forest using high spatial and spectral resolution imagery and 3D canopy modeling methods. A combined observation and modeling-based approach was applied to assess the influence of leaf and canopy parameters on various narrow-band vegetation indices proposed to estimate carotenoid content. The objectives of the analysis were the following: i) assess the influence of carotenoid and chlorophyll content on the indices proposed, ii) evaluate the performance of existing narrow-band carotenoid indices at both leaf and canopy scales, iii) evaluate the sensitivity of *Cx+c* -related vegetation indices to canopy structure, and iv) propose a new formulation for *Cx+c* estimation at canopy level, assessing its performance with high-resolution airborne imagery.

3.2. Materials and methods

3.2.1. Leaf measurements

Mean crown pigment and spectral measurements were obtained from a total of 5 young needles (one year-old needles) collected from the top of the crown. Analyses were performed on young needles to avoid non-representative outliers in current and mature needles. Needle pigment concentration was determined as reported by Abadía and Abadía (1993). Pigment extracts were obtained from a mixed sample of 5 cm of needle material, using 1 linear cm per needle. The area was calculated by assuming that the needle was a half cylinder and the diameter was the measured width of each needle. Needle diameter was measured with a digital caliper precision instrument. Five additional needle samples were used to take structural measurements (thickness and width) and determine water content and dry mass. The needles were ground in a mortar on ice with liquid nitrogen and diluted in acetone up to 5 ml (in the presence of Na ascorbate). After that, the extracts were filtered through a 0.45 μm filter to separate the pigment extracts from the Na ascorbate. Spectrophotometric and High-Performance Liquid Chromatography (HPLC) determinations were conducted simultaneously on the same extracts. A total of 20 μl were injected into the HPLC, and 1 ml was inserted into the spectrophotometer. The pigment extractions and HPLC measurements were undertaken concurrently to avoid pigment degradation. Absorption at 470, 644.8 and 661.6 nm was measured with the spectrophotometer to derive chlorophyll *a* and *b* and total carotenoid concentrations (Abadía and Abadía, 1993). Total chlorophyll and carotenoid concentration were related linearly with a mean average coefficient of determination value of 0.59 per plot. Pigment extracts were analyzed using an isocratic HPLC method (Larbi et al., 2004). Samples were injected into a 100×8 mm Waters Novapak C18 radial compression column (4 μm particle size) with a 20 μl loop, and mobile phases were

pumped by a Waters M45 high pressure pump at a flow of 1.7 ml/min. The EPS ratio between the pigment concentration was calculated as (V+0.5A)/(V+A+Z) (Thayer & Björkman, 1990), where V is violaxanthin, A is antheraxanthin and Z is zeaxanthin.

Needle spectral reflectance was also measured with a UniSpec Spectral Analysis System (PP Systems, Herts, UK), following a similar procedure to that described by Richardson and Berlyn (2002). The UniSpec measurements were conducted in the field minutes before the needles were collected. Bidirectional reflectance obtained from the field was used to evaluate the relationships between hyperspectral indices and pigment content.

3.2.2. Airborne campaigns

An unmanned aerial vehicle (UAV) platform for remote sensing research was developed at the Laboratory for Research Methods in Quantitative Remote Sensing (QuantaLab, IAS-CSIC, Spain) to carry a payload with narrow-band multispectral imaging sensors (Berni et al., 2009; Zarco-Tejada et al., 2009). The UAV was a 2-m fixed-wing platform capable of carrying a 3.5 kg payload. It had 1 hour endurance and 5.8 kg take-off weight (TOW) (mX-SIGHT, UAV Services and Systems, Germany). The UAV was controlled by an autopilot for autonomous flight (AP04, UAV Navigation, Madrid, Spain) to follow a flight plan using waypoints. The autopilot consisted of a dual CPU that controlled an integrated Attitude Heading Reference System (AHRS) based on a L1 GPS board, 3-axis accelerometers, yaw rate gyros and a 3-axis magnetometer (Berni et al., 2009). Communication with the ground was conducted through a radio link where position, attitude and status data were transmitted at 20 Hz frequency;

this also acted as a communication link for operating remote sensing multispectral cameras on board the UAV.

The multispectral sensor used in this study was a 6-band multispectral camera (MCA-6, Tetracam, Inc., California, USA). The camera consisted of 6 independent image sensors and optics with user-configurable spectral filters. The image had a resolution of 1280×1024 pixels with 10-bit radiometric resolution and an optical focal length of 8.5 mm, yielding an angular FOV of 42.8°×34.7° and 15 cm pixel spatial resolution at 150 m flight altitude. The detector used was a CMOS sensor with ~5.2 μm pixel size and 6.66 mm×5.32 mm image area operated in a progressive scan mode at 54 dB signal-to-noise ratio, with 0.03% fixed pattern noise, 28 mV/s dark current and 60 dB dynamic range. Different bandsets were selected depending on the objectives of the remote sensing study, including 25 mm diameter bandpass filters of 10 nm FWHM (Andover Corporation, NH, USA), with center wavelengths at 515 nm, 530 nm, 570 nm, 670 nm, 700 nm, 800 nm bands. The 10 nm filter measurements yielded ca. 60% transmission and 10.4 nm FWHM.

Multispectral imagery was radiometrically calibrated using coefficients derived from measurements taken with a calibrated uniform light source (integrating sphere, CSTM-USS-2000C Uniform Source System, LabSphere, NH, USA) at four different levels of illumination and six different integration times. Radiance values were later converted to reflectance using the total incoming irradiance simulated with the SMARTS model developed by the National Renewable Energy Laboratory of the US Department of Energy (Gueymard, 1995, 2001) using aerosol optical depth measured with a

Micro-Tops II sun photometer (Solar LIGHT Co., Philadelphia, PA, USA) collected in the study areas at the time of the flights. SMARTS computes clear sky spectral irradiance, including direct beam, circumsolar, hemispherical diffuse and total irradiance on a tilted or horizontal plane in specific atmospheric conditions. This radiative transfer model has previously been used in other studies to perform the atmospheric correction of narrow-band multispectral imagery. Some examples are the studies of Zarco-Tejada et al. (2012) and Suárez et al. (2010). The calibrated multispectral reflectance imagery obtained at 10 nm FWHM is shown in Fig. 3.1b, targeting pure components such as crowns, shaded and sunlit soil spectra (Fig. 3.1b). Each individual pure tree crown in the entire forest canopy was identified using automatic object-based crown-detection algorithms (Ardila et al., 2012; Kurtz et al., 2012) based on the Normalized Difference Vegetation Index (NDVI) calculated from the high spatial resolution image. This made it possible to extract the mean crown reflectance.

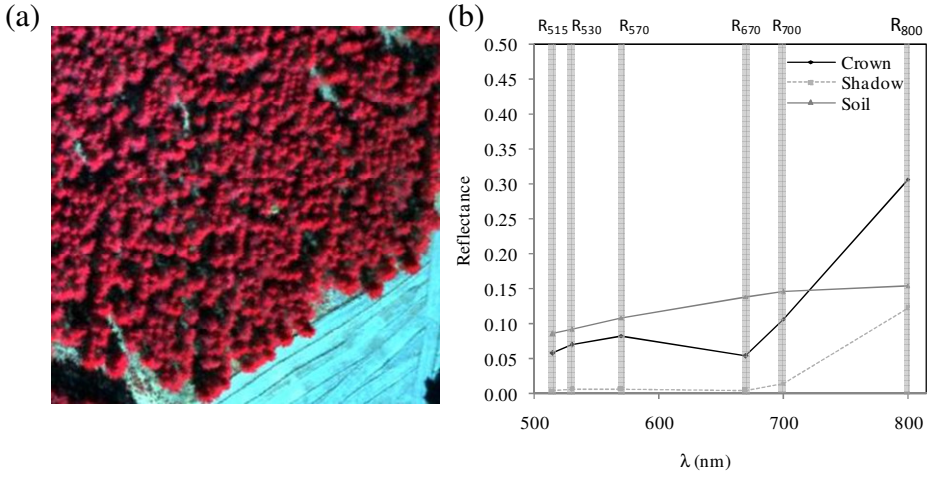

Figure 3.1. (a) Example of imagery acquired with the high resolution narrow-band airborne multispectral camera on board the UAV platform; (b) spectral reflectance extracted from the imagery for pure tree crown, shadow and soil pixels.

Field sampling campaigns were conducted concurrently with unmanned aerial vehicle overflights in the last week of August 2009. The flight campaigns were performed at 10 a.m. (GMT). A total of 35 individuals of *Pinus sylvestris* were subjected to field and airborne monitoring (Fig. 3.1). The measurements were taken on trees of a similar age (~40 years old) and height (~10 m) growing in low slope areas (<10%) and therefore with a similar sun/shade fraction.

3.2.3. Optical indices for Cx+c *estimation*

The purpose of this analysis was to evaluate the performance of a set of hyperspectral vegetation indices in carotenoid content estimation. The performance of each vegetation index was evaluated based on simulation analysis and field measurements. At the leaf level, vegetation indices calculated from directional hemispherical reflectance simulations were compared to the results obtained from field bidirectional measurements. At the canopy level, vegetation indices based on hemispherical reflectance simulations were compared to results obtained from the image reflectance acquired with a narrow-band multispectral camera after this. A detailed summary of the narrow-band vegetation indices applied in this study is shown in Table 3.1. The narrow-band vegetation indices selected from previous studies for *Cx+c* estimation were combinations of bands located in the visible and visible/NIR region. The Photochemical Reflectance Index (PRI) has been widely used to assess changes in carotenoid pigments (e.g. xanthophyll pigments). The PRI was initially formulated by Gamon et al. (1992). It was calculated with the 570 nm band as a reference (PRI_{570}) and later with the 515 nm band as a reference (PRI_{515}) and has been found to minimize structural effects (Hernández-Clemente et al., 2011). Similar

wavelengths have been selected by Gitelson et al. (2003, 2006) to formulate the Carotenoid Content Index (CRI_{550}). Other indices have been formulated as a combination of bands around $R_{510-515}$ and $R_{700-770}$. A few examples are CRI_{700}, RNIR*CRI_{550} and RNIR*CRI_{700}, proposed by Gitelson et al. (2003, 2006); the Ratio Analysis of Reflectance Spectra, proposed by Chappelle et al. (1992) as RARS; the Carotenoid/Chlorophyll Ratio Index (PRI*CI), analyzed by Garrity et al. (2011); the Reflectance Band Ratio Index (RBRI), proposed by Datt (1998) and the Plant Senescence Reflectance Index (PSRI), proposed by Merzlyak et al., (1999). The last group of *Cx+c* -related optical indices found are combinations of visible bands with the bands R_{800} or R_{860}. Some examples are the Pigment-Specific Simple Ratio (PSSRa, PSSRb, PSSRc, PSNDc), analyzed by Blackburn (1998), and the $RBRI_{NIR}$, analyzed by Datt (1998).

New narrow-band ratio indices in the 500-600 nm regions were also assessed at both leaf and crown levels for sensitivity to *Cx+c*. Narrow-band ratio indices were formulated based on related to the absorption of Cx+c concentration (the blue region from 450-555 nm) divided by the immediately continuous bands located in the green region (560 and 570 nm reference bands).

Table 3.1. Hyperspectral vegetation and physiological indices proposed in other studies

Index	Index_ID	Formula	Reference	Scale
Leaf area Index				
Normalized Difference Vegetation Index	**NDVI**	$(R_{800}-R_{670})/(R_{800}+R_{670})$	Rouse et al., 1973	Leaf/Canopy
Chlorophyll estimation				
Structure insensitive pigment index	**SIPI**	$(R_{800}-R_{445})/(R_{800}+R_{680})$	Peñuelas et al. 1995 Gitelson and Merzlyak, 1996; Zarco-Tejada et al. 2004	Leaf Leaf/Canopy
Chlorophyll index Red Edge	$CI_{red\ edge}$	R_{750}/R_{710}		
Transformed Cab absorrption in reflectance index	**TCARI**	$3*[(R_{700}-R_{670})-0.2*(R_{700}-R_{550})*(R_{700}/R_{670})$	Haboudane at al., 2002; Meggio et al., 2010	Leaf/Canopy
Optimized soil-adjusted vegetation index	**OSAVI**	$(1+0.16)*(R_{800}-R_{670})/(R_{800}+R_{670}+0.16)$	Rondeaux et al., 1996; Meggio et al., 2010	Leaf/Canopy
	TCARI/OSAVI	$3*[(R_{700}-R_{670})-0.2*(R_{700}-R_{550})*(R_{700}/R_{670})/(1.16*(R_{800}-R_{670})/(R_{800}+R_{670}+0.16))$	Haboudane at al., 2002; Meggio et al., 2010	Leaf/Canopy
Carotenoid concentration				
Ratio Analysis of Reflectance Spectra	**RARS**	R_{746}/R_{513}	Chappelle et al. 1992	Leaf
Pigment-specific simple ratio	**PSSRa**	R_{800}/R_{680}	Blackburn (1998)	Leaf/Canopy
Pigment-specific simple ratio	**PSSRb**	R_{800}/R_{635}	Blackburn (1998)	Leaf/Canopy
Pigment-specific simple ratio	**PSSRc**	R_{800}/R_{470}	Blackburn (1998)	Leaf/Canopy
Pigment-specific normalized difference	**PSNDc**	$(R_{800}-R_{470})/(R_{800}+R_{470})$	Blackburn (1998)	Leaf/Canopy
Carotenoid Concentration Index	$\mathbf{CRI_{550}}$	$(1/R_{515})-(1/R_{550})$	Gitelson et al. (2003, 2006)	Leaf
Carotenoid Concentration Index	$\mathbf{CRI_{700}}$	$(1/R_{515})-(1/R_{700})$	Gitelson et al. (2003, 2006)	Leaf
Carotenoid Concentration Index	$\mathbf{R_{NIR}*CRI_{550}}$	$(1/R_{510})-(1/R_{550})*R_{770}$	Gitelson et al. (2003, 2006)	Leaf
Carotenoid Concentration Index	$\mathbf{R_{NIR}*CRI_{700}}$	$(1/R_{510})-(1/R_{700})*R_{770}$	Gitelson et al. (2003, 2006)	Leaf
Modified Photochemical Reflectance Index	$\mathbf{PRI_{m1}}$	$(R_{515}-R_{530})/(R_{515}+R_{530})$	Hernández-Clemente et al., 2011	Leaf/Canopy
Photochemical Reflectance Index	**PRI**	$(R_{570}-R_{530})/(R_{570}+R_{530})$	Gamon et al., 1992	Leaf
Carotenoid/Chlorophyll Ratio Index	**PRI*CI**	$((R_{570}-R_{530})/(R_{570}+R_{530}))*((R_{760}/R_{700})-1)$	Garrity et al., 2011	Leaf
Plant senescencing reflectance Index	**PSRI**	$(R_{680}-R_{500})/R_{750}$	Merzlyak et al., 1999	Leaf
Reflectance Band Ratio Index	$\mathbf{Datt\text{-}CabCx+c}$ $\mathbf{Datt_{NIR}}$	$R_{672}/(R_{550}*3R_{708})$	Datt 1998	Leaf
Reflectance Band Ratio Index	**CabCx+c**	$R_{860}/(R_{550}*R_{708})$	Datt 1998	Leaf

3.2.4. Simulations with PROSPECT-5 and DART models

A model simulation analysis was conducted to assess the sensitivity of the carotenoid-related optical indices on heterogeneous coniferous forest canopy images and to test the performance of new formulations. Radiative transfer modeling methods were applied with the *leaf optical PROperties SPECTra* (PROSPECT-5) model (Féret et al., 2008; Jacquemoud & Baret, 1990) coupled with the 3-dimensional *Discrete Anisotropic Radiative Transfer* (DART) model.

PROSPECT-5 was selected for the leaf-level simulations. This model simulates leaf directional-hemispherical reflectance and transmittance from the 400 to the 2500 nm spectral region with five input variables: *Ca+b, Cx+c*, leaf *dry* matter content (*Cm*), equivalent *water* thickness (*Cw*) and leaf structure parameter (*N*) (Féret et al., 2008). Although the PROSPECT model was originally developed for broad leaves, it has been validated and is widely used for needles (Malenovsky et al., 2007; Moorthy et al., 2008; Zarco-Tejada et al., 2004). Leaf-level simulations with PROSPECT-5 were performed to assess the effect of *Cx+c* and *Ca+b* concentration variations on the spectral signature in the 400-800 nm region and on the optical indices proposed, both at leaf and canopy levels when coupled with the DART model. Nominal values and input parameter ranges used for the leaf modeling are summarized in Table 3.2. Fixed values for Cw, Cm and N and the variation range for Cx+c and Ca+b were set based on previous studies carried out on conifer species (Hernández-Clemente et al., 2010; Moorthy et al., 2008). Fig. 3.2 shows an example of the spectral variation derived from the simulations performed had a range of 2-16 µg cm^{-2} for *Cx+c* and a mean *Ca+b* value of 10, 30 and 50 µg cm^{-2} (Fig. 3.2 a, b, c). Additional

simulations showed *Ca+b* variation, ranging from 10 to 60 µg cm^{-2} along with *Cx+c* values of 6, 8 and 14 µg cm^{-2} (Fig. 3.2 d, e, f).

Table 3.2. Nominal values range of parameters used for leaf modeling with PROSPECT-5.

Prospect-5 input variables	*Value*	*Unit*
Ca+b (varied parameter)	10-60	µ g cm^{-2}
Cx+c (varied parameter)	2-16	µ g cm^{-2}
Cw	0.03	cm
Cm	0.01	g cm^{-2}
N	2	

At crown level, DART was chosen because it simulates the radiative transfer reflectance of complex structures. This model was used in this study to generate coniferous canopy architectures at high spatial resolution. DART was developed by Gastellu-Etchegorry et al. (1996) on the basis of the discrete ordinate method (DOM). DART has been used to simulate heterogeneous coniferous forest canopies (Malenovsky et al., 2008) and has been validated for this use (Pinty et al., 2001; Widlowski et al., 2007). In order to simulate the forest canopy architecture of the study sites, the DART model was parameterized based on detailed field measurements.

The coupled PROSPECT and DART models were used to simulate the spectral reflectance of *Pinus sylvestris* forest stands assuming random variations of *Ca+b* and *Cx+c* content under two different scenarios: i) considering a random variation in LAI (Leaf Area Index) (1-10$m^{-2}m^{-2}$); ii) considering variations in both LAI (1-10) and tree density (800-1600trees per ha^{-1}). In both cases, PROSPECT simulations were based on random *Cx+c* (2-16 µg cm^{-2}) and *Ca+b* (10-60 µg cm^{-2}) values. Nominal values and the parameter range used for crown modeling are summarized in Table 3.3.

Table 3.3. Nominal values range of parameters used for canopy modeling with *DART*

DART input variables	*Value*	*Unit*
Central wavelength	400-800	nm
Spectral bandwidth	10	nm
Scene parameters	*Value*	*Unit*
Cell size	0.5	m
Scene dimensions	50 x 50	m
Spatial distribution	Random	
Canopy parameters		
Number of trees	1200 trees/ha	
Probability of presence	0.8	
Leaf area index (varied parameter)	1-10	
Crown shape	Truncated cone	
Crown height (mean)	6	m
Crown height (std dev)	0.9	m
Height below crown (mean)	4	m
Height below crown (std dev)	0.8	m
Diameter below crown (mean)	0.4	m
Diameter below crown (std dev)	0.1	m
Height within the tree crown	5	m
Diameter within the tree crown	0.35	m

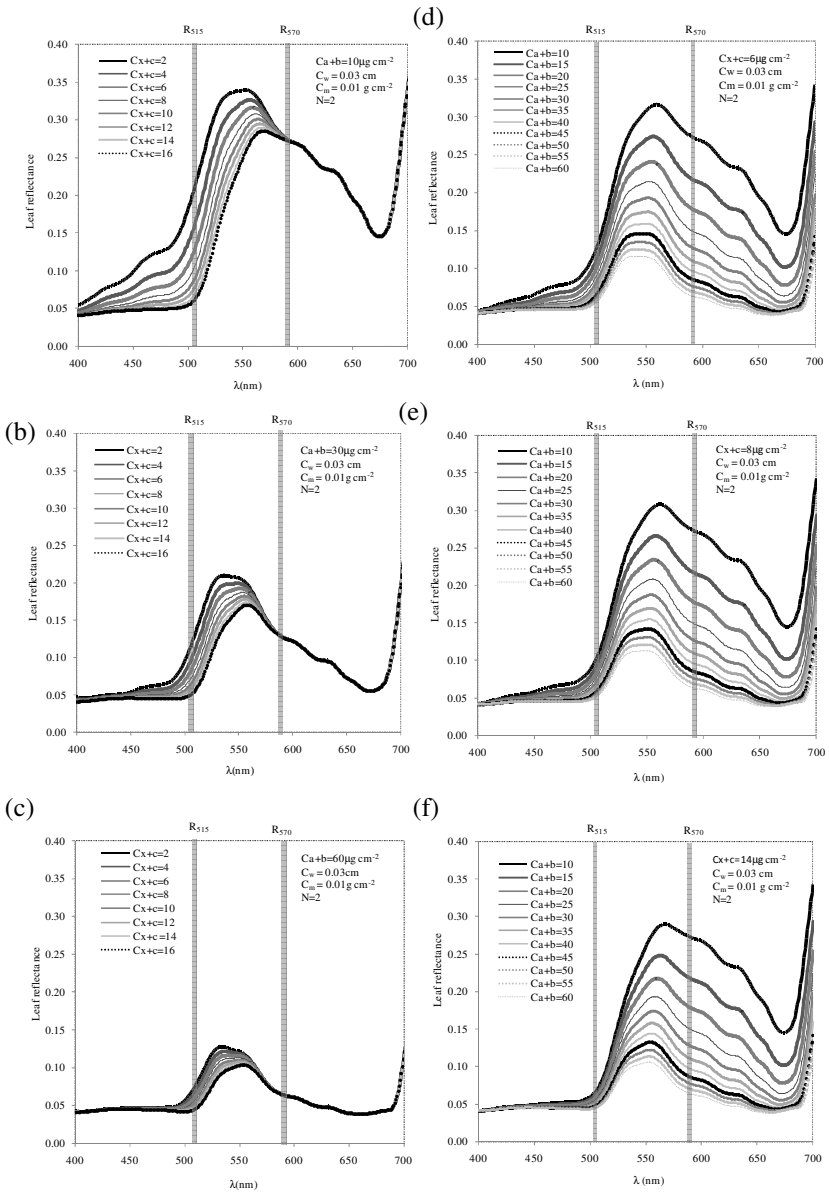

Figure 3.2. Leaf-level modeling simulations conducted with the PROSPECT-5 model to assess the effects of *Cx+c* and *Ca+b* content on the spectral signature in the 400-700 nm spectral range. Simulations performed for *Cx+c* variation between 2 and 16 µg cm^{-2} for mean *Ca+b* values of 10, 30 and 60 µg cm^{-2} (a,b,c). Simulations conducted for *Ca+b* variation between 10 and 60 µg cm^{-2} for mean *Cx+c* values of 6, 8 and 14 µg cm^{-2} (d,e,f).

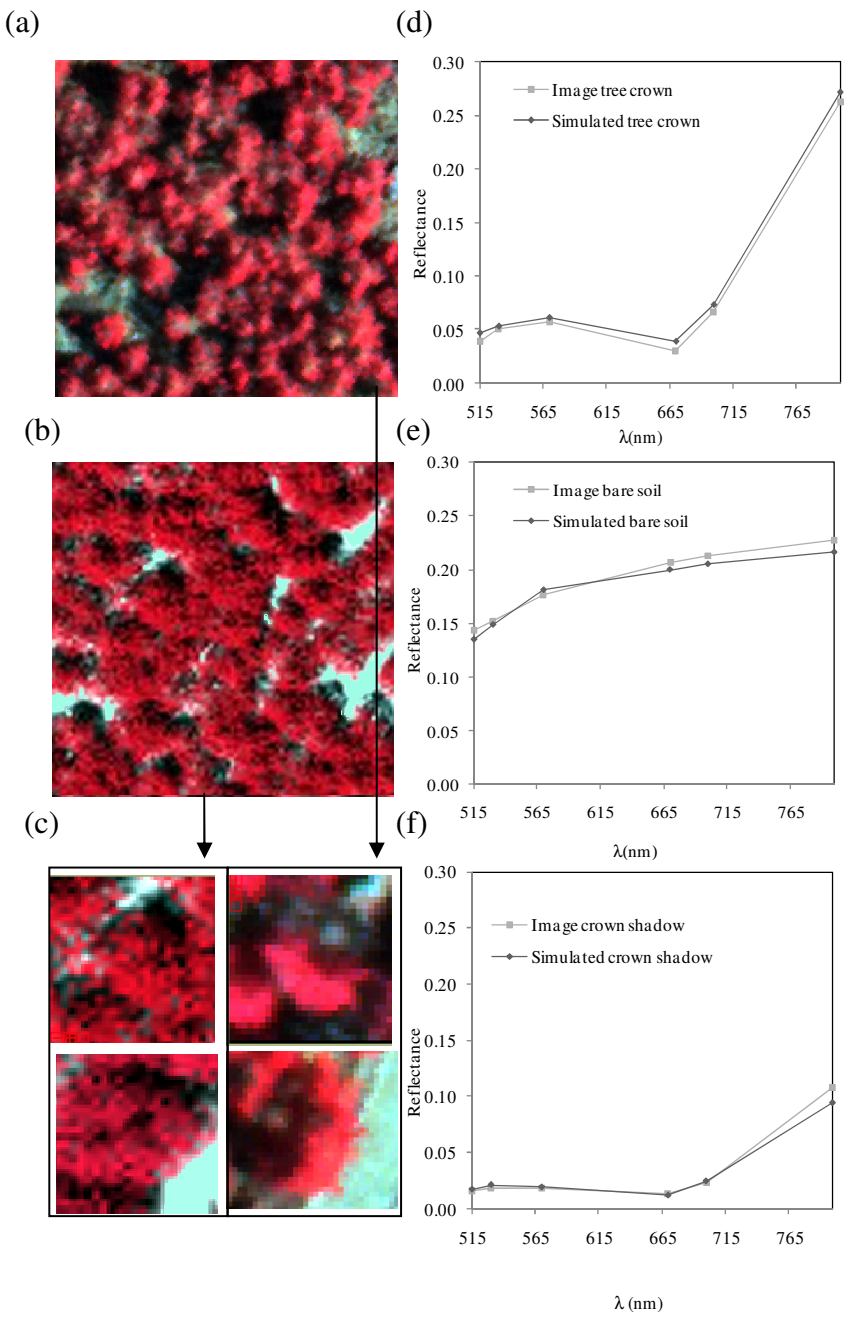

Figure 3.3. High-resolution multispectral image acquired from the UAV platform (a) and the PROSPECT-5+DART simulated image for the same study site (b); zoomed-in image detail of the multispectral image (right) and the simulated image (left) (c); tree crown (d), bare soil (e) and shaded crown (f) spectral reflectance extracted from the multispectral image and the simulated scenes.

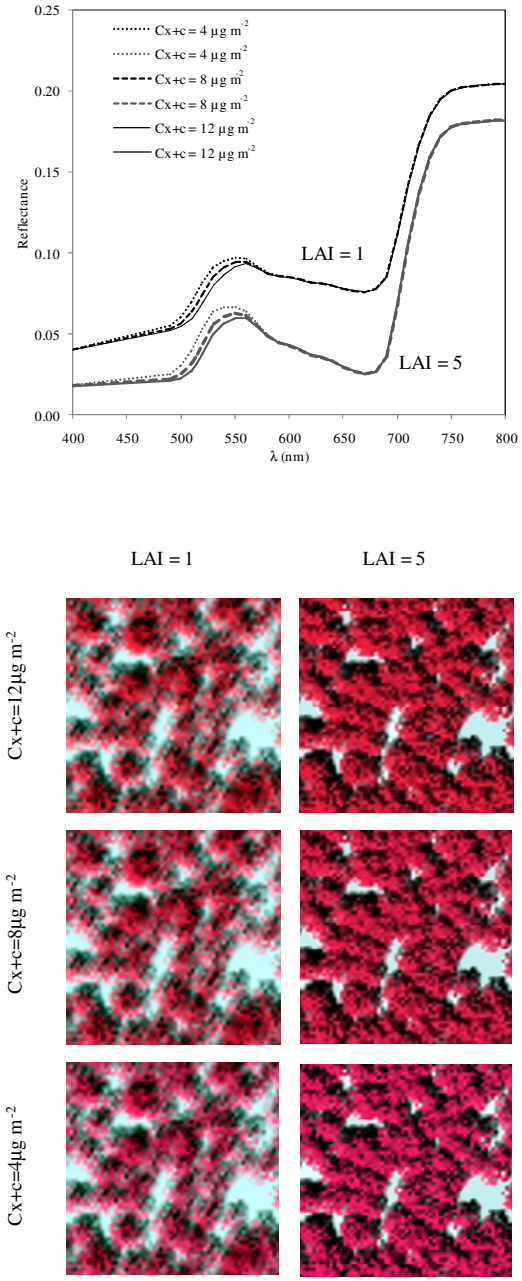

Figure 3.4. Canopy reflectance simulated with PROSPECT-5+DART models considering low LAI (LAI=1) and high LAI values (LAI=5) for different concentrations of *Cx+c* (4, 8 and 12 µg cm^{-2}) and a mean *Ca+b* value of 35 µg cm^{-2}.

Canopy level simulations were performed using the hemispherical reflectance simulated at the leaf level with PROSPECT. An example of the canopy reflectance simulated with PROSPECT coupled with DART is shown in Fig. 3.3. Fig. 3.4 shows the crown reflectance of trees with low (LAI=1) and high (LAI=5) LAI values simulated with DART based on leaf reflectance and transmittance. Leaf reflectance and transmittance were simulated with PROSPECT-5 considering different values of carotenoid content (4, 8 and 12 μg m^{-2}) and a mean value of chlorophyll content (35 μg m^{-2}).

3.3. Results

3.3.1. Leaf-level simulation results

Simulations conducted with the PROSPECT-5 model assessed the sensitivity of the various vegetation indices to different values of *Ca+b* and *Cx+c* content. The simulations showed that chlorophylls a and b have strong absorbance peaks in the blue and red regions of the spectrum (from 500 to 700 nm) (Fig. 3.2 d, e, f). Carotenoid absorbance mainly affected the 450 to 555 nm region (Fig. 3.2 a, b, c), overlapping chlorophyll absorption peaks from 500 to 555 nm. The vegetation indices proposed were formulated as a simple ratio between bands located in the carotenoid and chlorophyll absorbance spectral range (Fig 3.2).

Coefficients of determination (r^2) of all the indices studied are provided in Fig. 3.5, which shows the relationships found between simulated hyperspectral vegetation indices and pigment content. Most of the *Cx+c* -related vegetation indices tested at leaf level showed good agreement with *Cx+c* content. The best relationships were obtained when the CRI_{550} and CRI_{700} indices were used. The linear relationship between such CRI indices

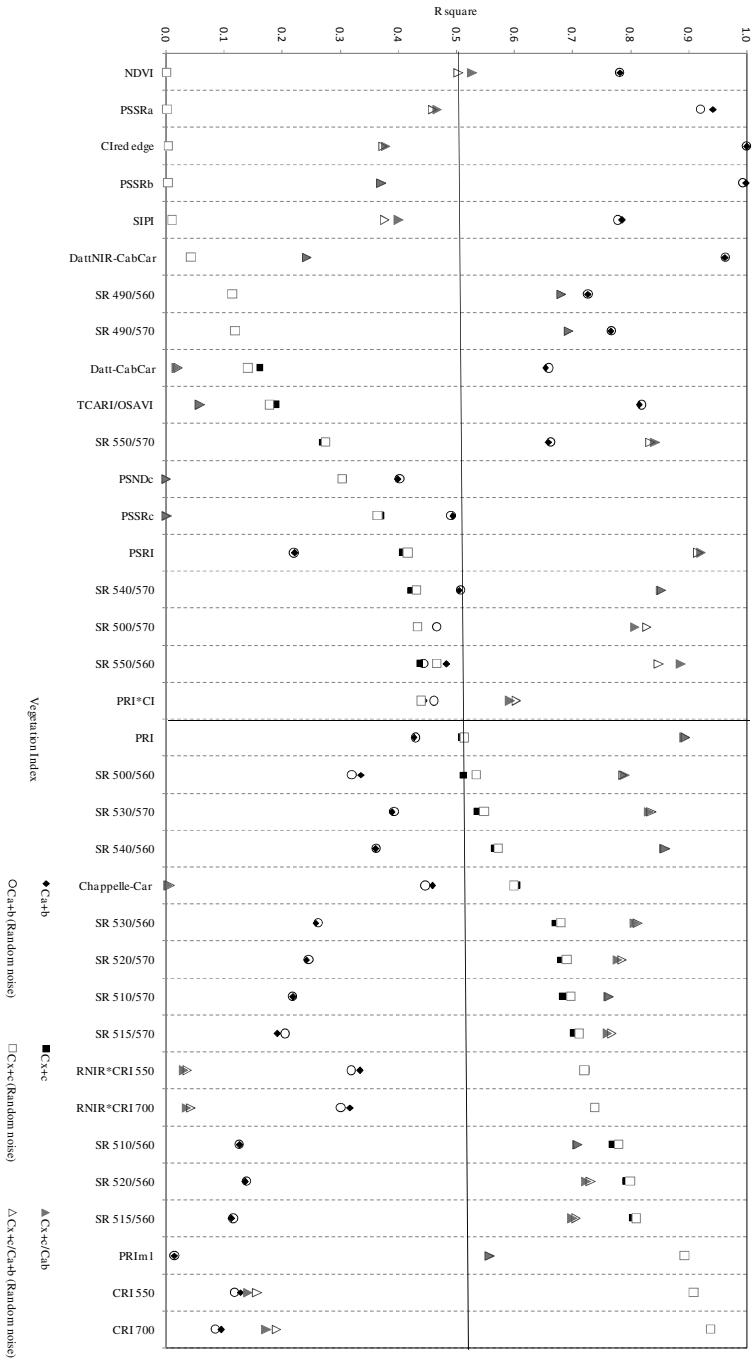

Figure 3.5. Relationships obtained between *Ca+b, Cx+c* content and the *Ca+b/Cx+c* ratio when compared with vegetation indices proposed for *Cx+c* estimation. Data were simulated at leaf level with PROSPECT-5 model assuming random *Cx+c* (2-16 µg cm^{-2}) and *Ca+b* content (10-60 µg cm^{-2}).

and *Cx+c* was significant (P<0.001), with a coefficient of determination of r^2> 0.9. By contrast, the relationship between these CRI indices and *Ca+b* had a coefficient of determination of less than 0.15. These results showed the sensitivity of CRI indices to *Cx+c* content and their low sensitivity to chlorophyll content at leaf level. Other indices such as RNIR·CRI_{550} and RNIR·CRI_{700} were found to be highly correlated with *Cx+c,* with a coefficient of determination of r^2=0.72 and r^2=0.74 respectively, but were more influenced by *Ca+b* (r^2 >0.3) (Fig. 3.5). In the leaf-level simulations a 1% Gaussian random noise was added to the leaf simulations (Fig. 3.5). This step aimed at assessing noise-sensitive indices as shown in le Maire et al. (2004). According to the results obtained with and without the Gaussian noise (Fig. 3.5), the simulated spectral vegetation indices showed similar sensitivity to Ca+b, Cx+c and to the Ca+b/Cx+c ratio.

The comparative analysis performed by testing a large number of *Cx+c* indices identified a new group of indices that were significantly related to *Cx+c* (P<0.001) but showed low sensitivity to *Ca+b* content (r^2 < 0.15). This was the case of PRI_{m1}, with a coefficient of determination of r^2=0.86 and the following ratio indices: R_{515}/R_{560} (r^2=0.80), R_{520}/R_{560} (r^2=0.79), R_{510}/R_{560} (r^2=0.77), R_{515}/R_{570} (r^2=0.71), R_{510}/R_{570} (r^2=0.69), R_{520}/R_{570} (r^2=0.68) and R_{530}/R_{570} (r^2=0.54).

The relationship between the indices SR_{560} (R_{510}, R_{515}, R_{520} and R_{530} over R_{560}) and SR_{570} (R_{510}, R_{515}, R_{520} and R_{530} over R_{570}) and *Cx+c* is presented in Fig. 3.6, which shows the behavior of the new ratio indices proposed in this study. These indices showed similar trends and coefficients of determination to *Cx+c* content, with the best relationships observed for

R_{515}/R_{570} (r^2=0.72) (Fig. 3.6a) and R_{515}/R_{560} (r^2=0.80) (Fig. 3.6b). Other *Cx+c* -related vegetation indices showed significant relationships (P<0.001) with *Cx+c* content (r^2>0.5), but were more affected by chlorophyll content (r^2>0.3). This was the case of the indices PRI and RARS, as well as the simple ratios R_{500}/R_{560}, R_{530}/R_{570}, R_{540}/R_{560}.

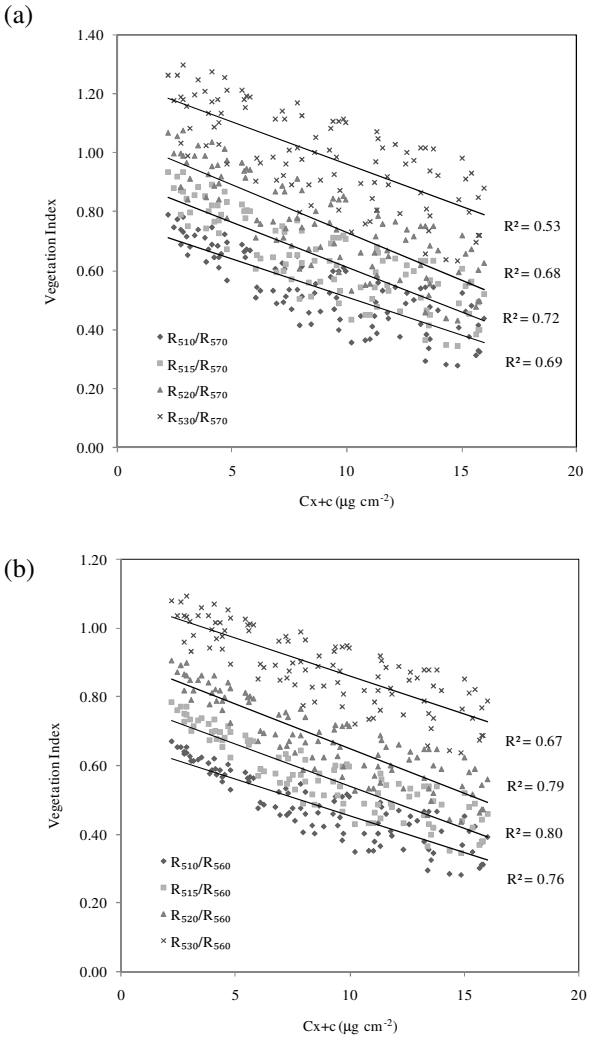

Figure 3.6. Relationships obtained between *Cx+c* content and the simple ratio vegetation indices $R_{510/570}$, $R_{515/570}$, $R_{520/570}$, and $R_{530/570}$ (a) and $R_{510/560}$, $R_{515/560}$, $R_{520/560}$, $R_{530/560}$ (b). Simulations conducted at leaf level with the PROSPECT-5 model considering random *Cx+c* (2-16 µg cm^{-2}) and *Ca+b* content (10-60 µg cm^{-2}).

In the case of Ca+b, the best relationships were obtained using the vegetation indices CIred edge and PSSRb, yielding a coefficient of determination higher than 0.98 (Fig.3.5). Despite using other indices such us PSSRa, DattNIR-CabCar or TCARI/OSAVI, relationships from (r^2=0.8) to (r^2=0.9) were found. In addition, the Cx+c/Ca+b ratio was found to be a variable highly related with a wide range of vegetation indices due to the sensitivity of such indices either to Cx+c or Ca+b concentration (Fig.3.5). The best relationship with Cx+c/Ca+b was found for indices such as PSRI and PRI, yielding a coefficient of determination around 0.9.

3.3.2. Canopy-level simulation results

Simulations conducted with DART at canopy level were used to assess the effect of the structure on the *Cx+c* indices when targeting pure crowns. Results of the modeling analysis showed that vegetation indices behaved differently at leaf and crown level (Fig. 3.7). These results show that the closest relationships between *Cx+c* content and vegetation indices at crown level were obtained by the indices R_{515}/R_{570} and R_{520}/R_{570}, yielding r^2 values of 0.70 and 0.71 respectively. Simple ratios formulated with bands from R_{510} to R_{540} and the reference bands R_{560} and R_{570} showed significant relationships ($P<0.001$) and coefficients of determination greater than 0.55 (Fig. 3.7). Other vegetation indices highly correlated with *Cx+c* content at leaf level showed high effects due to the structure and did not obtain high coefficients of determination at crown level. This was the case of CRI_{550} (r^2=0.44) and CRI_{700} (r^2=0.43). These results are in agreement with studies that have shown that leaf-level indices may not work well at canopy level due to the confounding effects of the structure on the indices. The vegetation indices proposed by Gitelson were formulated based on spectral bands simulated with 10 and 30 nm FWHM. This analysis was conducted to assess

the effect of considering different band width for the 510 - 520 nm and 540 - 560 nm ranges. The results shown in Fig. 3.8 demonstrate that comparable results were obtained for (10 and 30 nm FWHM).

A comparison of the relationships found in a selection of indices at both leaf and crown levels is provided in 3.9. While R_{515}/R_{570} showed similar agreement with $Cx+c$ at leaf and crown levels (r^2=0.7) (Fig. 3.9a and 3.9c), other indices such as CRI_{550} and CRI_{700} showed a high coefficient of determination at leaf level (r^2=0.9) (Fig. 3.9b) but poorer performance at crown level (r^2=0.44) (Fig. 3.9d). These results demonstrate the importance of accounting for canopy-level effects on the indices and assessing the performance at both leaf and canopy levels. These results can be explained by the different sensitivity of these indices to structural effects. As shown in Fig. 3.10, the coefficients of determination between the vegetation indices CRI_{550} and CRI_{700} and LAI values were r^2=0.48 and r^2=0.45 respectively (Fig. 3.10a and 3.10b). By contrast, the relationship between simple ratio indices such as R_{515}/R_{570} and R_{540}/R_{560} and LAI showed coefficients of determination of less than 0.05 (Fig. 3.10c and 3.10d). These simulation results demonstrate the low effects of LAI variation on the $Cx+c$ index proposed in this study (R_{515}/R_{570}), with coefficients of determination of r^2=0.72 for $Cx+c$ and r^2=0.19 for $Ca+b$ at leaf level and and r^2=0.71 for $Cx+c$ and r^2=0.16 for $Ca+b$ at canopy level. A more detailed analysis of the structural variation affecting $Cx+c$ -related indices was performed normalizing the values of vegetation indices to LAI=1.

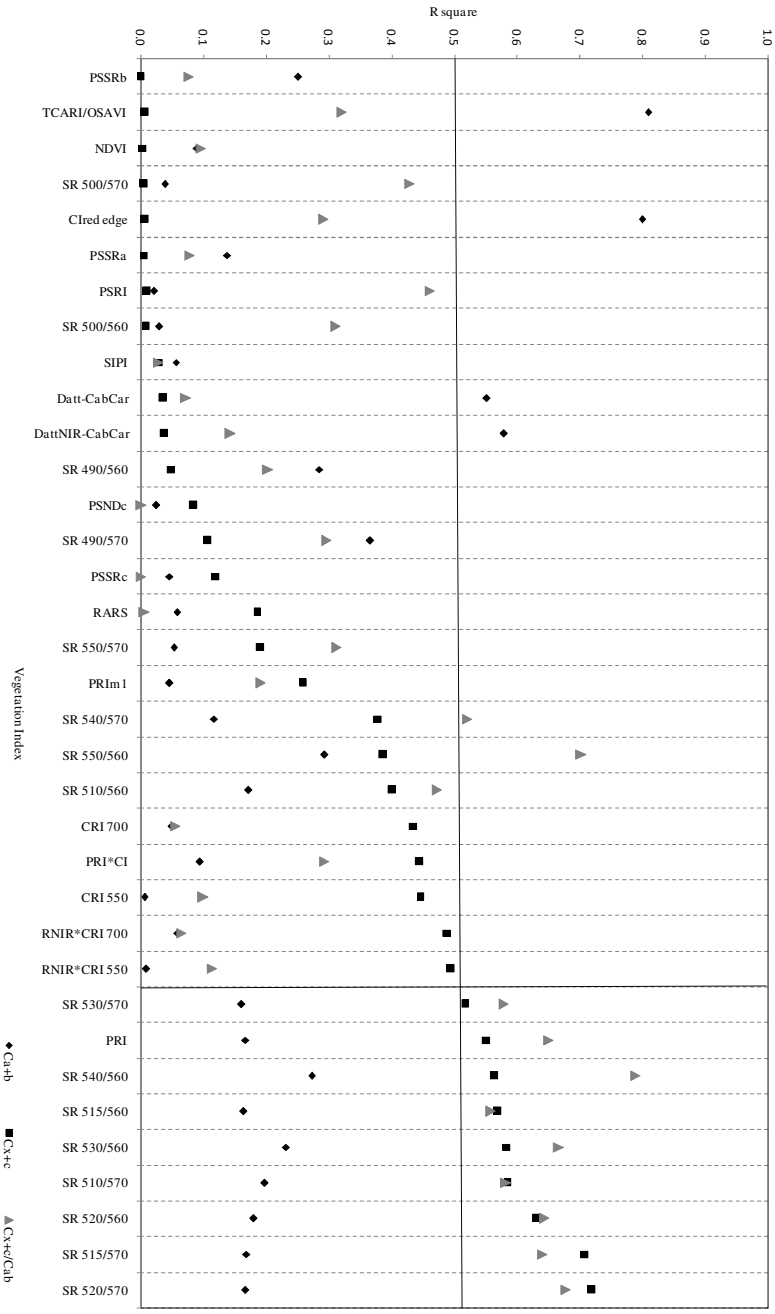

Figure 3.7. Relationships obtained between *Ca+b, Cx+c* content and the *Ca+b/Cx+c* ratio when compared with vegetation indices proposed for *Cx+c* estimation. Data were simulated at crown level with PROSPECT-5 model coupled with DART assuming random variation of leaf *Cx+c* (2-16 µg cm^{-2}) and *Ca+b* (10-60 µg cm^{-2}) and crown LAI ranging between 1 and 8.

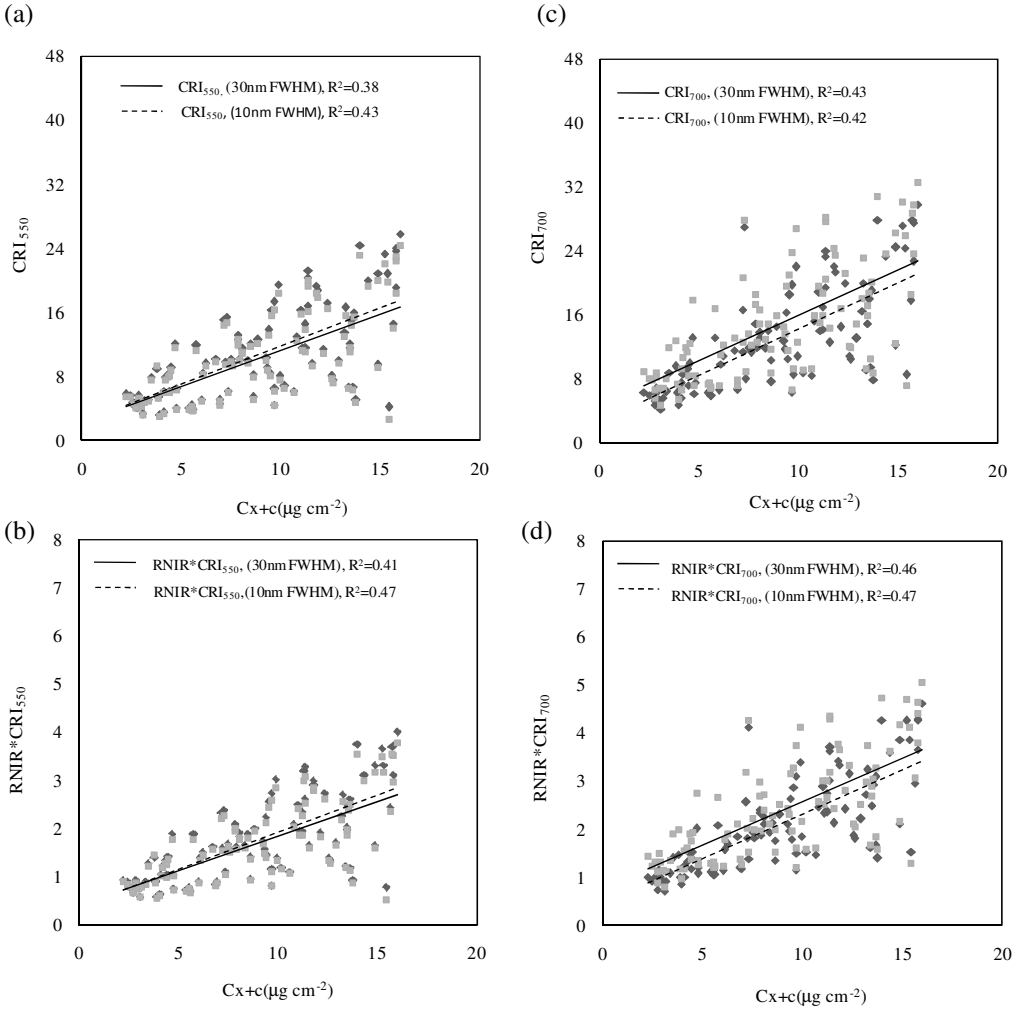

Figure 3.8. Relationships obtained between *Cx+c* and vegetation indices CRI_{550} (a), $RNIR*CRI_{550}$ (b). CRI_{700} (c) and $RNIR*CRI_{700}$ (d) formulated with 10 and 30 nm FWHM at crown level.

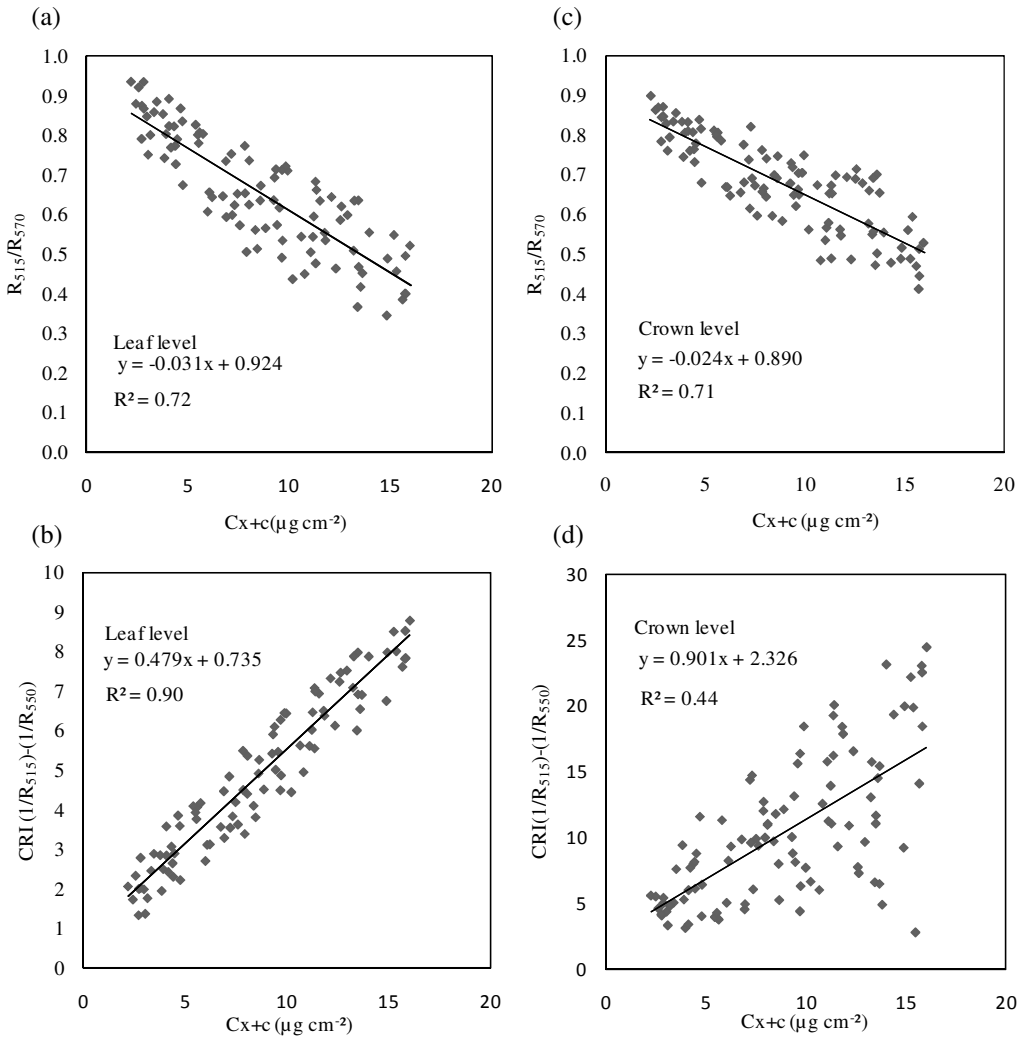

Figure 3.9. Relationships obtained between *Cx+c* and vegetation indices R_{515}/ R_{570} (a) and CRI $(1/R_{515})-(1/R_{550})$ (b) at leaf level and crown level (c) and (d). Simulations conducted considering random variation of leaf *Cx+c* (2-16 µg cm^{-2}) and *Ca+b* (10-60 µg cm^{-2}) for crown LAI ranging between 1 and 8.

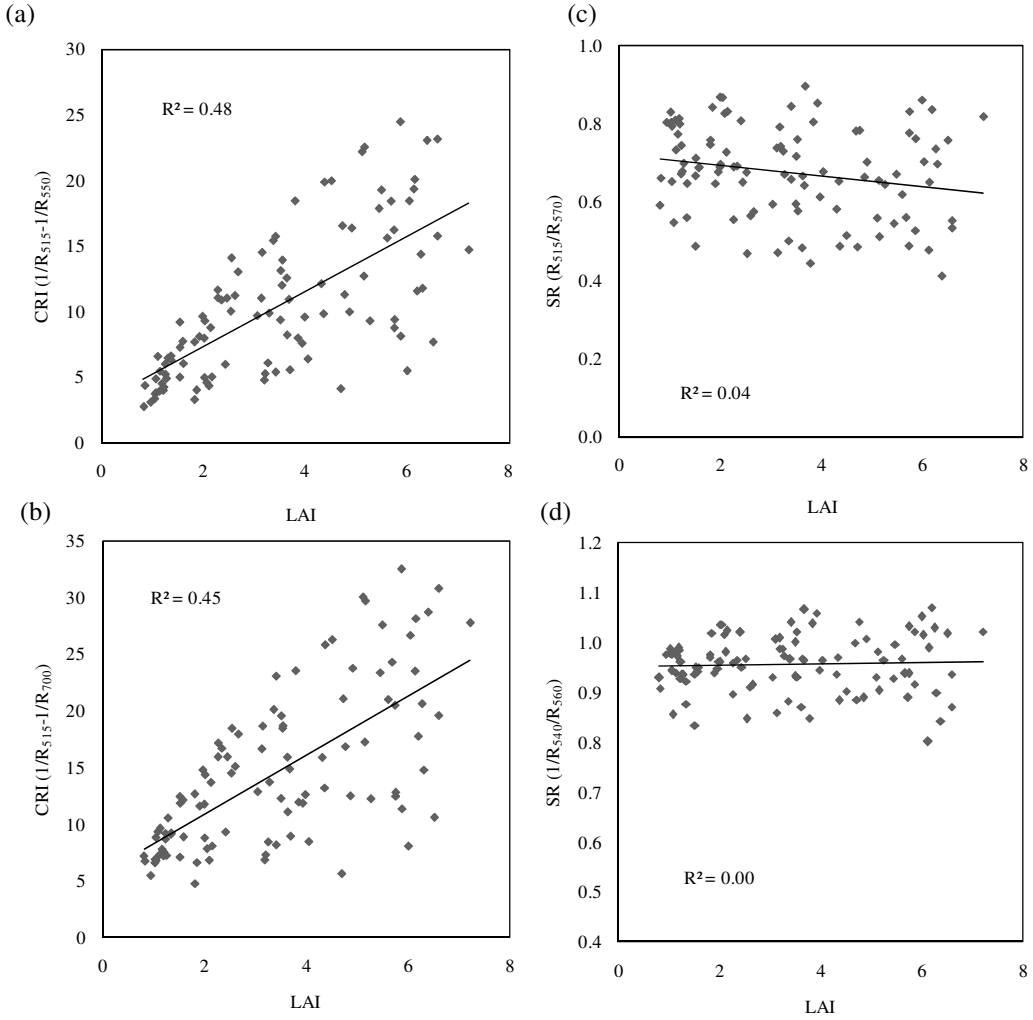

Figure 3.10. Crown-level simulations performed with PROSPECT-5 leaf model coupled with DART considering random leaf *Cx+c* (2-16 µg cm^{-2}) and *Ca+b* (10-60 µg cm^{-2}) values and LAI ranging between 1 and 8 to assess the effects of the canopy density variation on indices $(1/R_{515})$-$(1/R_{550})$ (a), $(1/R_{515})$-$(1/R_{700})$ (b), (R_{515}/R_{570}) (c) and (R_{520}/R_{570}) (d).

Fig. 3.11 shows the variations of CRI_{550} (Fig. 3.11a), RARS (Fig. 3.11b), R_{515}/R_{570} (Fig. 3.11c) and R_{540}/R_{560} (Fig. 3.11d), considering a range for LAI (1-10 m^2 m^{-2}) and tree density (800-2800 trees per ha^{-1}). While some vegetation indices such as R_{515}/R_{570} and R_{540}/R_{560} were not affected, the RARS and CRI_{550} indices showed higher sensitivity to LAI and tree density variation.

LAI variations also seem to affect the relationships between Cx+c-related vegetation indices and the Cx+c/Ca+b ratio. Indices with high coefficient of determination values (r^2=0.9) at leaf level such as PSRI or PRI yielded coefficients of determination of r^2=0.46 and r2=0.64 at crown level (Fig. 3.7).

3.3.3. Relationships between optical indices and Cx+c *obtained from leaf measurements and airborne imagery*

The analysis of the leaf measurements showed significant relationships between *Cx+c* indices and needle *Cx+c* content obtained by destructive sampling. The coefficients of determination calculated by the linear regression analysis are shown in Fig. 3.12. The experimental results agree with the results obtained with model simulations, in which indices such as CRI_{700} (r^2=0.73) or CRI_{550} (r^2=0.72) (Fig. 3.12 a and c) showed better results than the R_{515}/R_{570} index (r^2=0.57) at leaf level (Fig. 3.12 b). A further comparison between the R_{515}/R_{570} vegetation index and the *epoxidation state* (EPS) of the xanthophyll cycle yielded a coefficient of determination of r^2=0.12 (Fig. 3.12 d). These results demonstrate that SR (R_{515}/R_{570}) was correlated with *Cx+c* content but was not sensitive to variations in the xanthophyll cycle. The R_{515}/R_{570} index showed a weak relationship with *Ca+b* content, with a coefficient of determination of r^2=0.10 (Fig. 3.13a).

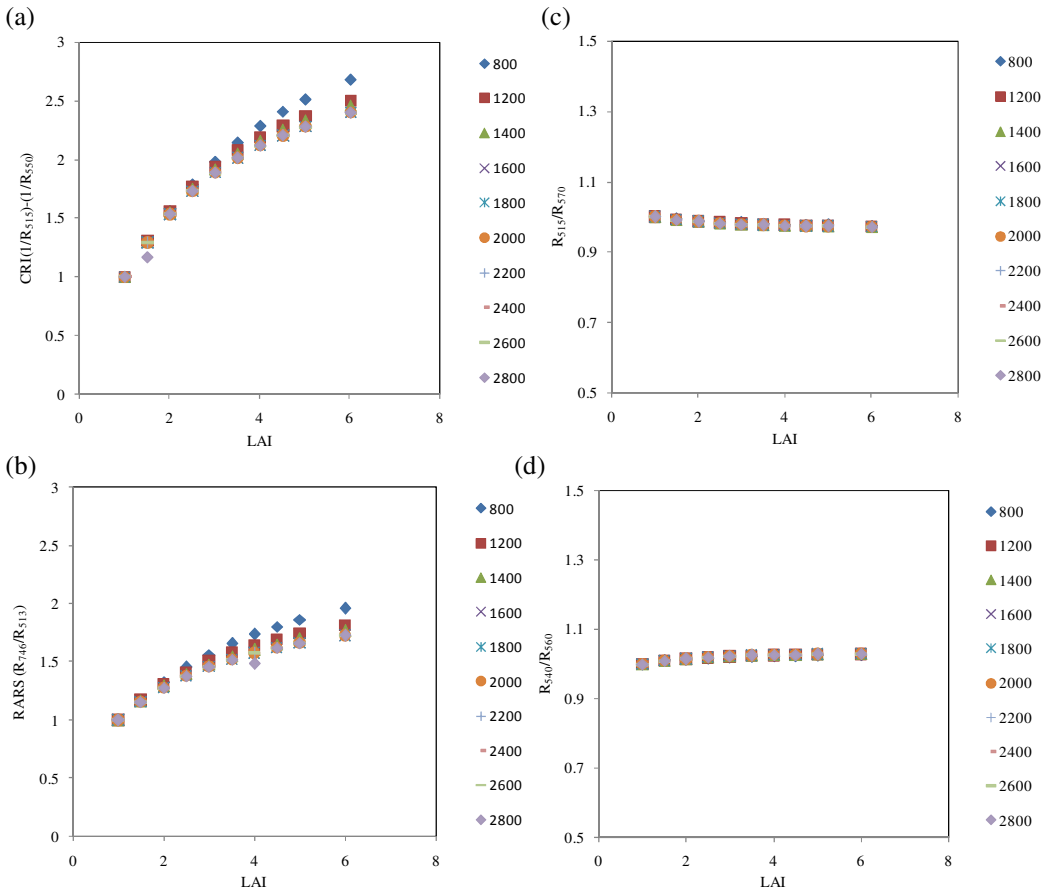

Figure 3.11. Canopy-level model simulations conducted with PROSPECT-5 coupled with DART to assess the effect of the *Cx+c* and *Ca+b* content variation on indices used for *Cx+c* estimation such as $(1/R_{515})-(1/R_{550})$ (a), (R_{746}/R_{513}) (b), (R_{515}/R_{570}) (c) and (R_{540}/R_{560}) (d). Simulations were performed for LAI ranging 1-6 and tree density variations from 800-2800 trees ha^{-1}. Values normalized to LAI=1.

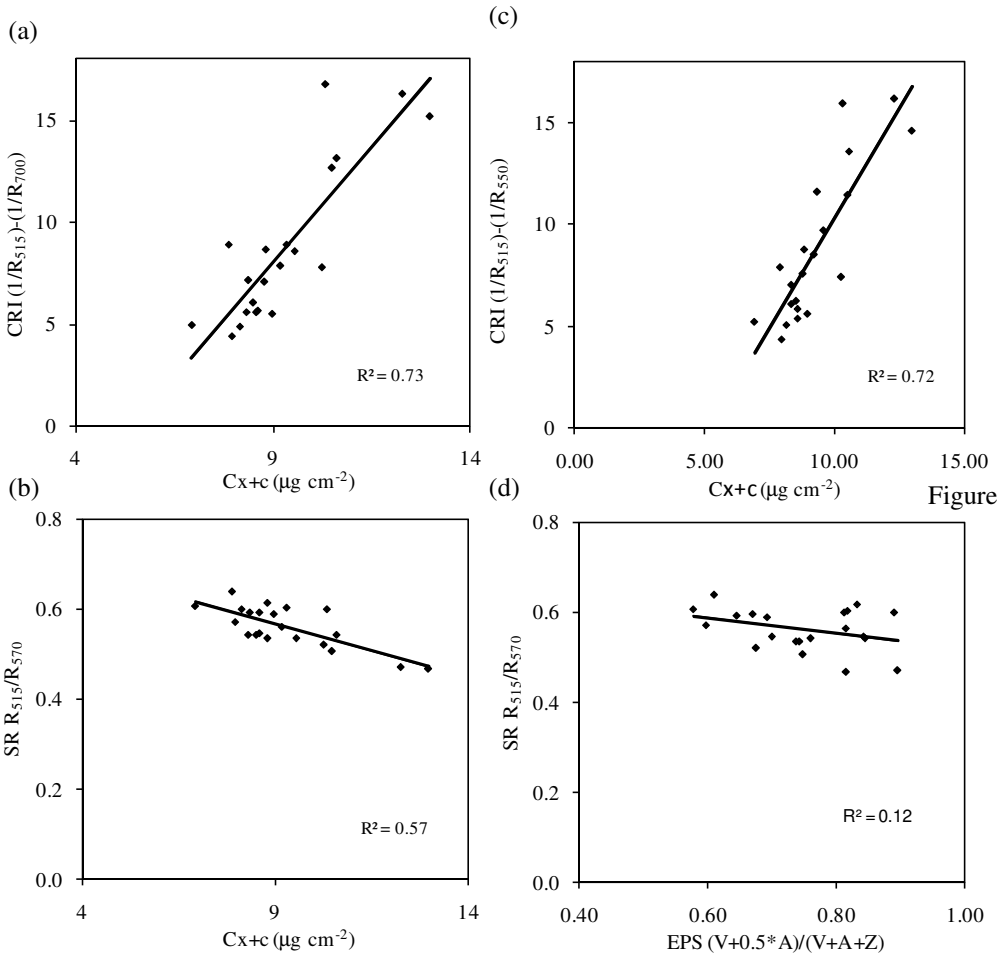

Figure

Figure 3.12. Relationships between *Cx+c* content and the following indices: Gitelson ($1/R_{515}$)-($1/R_{700}$) (a), simple ratio index (R_{515}/R_{570}) (b) and Gitelson ($1/R_{515}$)-($1/R_{550}$)(c). Relationships obtained between EPS and the simple ratio index (R_{515}/R_{570}) (d). Results obtained from leaf-level measurements.

This result agrees with the modeling results obtained with PROSPECT-5, where the relationship between R_{515}/R_{570} and *Ca+b* was lower than 0.15. As expected, the strongest relationships were found between *Ca+b* content and the red edge index R_{750}/R_{710} (Fig. 3.13 b).

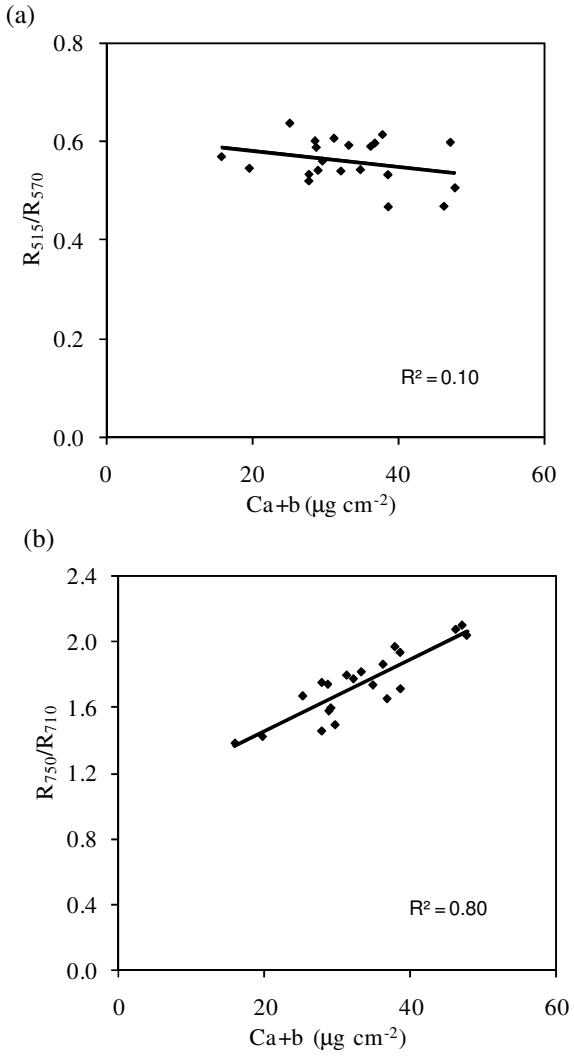

Figure 3.13. Relationships obtained between R_{515}/R_{570} (a) and R_{750}/R_{710} (b) when compared to *Ca+b* content. Results obtained from leaf-level measurements.

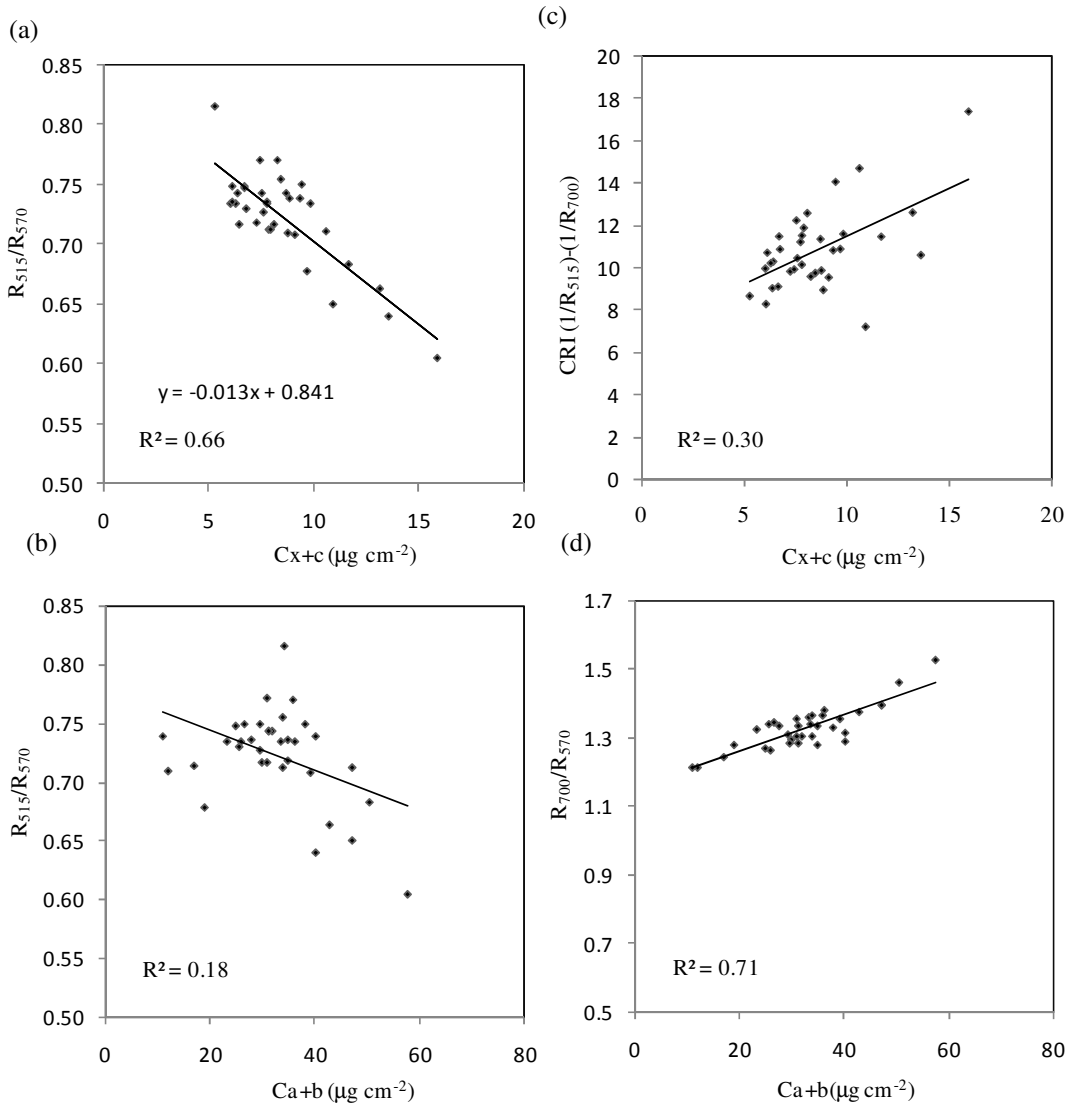

Figure 3.14. Relationships obtained between *Cx+c* (a;c) and *Ca+b* content (b;d) when compared to vegetation indices R_{515}/R_{570} (a;b), CRI_{700} (c) and R_{700}/R_{570} (d). Indices calculated at canopy level from the high-resolution multispectral camera on board the UAV platform.

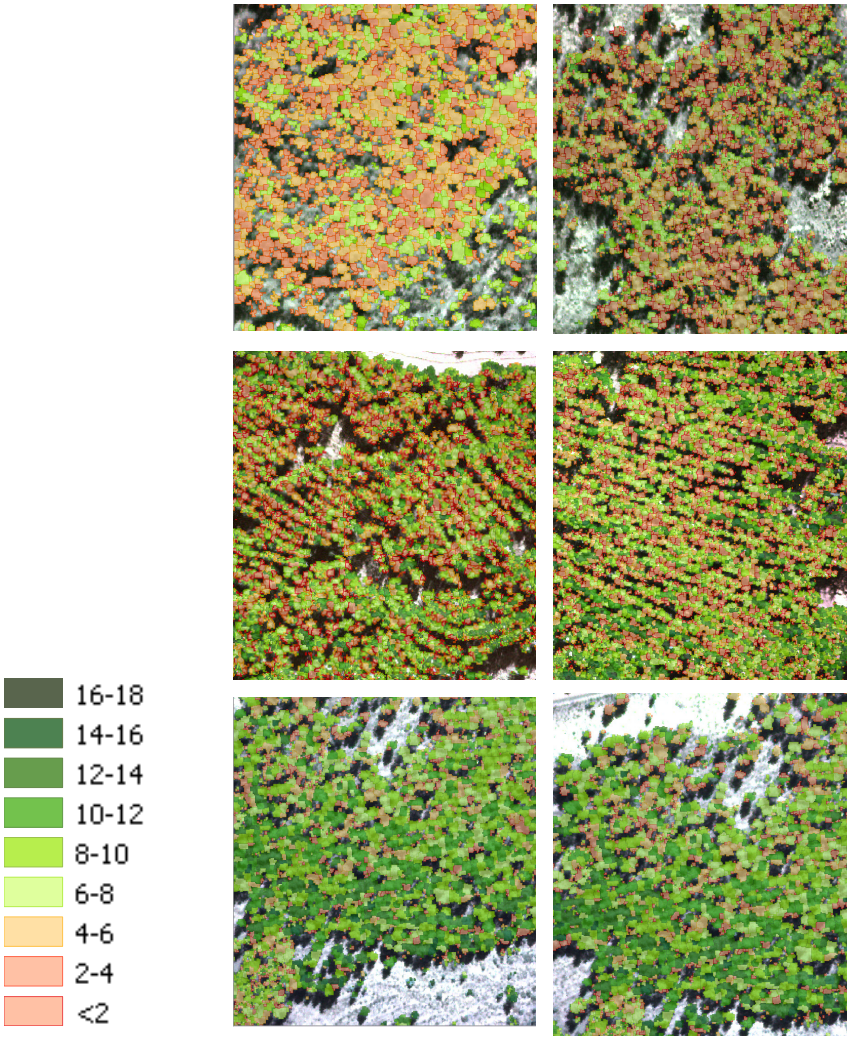

Figure 3.15. Maps showing the spatial variation of $Cx+c$ content µg cm^{-2}) using the index R_{515}/R_{570} through scaling-up. Imagery acquired with the narrow-band multispectral camera on board the UAV platform. Maps with different mean values of carotenoid content are shown for 2-6 µg cm^{-2} (a), 6-12 µg cm^{-2}(b), and 12-18 µg cm^{-2} (c).

The high spatial resolution imagery (50 cm) obtained with the narrow-band multispectral camera enabled the identification of pure crowns and the assessment of pigment measurements by applying vegetation indices to the crown level. Linear relationships obtained between *Cx+c* content and the simple ratio index R_{515}/R_{570} showed a significant relationship ($p<0.001$), with a coefficient of determination of $r^2=0.66$ (Fig 3.14 a). Other traditional indices sensitive to *Cx+c* content at leaf level (CRI) showed weaker relationships at crown level (Fig 3.14c). These results agree with the results of coupling PROSPECT-5 with DART simulations, where the R_{515}/R_{570} index behaved better than the CRI indices at crown level. The relationships obtained between the simple ratio index R_{515}/R_{570} and *Ca+b* content showed a low coefficient of determination ($r^2=0.18$) (Fig. 3.14b). By contrast, *Ca+b*-related vegetation indices were found to be highly related with *Ca+b* content ($r^2=0.71$) (Fig. 3.14d). These results agree with the findings obtained at leaf level, where the simple ratio index R_{515}/R_{570} was highly related with *Cx+c* content and slightly related with *Ca+b*, while the *Ca+b* –related vegetation index R_{700}/R_{570} was highly related with *Ca+b* content.

The relationship found between *Cx+c* and R_{515}/R_{570} (Fig. 3.14a) was used to map carotene spatial variability at crown level using high-resolution imagery. Fig. 3.15 shows a map of the *Cx+c* content of the study area aggregated into different classes, where values correspond to very low *Cx+c* content (< 2 μg cm^{-2}), low *Cx+c* content (range 2-4 μg cm^{-2}), below average *Cx+c* content (range 4-6 μg cm^{-2}), average *Cx+c* content (range 6-8 μg cm^{-2}), average to above-average *Cx+c* content (range 8-10 μg cm^{-2}), above-average *Cx+c* content (range 10-12 μg cm^{-2}), high *Cx+c* content (range 12-14 μg cm^{-2}) and very high *Cx+c* content (range 14-16 μg cm^{-2}).

4. Discussion

The quantitative link between foliar carotenoid content and spectral properties constitutes the basis of pigment retrieval analysis. Several studies have been conducted at leaf scale (Chappelle et al., 1992; Gitelson et al., 2002; Merzlyak et al., 1999). The present study includes a comprehensive review of narrow-band vegetation indices related to carotenoid content based on empirical and modeling methods. Formulating *Cx+c* -related vegetation indices is more challenging than retrieving other biophysical parameters mainly due to the overlap between the chlorophyll and carotenoid absorption peaks. Red edge and TCARI/OSAVI vegetation indices obtained from the simulation analysis showed high sensitivity to Ca+b at leaf and canopy level. These results agree with previous studies that used red edge vegetation indices in forest canopies (Moorthy et al., 2008, Zarco-Tejada et al., 2001) and applied combined indices such as TCARI/OSAVI in tree orchards (Zarco-Tejada et al., 2004) and vineyards (Meggio et al., 2010). Simulation results performed at leaf level provide additional information about the sensitivity of these indices to Ca+b concentration and the Cx+c/Ca+b ratio. The interest of analyzing the relationships between those variables and the response of Ca+b sensitivity to Cx+c -related vegetation indices has been previously studied for some of the indices included in this study such as the CRI (Gitelson et al., 2002) and the PRI (Garity et al. 2011). The Cx+c/Ca+b ratio was found to be highly related with a wide range of Cx+c -related vegetation indices at the leaf level, although the best relationship was found using the PSRI and PRI vegetation indices. These results agree with those obtained by Merzlyak et al., 1999 (PSRI) and Garrity et al. (2011) (PRI) at

the leaf level. However, according to the results obtained at crown level, these indices seem to be highly affected by structural parameters.

A detailed sensitivity analysis of the effect of structural parameters such as LAI or tree density introduced into the Discrete Anisotropic Radiative Transfer (DART) model was performed to show the potential scaling-up of *Cx+c* -related vegetation indices in heterogeneous canopies. Coefficients of determination resulting from the linear relationships between *Cx+c* content and narrow-band vegetation indices revealed the ability of simple ratio indices to assess variations in *Cx+c* content, showing better results than traditional *Cx+c* -related vegetation indices at crown level. Traditional indices formulated as a combination of visible and infrared bands showed greater sensitivity to structural variable effects than simple ratio indices formulated as a combination of bands influenced by *Cx+c* and *Ca+b* absorption.

The new simple ratio vegetation indices proposed in this study were found to be significantly related with *Cx+c* content (r^2>0.6; P<0.001) at leaf and crown level. Nevertheless, this study confirms the robustness of other indices such as the CRI_{550} (r^2>0.93; P<0.001) and CRI_{700} (r^2>0.91; P>0.001) reported in previous studies at leaf level (Gitelson et al., 2003, 2006). Model simulations were validated with detailed laboratory/field leaf pigment content measurements (*Ca+b*, *Cx+c* and xanthophyll pigment content) and needle spectral reflectance.

Spectral vegetation indices used to estimate biophysical variables are usually developed to detect changes in the physical or chemical composition of leaves based on narrow-band optical properties (Zarco Tejada et al.,

2001). The scaling-up of these results is not always feasible because of the heterogeneity and geometry of the crown. In fact, this study demonstrates that most of the spectral indices related to *Cx+c* content at leaf level were not directly applicable to the higher spatial scale of the crown. These results agree with previous studies that have highlighted the need to assess the structural and viewing geometry effects to properly scale-up physiological indices from leaf to crown level (Meggio et al., 2010; Suárez et al., 2008).

5. Conclusions

This study highlights that traditional vegetation indices related to *Cx+c* content behave differently at the leaf and at crown level based on radiative transfer modeling and field and airborne data validation. The study was conducted in a conifer forest, where structure plays an important role. The modeling simulation analysis showed that a new narrow-band vegetation index tested in this study (R_{515} /R_{570}) was sensitive to *Cx+c* content variations at leaf level and were the most robust indices at canopy level. The present study combined field, laboratory and modeling methods to assess the scaling-up of *Cx+c* -related vegetation indices to the canopy level. Results demonstrated that simple ratios formulated with bands R_{515} and R_{520} using reference bands R_{560} and R_{570} showed an adequate relationship with *Cx+c* content at leaf and crown level. In particular, index R_{515} /R_{570} showed the best relationship with *Cx+c* at both leaf and canopy levels and was the least affected by the canopy structure. The robustness of other indices at leaf level was highly correlated to LAI and tree density values at crown level. The results obtained in this study show that when the scale increases to stand level, relationships between the spectral response and leaf chemistry tend to

break down due to confounding factors related to the structure of the crown and background contributions.

Modeling simulation results were in agreement with empirical results obtained at leaf and crown level. The use of narrow-band multispectral cameras on board UAV platforms made it possible to validate this study and obtain high-resolution image data to map biophysical variables. These results demonstrate the feasibility of estimating $Cx+c$ with narrow-band multispectral imagery and confirm the findings obtained by modeling methods.

References

Abadía, A. & Abadía, J. (1993). Iron and plant pigments. In L. L. Barton & B. C. Hemming (Eds.), *Iron Chelation in Plants and Soil Microorganisms* (pp. 327-344). Academic: San Diego.

Ardila, J. P., Bijker, W., Tolpekin, V. A., Alfred Stein. (2012). Context-sensitive extraction of tree crown objects in urban areas using VHR satellite images. *International Journal of Applied Earth Observation and Geoinformation*, *15*, 57-69.

Berni, J. A. J., Zarco-Tejada, P. J., Sepulcre-Cantó, G., Fereres, E., & Villalobos, F. J. (2009). Mapping canopy conductance and CWSI in olive orchards using high resolution thermal remote sensing imagery. *Remote Sensing of Environment*, *113*, 2380-2388.

Blackburn, G. A. (1998). Quantifying chlorophylls and carotenoids at leaf and canopy scales: An evaluation of some hyperspectral approaches. *Remote Sensing of the Environment*, *66*, 273-285.

Broge, N. H., & Leblanc, E. (2001). Comparing prediction power and stability of broadband and hyperspectral vegetation indices for estimation of green leaf area index and canopy chlorophyll density. *Remote Sensing of Environment*, *76*, 156-172.

Carter, G. A. (1994). Ratios of leaf reflectances in narrow wavebands as indicators of plant stress. *International Journal of Remote Sensing*, *15*, 697-704.

Carter, G. A., & Spiering, B. A. (2002). Optical properties of intact leaves for estimating chlorophyll content. *Journal of Environmental Quality*, *31*, 1424-1432.

Chappelle, E. W., Kim, M. S., & McMurtrey, J. E., III (1992). Ratio analysis of reflectance spectra (RARS): An algorithm for the remote estimation of the concentrations of chlorophyll a, chlorophyll b, and carotenoids in soybean leaves. *Remote Sensing of Environment*, *39*, 239-247.

Datt, B. (1998). Remote sensing of chlorophyll a, chlorophyll b, chlorophyll a + b, and total carotenoid content in Eucalyptus leaves. *Remote Sensing of Environment*, *66*, 111-121.

Demmig-Adams, B., & Adams, W. W. (1996). The role of xanthophyll cycle carotenoids in the protection of photosynthesis. *Trends in Plant Science*, *1*, 21-26.

Demmig-Adams, B., & Adams, W. W. III (1992). Photoprotection and other responses of plants to high light stress. *Annual Review of Plant Physiology and Plant Molecular Biology*, *43*, 599-626.

Faria T., García-Plazaola, J. I., Abadia, A., Cerasoli, S., Pereira, J. S., & Chaves, M. M. (1996). Diurnal changes in photoprotective mechanisms in leaves of cork oak (*Quercus suber*) during summer. *Tree Physiology*, *16*, 115-123.

Feret, J. B., François, C., Asner, G.P., Gitelson, A.A., Martin, R.E., Bidel, L.P.R., Ustin, S.L., le Maire, G., & Jacquemoud, S. (2008). PROSPECT-4 and 5: Advances in the leaf optical properties model separating photosynthetic pigments. *Remote Sensing of Environment*, *112*, 3030-3043.

Feret, J. B., François, C., Gitelson, A., Asner, G. P., Barry, K. M., Panigada, C., Richardson A. D., & Jacquemoud, S. (2011). Optimizing spectral indices and chemometric analysis of leaf chemical properties using radiative transfer modeling. *Remote Sensing of Environment*, *115*, 2742-2750.

Frank, H. A., & Cogdell, R. J. (1996) Carotenoids in photosynthesis. *Photochemistry. Photobiology*, *63*, 257-264.

Gamon, J. A., Peñuelas, J., & Field, C. B. (1992). A narrow-wave band spectral index that tracks diurnal changes in photosynthetic efficiency. *Remote Sensing of Environment*, *41*, 35-44.

Garrity S. R., Eitel, J. U. H., & Vierling, L. A. (2011) Disentangling the relationships between plant pigments and the photochemical reflectance index reveals a new approach for remote estimation of carotenoid content. *Remote Sensing of Environment*, *115*, 628-635.

Gastellu-Etchegorry, J. P., Demarez, V., Pinel, V., & Zagolski, F., (1996). Modeling radiative transfer in heterogeneous 3-D vegetation canopies. *Remote Sensing of Environment*, *58*, 131-156.

Gastellu-Etchegorry, J. P., & Bruniquel-Pinel, V. (2001): A model approach to assess the robustness of spectrometric predictive equations for canopy chemistry. *Remote Sensing of Environment*, *76*, 1-15.

Gastellu-Etchegorry, J. P., Martin E., & Gascon, F. (2004). DART: a 3D model for simulating satellite images and studying surface radiation budget. *Internation Journal of Remote Sensing*, *25*, 73-96.

Gitelson A. A. & Merzlyak M. N. (1996). Signature analysis of leaf reflectance spectra: Algorithm development for remote sensing of chlorophyll. *Journal of Plant Physiology*, *148*, 494-500.

Gitelson, A. A., Zur, Y., Chivkunova, O. B., & Merzlyak, M. N. (2002). Assessing carotenoid content in plant leaves with reflectance spectroscopy. *Journal of Photochemistry and Photobiology B-Biology*, *75*, 272-281.

Gitelson, A. A., Gritz, U., & Merzlyak, M. N. (2003). Relationships between leaf chlorophyll content and spectral reflectance and algorithms for non-destructive chlorophyll assessment in higher plant leaves. *Journal of Plant Physiology*, *160*, 271-282.

Gitelson, A. A., Keydan, G. P., & Merzlyak, M. N. (2006). Three-band model for noninvasive estimation of chlorophyll, carotenoids, and

anthocyanin content in higher plant leaves. *Geophysical Research Letters*, *33*, L11402.

Gueymard, C.A. (1995). SMARTS, A Simple Model of the Atmospheric Radiative Transfer of Sunshine: Algorithms and Performance Assessment. Technical Report No. FSECPF- 270-95. Cocoa, FL: Florida Solar Energy Center.

Gueymard, C. A. (2001). Parameterized Transmittance Model for Direct Beam and Circumsolar Spectral Irradiance. *Solar Energy*, *71*, 325-346.

Haboudane, D., Miller, J. R., Tremblay, N., Zarco-Tejada, P. J., & Dextraze, L. (2002). Integrated narrow-band vegetation indices for prediction of crop chlorophyll content for application to precision agriculture. *Remote Sensing of Environment*, *81*, 416-426.

Hernández-Clemente, R., Navarro-Cerrillo, R. M., Suárez, L., Morales, F., & Zarco-Tejada, P. J. (2011). Assessing structural effects on PRI for stress detection in conifer forests. *Remote Sensing of Environment*, *115*, 2360-2375.

Jacquemoud S., & Baret F. (1990). PROSPECT: a model of leaf optical properties spectra. *Remote Sensing of Environment*, *34*, 75-91.

Kirchgebner, H. D., Reichert, K., Hauff, K., Steinbrcher, R., Schnitzler J.P., & Pfündel, E.E. (2003). Light and temperature, but not UV radiation, affect chlorophylls and carotenoids in Norway spruce needles (*Picea abies* (L.) Karst.). *Plant, Cell & Environment*, *26*, 1169-1179.

Kurtz, C., Passat, N., Gançarski, P. Puissant, A. (2011). Extraction of complexpatterns from multiresolutionremotesensing images: Ahierarchicaltop-downmethodology. *Pattern Recognition*, *45*, 685-706.

Larbi, A., Abadía, A., Morales, F., & Abadía, J. (2004). Fe resupply to Fe-deficient sugar beet plants leads to rapid changes in the violaxanthin cycle and other photosynthetic characteristics without significant de novo chlorophyll synthesis. *Photosynthesis Research*, *79*, 59-69.

le Maire, G., François, C., & Dufrêne, E. (2004). Towards universal broad leaf chlorophyll indices using PROSPECT simulated database and

hyperspectral reflectance measurements. *Remote Sensing of Environment*, *89*, 1-28.

Lichtenhaler, H. K., (1998). The stress concept in plants: An introduction. *Annals of the New York Academy of Science*, *851*, 187-198.

Main, R., Cho, M. A., Mathieu, R., O'Kennedy, M. M., Ramoelo, A. & Koch, S. (2011). An investigation into robust spectral indices for leaf chlorophyll estimation. *ISPRS Journal of Photogrammetry and Remote Sensing* , *66*, 751-761

Malenovsky, Z., Homolova, L., Cudlin, P., Zurita Milla, R., Schaepman, M.E., Clevers, J.G.P.W., Martin, E., & Gastellu-Etchegorry, J.P. (2007). Physically-based retrievals of Norway spruce canopy variables from very high spatial resolution hyperspectral data. In Proc. IEEE International Geoscience and Remote Sensing Symposium (IGARSS'07), Barcelona, Spain.

Malenovsky, Z., Martinb, E., Homolovác, L.,Gastellu-Etchegorry, J. P., Zurita-Milla, R., Schaepmana, M. E., Pokornýc, R., Cleversa, J. G. P. W., & Cudlínc, P. (2008). Influence of woody elements of a Norway spruce canopy on nadir reflectance simulated by the DART model at very high spatial resolution. *Remote Sensing of Environment*, *112*, 1-18.

Meggio, F., Zarco-Tejada, P. J., Miller, J. R., Martín, P., González, M. R., & Berjón, A. (2008). Row orientation and viewing geometry effects on row-structured vine crops for chlorophyll content estimation. *Canadian Journal of Remote Sensing*, *34*, 220-234.

Meggio F., Zarco-Tejada, P.J., Núñez L.C., Sepulcre-Cantó G., Gonzalez M.R. & Martin, P. (2010). Grape quality assessment in vineyards affected by iron deficiency chlorosis using narrow-band physiological remote sensing indices. *Remote Sensing of Environment*, *114*, 1968-1986.

Merzlyak, M. N., Gitelson, A. A., Chivkunova, O. B., & Rakitin, V. Y. (1999). Non-destructive optical detection of leaf senescence and fruit ripening. *Physiologia Plantarum*, *106*, 135- 141.

Miller, J. R., Hare, E. W., & Wu, J. (1990). Quantitative characterization of the vegetation red edge reflectance. An inverted-Gaussian reflectance model. *International Journal of Remote Sensing*, *11*, 1755-1773.

Moorthy I., Miller J. R., & Noland T. L. (2008). Estimating chlorophyll concentration in conifer needles with hyperspectral data: An assessment at the needle and canopy level. *Remote Sensing of Environment*, *112*, 2824-2838.

Munné-Bosch, S., & Peñuelas, J. (2003). Photo- and antioxidative protection, and a role for salicylic acid during drought and recovery in field-grown *Phillyrea angustifolia* plants. *Planta*, *217*, 758-766.

Peñuelas, J., Gamon, J., Freeden, A., Merino, J., & Field, C. (1994). Reflectance indices associated with physiological changes in nitrogen- and water-limited sunflower leaves. *Remote Sensing of Environment*, *48*,135-146.

Peñuelas, J., Baret, F., & Filella, I. (1995). Semi-empirical indices to assess carotenoids/ chlorophyll a ratio from leaf spectral reflectance. *Photosynthetica*, *31*, 221-230.

Richardson, A. D. & Berlyn, P. (2002). Changes in foliar spectral reflectance and chlorophyll fluorescence of four temperate species following branch cutting. *Tree Physiology*, *22*, 499-506.

Pinty, B., Gobron, N., Widlowski, J.L., Gerstl, S.A.W., Vertraete, M.M., Antunes, M., Bacour, C., Gascon, F., Gastellu-Etchegorry, J.P., Jacquemoud, S., North, P., Qin, W., Thompson, R. (2001). Radiation transfer model intercomparison (RAMI) exercice. *Journal of Geophysical Research*, *106*, 11937-11956.

Ritz T., Damjanovic, A., Schulten, K., Zhang, J. P. & Koyama, Y. (2000). Understanding efficient light-harvesting through carotenoids with novel theoretical and experimental techniques. *Photosynth Research*, *66*, 125-144.

Rondeaux G., Steven M. & Baret F. (1996). Optimization of Soil-adjusted vegetation indices. *Remote Sensing of Environment*, *55*, 95-107.

Rouse, J. W., Haas, R. H., Schell, J. A., Deering, D. W., & Harlan, J. C. (1974). Monitoring the vernal advancement and retrogradation (Greenwave Effect) of natural vegetation. Type III Final Report, NASA Goddard Space Flight Center, Greenbelt, Maryland, 20771, USA 371 pp.

Sims, D. A., & Gamon, J. A. (2002). Relationships between leaf pigment content and spectral reflectance across a wide range of species, leaf structures and developmental stages. *Remote Sensing of Environment*, *81*, 337-354.

Suárez, L., Zarco-Tejada, P. J., Sepulcre-Cantó, G., Pérez-Priego, O., Miller, J. R., Jiménez-Muñoz, J. C., & Sobrino, J. (2008). Assessing canopy PRI for water stress detection with diurnal airborne imagery. *Remote Sensing of Environment*, *112*, 560-575.

Suárez, L., Zarco-Tejada, P. J., Berni, J. A. J., González-Dugo, V., & Fereres, E., (2009). Modelling PRI for water stress detection using radiative transfer models. *Remote Sensing of Environment*, *113*, 730-744.

Suárez, L., Zarco-Tejada, P. J., González-Dugo, V., Berni, J. A. J., Sagardoy, R., Morales, F. & Fereres, E. (2010). Detecting water stress effects on fruit quality in orchards with time-series PRI airborne imagery. *Remote Sensing of Environment*, *114*, 286-298.

Thayer, S. S., & Björkman, O. (1990). Leaf xanthophyll content and composition in sun and shade determined by HPLC. *Photosynthesis Research*, *23*, 331-343.

Widlowski, J. L., Taberner, M., Pinty, B., Bruniquel-Pinel, V., Disney, M., Fernandes, R., Gastellu-Etchegorry, J.-P., Gobron, N., Kuusk, A., Lavergne, T., Leblanc, S., Lewis, P. E., Martin, E., Mottus, M., North, P. R. J., Qin, W., Robustelli, M., Rochdi, N., Ruiloba, R., Soler, C., hompson, R., Verhoef, W., Verstraete, M.M. & Xie, D. (2007), Third Radiation Transfer Model Intercomparison (RAMI) exercise: Documenting progress in canopy reflectance models. *Journal of Geophysical Research*, *112*, D09111.

Wu, S. L., Mickley L. J., Jacob D.J., Rind D. & Streets, D.G. (2008). Effects of 2000-2050 changes in climate and emissions on global tropospheric ozone and the policy-relevant background surface ozone in the United States. *Journal of Geophysical Research*, *108*, D18312.

Young, A. & Britton, G. (1990). Carotenoids and stress. In Alscher, R. G., Cumming, J. R. (Ed.), *Stress responses in plants: adaptation and acclunation mechanisms* (pp. 87-112). New York; Wiley- Liss.

Young, A. J., Phillip, D. & Savill, J. (1997). Carotenoids in higher plant photosynthesis. In Pessaraki M. (Ed.), *Handbook of Photosynthesis* (pp 575-596). New York: Marcel Dekker.

Zarco-Tejada, P. J., Miller J. R., Mohammed G. H., Noland T. L., & Sampson, P.H. (2001). Scaling-up and model inversion methods with narrow-band optical indices for chlorophyll content estimation in closed forest canopies with hyperspectral data. *IEEE Transactions on Geoscience and Remote Sensing*, *39*, 1491-1507.

Zarco-Tejada, P.J., Miller J. R., Harron, J., Hu, B., Noland, T. L., Goel, N., Mohammed, G. H. & Sampson P. H. (2004). Needle chlorophyll content estimation through model inversion using hyperspectral data from boreal conifer forest canopies. *Remote Sensing of Environment*, *89*, 189-199.

Zarco-Tejada, P. J., Berni, J. A. J., Suárez, L., Sepulcre-Cantó, G., Morales, F. & Miller, J. R**.** (2009). Imaging Chlorophyll Fluorescence from an Airborne Narrow-Band Multispectral Camera for Vegetation Stress Detection. *Remote Sensing of Environment*, *113*, 1262-1275.

Zarco-Tejada, P. J., González-Dugo, V., & Berni, J. A. J., (2012). Fluorescence, temperature and narrow-band indices acquired from a UAV platform for water stress detection using a micro-hyperspectral imager and a thermal camera. *Remote Sensing of Environment*, *117*, 322-337.

4. Scaling-up methods for chlorophyll and carotenoid content estimation using narrow-band optical indices and radiative transfer model in conifer forest.

Chapter 4

Scaling-up methods for chlorophyll and carotenoid content estimation using narrow-band optical indices and radiative transfer model in conifer forest.

Abstract

This Quantifying leaf pigments associated with photosynthesis, light harvesting, energy transfer and photoprotection is critical to evaluate forest species affected by decline processes. This paper focuses on the retrieval of chorophyll a+b (Ca+b) and carotenoids (Cx+c) pigments, which are critical bio-indicators of plant physiological state. Radiative transfer theory and modelling assumptions were applied at both laboratory and field scales to develop methods for the simultaneous estimation of Ca+b and Cx+c content using high resolution hyperspectral imagery. Airborne campaigns were conducted with the Airborne Hyperspectral Scanner (AHS) over Pinus sylvestris and Pinus nigra forest areas affected by decline processes, acquiring 2 m spatial resolution imagery in 80 spectral bands in the 0.43-12.5 μm spectral range. Needle samples were collected from P. sylvestris and P. nigra plots for destructive sampling and biochemical determination of Ca+b and Cx+c content conducted in the laboratory. Chlorophyll content retrieval was investigated based on the red edge (R_{750}/R_{710}) and TCARI/OSAVI narrow-band indices. The carotenoid retrieval was assessed with the R_{515}/R_{570} index recently demonstrated sensitive to carotenoid pigment content in conifer forests. Simpler canopy modelling methods based on infinite reflectance by Lillestaeter, Yamada and Fujimura and Hapke, and the 3D approach such as the Discrete Anisotropic Radiative Transfer (DART) model were evaluated along with PROSPECT-5 leaf model for the scaling-up of the optical indices. The model simulation results with synthetic spectra demonstrated the feasibility of R_{515}/R_{570} index combined with the R_{750}/R_{710} red edge index for Cx+c content estimation on conifer forest. Among the canopy reflectance approximations assessed, simpler modelling methods yielded comparable results to more complex 3-D approximations due to the high resolution acquired which enabled targeting pure crowns. The scaling up methods based on PROSPECT-5+DART yielded root mean square errors of 1.42 $\mu g/cm^{-2}$ (Cx+c) and 4.87 $\mu g/cm^{-2}$ (Ca+b) and based on PROSPECT-5+Hapke infinitive model of 4.37 $\mu g/cm^{-2}$ (Cx+c) and 4.71

μg/cm^{-2} (Ca+b). These predictive algorithms validated on high resolution hyperspectral imagery provide a methodology to monitor chlorophyll and carotenoid pigment content on conifer forest canopies.

Keywords: chlorophyll, carotenoids, hyperspectral, airborne, R_{515}/R_{570}, R_{750}/R_{710}, TCARI/OSAVI, conifers, forest, scaling up.

2.1. Introduction

Photosynthetic pigments have been shown to be important bio-indicators of plant physiological state, mainly due to their roles in photosynthesis (Carter and Miller, 1994; Lichtenhaler, 1998). The early diagnosis of forest decline processes have been previously reported using photosynthetic pigments content as stress indicators (Batic et al, 1999; Tausz et al., 1998). The main short-term physiological response of trees under decline is a general reduction in photosynthesis due a large decrease in the levels of chlorophylls and carotenoids (Lippert et al., 1996). Several authors (eg Hoshizaki, 1988; Matyssek et al., 1993) have been demonstrated that declining physiological state is connected with decline in chlorophyll content and with decreasing rate of photosynthesis, whereas the values of ratio Ca/Cb are increasing. On the other hand, the ratio C a+b/C x+c shows a decreasing trend.

The decrease in chlorophyll and carotenoid content in leaves leads to less overall absorption in the 430-700 nm region due to the decrease of the proportion of light-absorbing pigments. Several narrowband leaf-level optical indices have been reported in the literature demonstrating the sensitivity to chlorophyll content at the leaf level (see Main et al., 2011 for a review of vegetation indices) and at the canopy level (Zarco-Tejada et al., 2001). Carotenoid-sensitive indices had been also widely analyzed at the leaf level (Gitelson et al., 2002; Peñuelas et al., 1995) and recently evaluated at the crown level (Hernández-Clemente et al., (submitted)). Despite the extensive work on broadleaf species, strategies to link biochemistry and

optical properties for coniferous species have been limited due to difficulties in measuring coniferous species. The main narrow band indices proposed for the retrieval of chlorophyll content are based on band ratios calculated in the red edge region. The red edge is the point of maximum slope in vegetation reflectance spectra, between 680-750 nm. It occurs because the absorption region of the chlorophylls dramatically changes from the red to the near-infrared. In forest canopies, one of the best red edge formulations was found by Zarco-Tejada et al., (2001) who demonstrated that the R_{750}/R_{710} red edge index was less sensitive than other chlorophyll indices to forest shadows. Later, the same red index formulation was also validated by other authors (eg. Moorthy et al., 2008; Zhang et al., 2008). Recently, combined indices sensitive to Ca+b content had been developed with the Transformed Chlorophyll Absorption in reflectance Index, TCARI (Haboudane et al., 2002), and the Optimized Soil-Adjusted Vegetation Index, OSAVI (Rondeaux et al., 1996), used to minimize soil and leaf area index (LAI) effects in crops (Meggio et al., 2010; Zarco-Tejada et al., 2004b, 2005). Nevertheless, these potential valuable indices suitable for field crops (Haboudane et al., 2002), olive orchards (Zarco-Tejada et al., 2004b), and vineyards (Meggio et al., 2010; Zarco-Tejada et al., 2005) are not currently validated for forest canopies. Due the confounding factors related to the crown structure, shadows and background, the optical vegetation indices performs differently according to the canopy type analyzed.

Several methods have been proposed to retrieve biophysical parameters from hyperspectral reflectance in forest canopies, including scaling up and model inversion methods though coupling leaf and canopy transfer models

(Zarco-Tejada et al., 2001). Radiative transfer models had been widely used in modelling the bidirectional reflectance distribution of vegetation canopies based on different approximations (Pinty et al., 2004). Infinitive reflectance models (Hapke 1993; Lillestaeter, 1982; and Yamada and Fujimura, 1991), as the basis for radiation transfer theory in turbid media, has been successfully applied for pigment content retrieval (Zarco-Tejada et al., 2004a). These simplified approximations express the optically thick medium in terms of single reflectance and transmittance ignoring multiple scattering, and considering equal reflectance for both sides of the leaf. In a recent study carried out in crops by Zarco-Tejada et al. (submitted) the feasibility of employing infinitive reflectance models for the retrieval of cholorophyll and carotenoid content was demonstrated when targeting pure vegetation pixels. So far, the successfully application of this model requires high spatial resolution data to enable the application pure crowns identification methods and therefore, the applicability of those results on heterogeneous forest canopies requires further research. Pigment content retrieval had been also estimated based on the Scattering Arbitrary Inclined Leaves (SAIL) model (Verhoef, 1984), taking into account the hotspot effects or the multiple scattering in the canopy. Based on PROSAIL (formed by the newly-calibrated leaf reflectance model PROSPECT coupled with the multi-layer version of the canopy radiative transfer model SAIL) the study of le Maire et al., (2008) on broadleaf forest species showed results with an RMSE of 8.2µg cm^{-2} for Ca+b estimation. Those results were obtained based an optical vegetation index previously determined, the $ND_{chl}=(R_{925}-R_{710})/(R_{925}+R_{710})$. Although, other studies have been showed improved results using the (R_{750}/R_{710}) red edge index like for instance, the

work carried on conifer species by Moorthy et al., (2008) In this case, Ca+b was estimated thought scaling up using PROSPECT+SAILH radiative models with a root mean square error of 5.3 mg/cm2, for a pigment range of 25.7 to 45.9 mg/cm2 using pure crowns reflectance from high spatial resolution hyperspectral imagery.

In an effort to overcome the reflectance simulation of complex structures 3D models have been developed such us SPRINT, FLIGHT or DART (Pinty et al., 2004). In particular, the validity of canopy-level indices for chlorophyll content estimation in conifer forest had been studied through the inversion of linked PROSPECT and SPRINT models by Zarco-Tejada et al., (2004a) by using the optical index R_{750}/R_{710} as the merit function in the numerical inversion to minimize the effect of shadows and LAI variation. In this case, the application of this methodology for Ca+b estimation yielded a root square error of 8.1 $\mu g/cm^2$, targeting sunlit crown pixels with pigment content ranging between 26.8 and 56.8 $\mu g/cm^2$. More complex approach such us the Discrete Anisotropic Radiative Transfer, DART model was developed (Gastellu et al., 2004) to simulate heterogeneous coniferous forest. It had been demonstrated that canopy structure significantly influences canopy near-infrared and visible reflectance and the application of 3-D vegetation models such us DART model significantly improved chlorophyll forest retrieval (Demarez & Gastellu-Etchegorry; 2000). For this proposed, the coupled PROSPECT+DART was used by Malenovsky et al. (2008) for chlorophyll content estimation through an inversion method using an artificial neural network (ANN) yielding a root square error of 2.95 $\mu g/cm^2$, and using an optical vegetation index calculated as the Area under curve

Normalized to maximal Chlorophyll absorption Band depth between 650-720 nm (ANCB650-720), yielding RMSE=3.36 μg cm^2. So far, the successfully application of this methodology requires high spectral resolution enabling the calculation of the band depth between 650-720 nm and large computational effort to perform DART simulations and ANN inversion methods.

Despite the efforts made to assess several Ca+b -related vegetation indices, further research is needed to study Cx+c -sensitive indices both at leaf and canopy levels. The R_{515}/R_{570} index proposed for carotenoid estimation in conifer forest (Hernández-Clemente et al., 2012) had been recently validated in crops (Zarco-Tejada et al., 2012) obtaining RMSE values below 0.95 ugr/cm2. This paper aims at analysing the retrieval of both Ca+b and Cx+c content on forest canopies using scaling-up approaches based on the model simulation of narrow band vegetation indices. This study involves the comparison of modelling methods using the leaf PROSPECT model coupled to three infinite reflectance models and a complex 3D DART model for the retrieval of chlorophyll and carotenoid content at the crown level. The study also evaluate the methodology proposed by Zarco-Tejada et al., 2012 for the retrieval of Cx+c content by combining narrow band vegetation indices sensitive to Cx+c and Ca+b simultaneously in order to reduce Ca+b effects. The performance of two Ca+b-related indices, the red edge R_{750}/R_{710} and the TCRI/OSAVI indices were compared through a scaling up approach.

2. Materials and Methods

2.1.1. Field experiments and data collection

Field data collections were conducted in August 2009 in Sierra de Filabres (Almeria province, southeastern Spain) (37° 13' 27" N, 2° 32' 54" W) (Fig. 4.1), the driest region in Western Europe. The elevation of the study area ranges from 1540 to 2000 m.a.s.l., and annual rainfall is between 300 and 400 mm. The annual average temperature is 11ºC, reaching a maximum of 32ºC during summer and a minimum of -8ºC during winter. The vegetation consists of a 40-year-old mixed pine afforestation of *Pinus nigra* Arnold and *Pinus sylvestri*s L. (Table 4.1). Forest decline processes have been previously reported in Sierra de Filabres (Allen et al., 2010). Artificial *forest plantations* of the *same age* allow studying forest canopies controlling structural parameters and the separate analysis of each species. The relevance of pine plantation is currently significant being the most intensively managed forest in the world. The field sampling campaigns were conducted concurrently with airborne overflights during the last week of July 2008. Needles were collected from the top of the crown by selecting branches of illuminated areas on a total of 21 trees. Needles were frozen in liquid nitrogen in the field and then stored at -80ºC prior to pigment determination. Mean crown pigment determinations were calculated from a total of 10 young needles (one year-old needles) collected from the top of the crown. The pigment concentration assessments measured chlorophyll *a* and *b* (*Cab*), and carotenoids (*Cx+c*).

Needle pigment concentration was determined as reported by Abadía and Abadía (1993). Pigment extracts were obtained from a mixed sample of 5 cm of needle material, using 1 linear cm per needle. The area was calculated by assuming that the needle was a half cylinder and the diameter was the measured width of each needle. Needle diameter was measured with a digital

caliper precision instrument. Five additional needle samples were used to take structural measurements (thickness and width) and determine water content and dry mass. The needles were ground in a mortar on ice with liquid nitrogen and diluted in acetone up to 5 ml (in the presence of Na ascorbate). After that, the extracts were filtered through a 0.45-μm filter to separate the pigment extracts from the Na ascorbate. Spectrophotometric determinations were then conducted on the same extracts.

Table 4.1. Variability ranges of measured parameters for the conifer forest sites.

		Mean		SD		Minimum		Maximum	
		Ps	Pn	Ps	Pn	Ps	Pn	Ps	Pn
Diameter at breast height	DBH(cm)	16.8	15.6	2.6	2.8	11.3	11.3	21	22
Tree height	H(m)	7.9	7.4	1.4	1.8	5.8	4.3	11.6	11.3
Crown diameter	Cd(m)	4.5	3.8	0.7	0.8	3.1	2.1	5.8	5.3
Crown Height	Ch(m)	5.8	5.8	1.4	1.5	3.4	2.7	10.2	9.4
Basal area	BA(m^2ha^{-1})	155.7	128.5	99.9	52	73.9	67.9	611	353
Stand density	SD (trees ha−1)	1050	925	418	353	100	100	1800	1600

2.1.2. Airborne campaigns

The airborne campaign was conducted by the Spanish Aerospace Institute (INTA) with the Airborne Hyperspectral Scanner AHS (Sensytech Inc., currently Argon St. Inc., Ann Arbor, MI, USA) during the last week of July 2008. The airborne data acquisition was carried out at 12:00 GMT, acquiring 2 m spatial resolution imagery in 38 bands in the 0.43-12.5 μm spectral range. The Field of View (FOV) and Instantaneous Field of View (IFOV) of the AHS sensor were 90º and 2.5 mrad respectively, and plots were located in the central region of the scene in order to avoid edge effects. *At-sensor* radiance processing and atmospheric correction were performed at the INTA facilities. Atmospheric correction was conducted with ATCOR4 based on the MODTRAN radiative transfer model (Berk *et al.*, 1998; 2000) using aerosol optical depth at 550 nm collected with a Micro-Tops II sun photometer (Solar Light, Philadelphia, PA, USA).

The hyperspectral imagery acquired enabled pure crowns identification of P. sylvestris and P.nigra trees (Fig. 4.1b) for validation purposes. Single-crown reflectance spectra was extracted using object-based crown delimitation algorithm applied to the hyperspectral imagery (Fig. 4.2a), which enabled calculation of the mean hyperspectral reflectance of sunlight and shadow pure crown (Fig. 4.2b,c,d).

Vegetation indices were calculated from the crown spectra for the retrieval of chlorophyll (Ca+b) and carotenoid content (Cx+c). The Ca+b-related vegetation indices were selected based on previous studies in forest canopies, using simple ratio indices located in the red edge region (Moorthy et al., 2008 and Zarco-Tejada et al., 2001) and including recent Ca+b-releted

indices validated for crops canopies such us TCAR/OSAVI (Haboudane et al., 2002). The Cx+c-related vegetation index used is based on previous work where R_{515}/R_{570} was proposed by Hernandez-Clemente et al., (Submitted), which demonstrated to be significantly related to Cx+c concentration both at leaf (r2>0.72;P<0.001) and canopy (r2>0.71; P<0.001) levels.

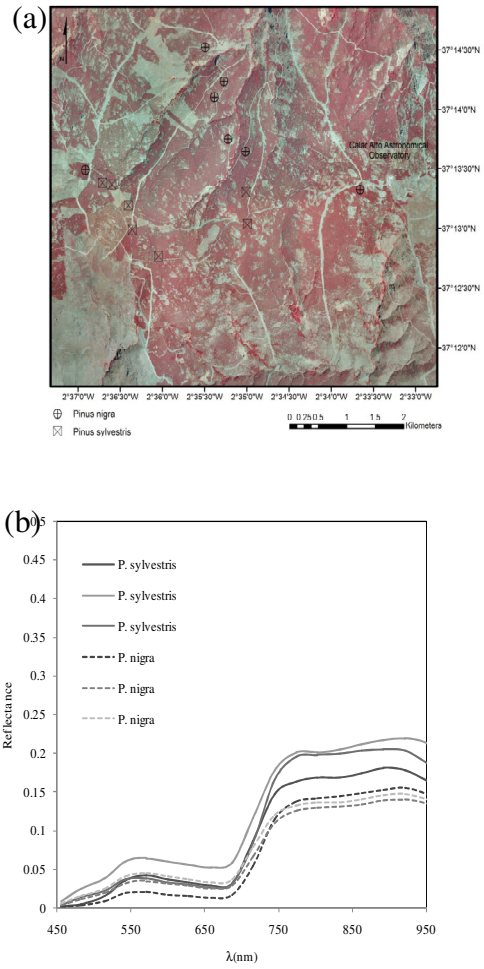

Figure 4.1. Overview of the area acquired with the AHS instrument and plot locations of the tree measured (a). Single pixel AHS spectra for pure crown pixels of *Pinus sylvestris* and *Pinus nigra* (b).

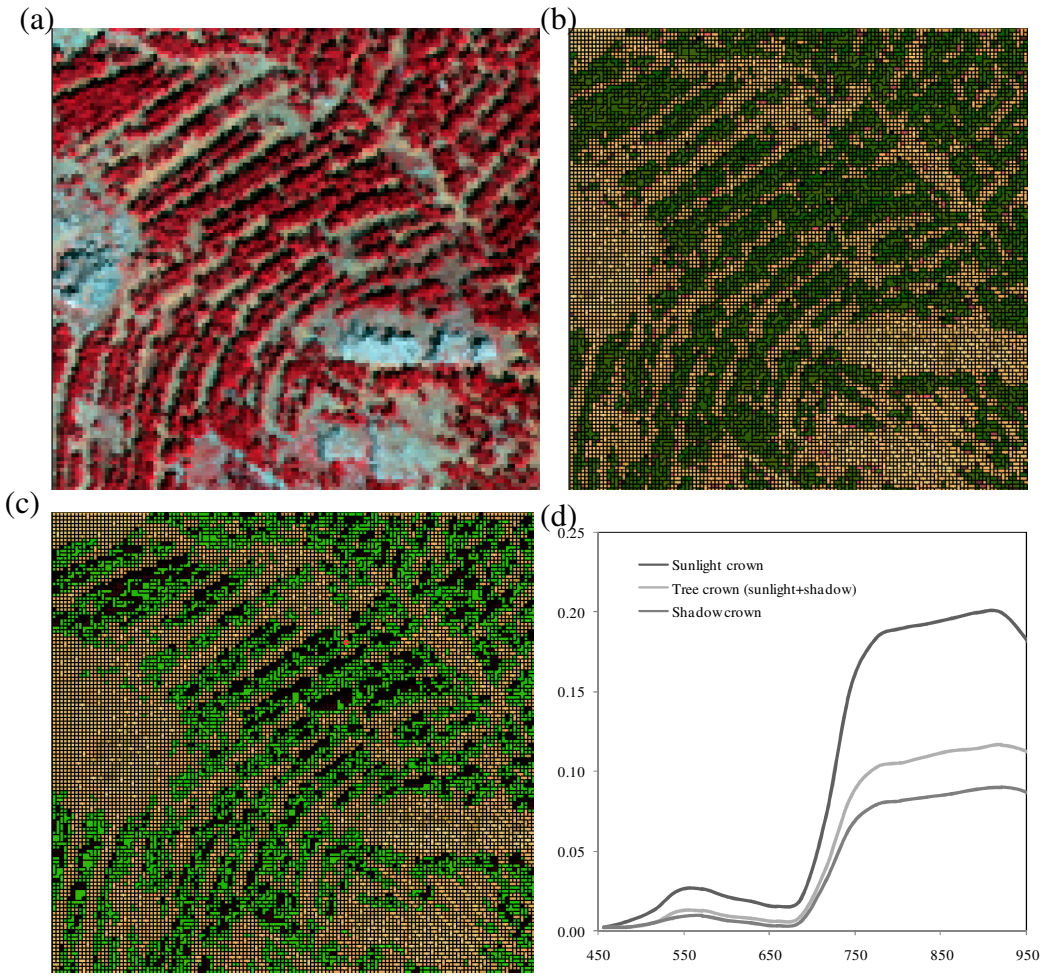

Figure 4.2. AHS airborne footprint (a). Overview of the area acquired with the AHS instrument (b). Single pixel AHS spectra for pure vegetation, soil and mixed vegetation-soil pixels (c). Automatic object-based crown detection algorithm applied to the hyperspectral imagery to identify pure crowns extraction (d).

2.2. Modelling the retrieval of chlorophyll and carotenoid content

The PROSPECT-5 model was used to simulate needle reflectance and transmittance for varying chlorophyll Ca+b (10-60 μg/cm^2) and carotenoid Cx+c (2-16 μg/cm2) content. Table 4.2 summarizes the nominal values used for leaf level modelling. The simulated leaf reflectance and transmittance spectra were used as input of canopy level radiative transfer models. Scaling-up methods were evaluated based on infinite reflectance R_∞ simulations and using 3-D canopy reflectance radiative transfer models. The aim of this analysis was to compare the scaling-up results obtained with different canopy reflectance approximations. The use of high resolution images enabled the extraction of pure crown vegetation pixels from the imagery, and therefore the applicability of simpler infinitive reflectance simulation approaches without considering canopy structure or viewing geometry effects. . The R_∞ formulations used were: Lillestaeter (1982) ($R_{\infty 1}$) [Equation 1a], Yamada and Fujimura (1991) ($R_{\infty 2}$) [Equation 1b] and Hapke (1993) ($R_{\infty 3}$) [Equation 1c].

$$R_{\infty 1} = \frac{\rho}{1-\tau^2} \qquad [1a]$$

$$R_{\infty 2} = \frac{\rho}{1-\dfrac{2\tau^2}{1+(1-4\tau^2)^{1/2}}} \qquad [1b]$$

$$R_{\infty 3} = \frac{1-\alpha^{1/2}}{1+\alpha^{1/2}} \; ; \quad \alpha = 1-\rho-\tau \qquad [1c]$$

In order to compare results obtained with infinitive reflectance approach, a more complex and computationally expensive approach used in this study consisted of simulating the crown reflectance using the the 3-dimensional *Discrete Anisotropic Radiative Transfer* (DART) model (Gastellu-Etchegorry et al., 1996; Gastellu-Etchegorry et al., 2004). The DART model was previously used to simulate forest canopy reflectance in Norway spruce for the retrieval of chlorophyll content (Malenovsky et al., 2008), and Scotch pine canopies for analysing Cx+c- related vegetation indices (Hernandez-Clemente et al., submitted). In this study, the DART model was used to simulate the pure crown reflectance from Scotch and Black pine canopies, extracting from the simulated crown the sunlight reflectance from each tree. The 3-D forest scene was conducted using structural inputs within the range of variation observed from field data measurements. Table 4.2 summarizes the input parameters defining geometrical and optical properties for DART simulations. Fig. 4.3 shows a sample area acquired with airborne imagery (Fig. 4.3a) and an example of the DART scene generation obtained (Fig. 4.3b), and the comparison of simulated and modelling spectral results for sunlight and shadows crowns (Fig. 4.3c).

Table 4.2. Nominal values used for leaf and canopy modelling parametrization with PROSPECT-5 and DART.

PROSPECT-5	*Nominal values and ranges*
Chlorophyll a+b, C_{a+b} *($\mu g\ cm^{-2}$)*	10-60
Carotenoid content, C_{x+c} *($\mu g\ cm^{-2}$)*	2-16
Leaf water content, C_w *(cm)*	0.03-0.01
Leaf dry matter content, C_m *($g\ cm^{-2}$)*	0.03
Leaf internal structure parameter, *N*	2-3
DART	*Nominal values and ranges*
Central wavelength*, (nm)*	400-800
Spectral bandwidth, *(nm)*	10
Scene parameters	*Value*
Cell size, *(m)*	0.5
Scene dimensions, *(m)*	50 x 50
Spatial distribution	Ramdom
Canopy parameters	
Number of trees	1200 trees/ha
Probability of presence	0.8
Leaf area index (varied parameter)	1-7
Crown shape	Truncated cone
Crown height (mean), *(m)*	6
Crown height (std dev), *(m)*	0.9
Height below crown (mean), *(m)*	4
Height below crown (std dev), *(m)*	0.8
Diameter below crown (mean), *(m)*	0.4
Diameter below crown (std dev), *(m)*	0.1
Height within the tree crown, *(m)*	5
Diameter within the tree crown, *(m)*	0.35

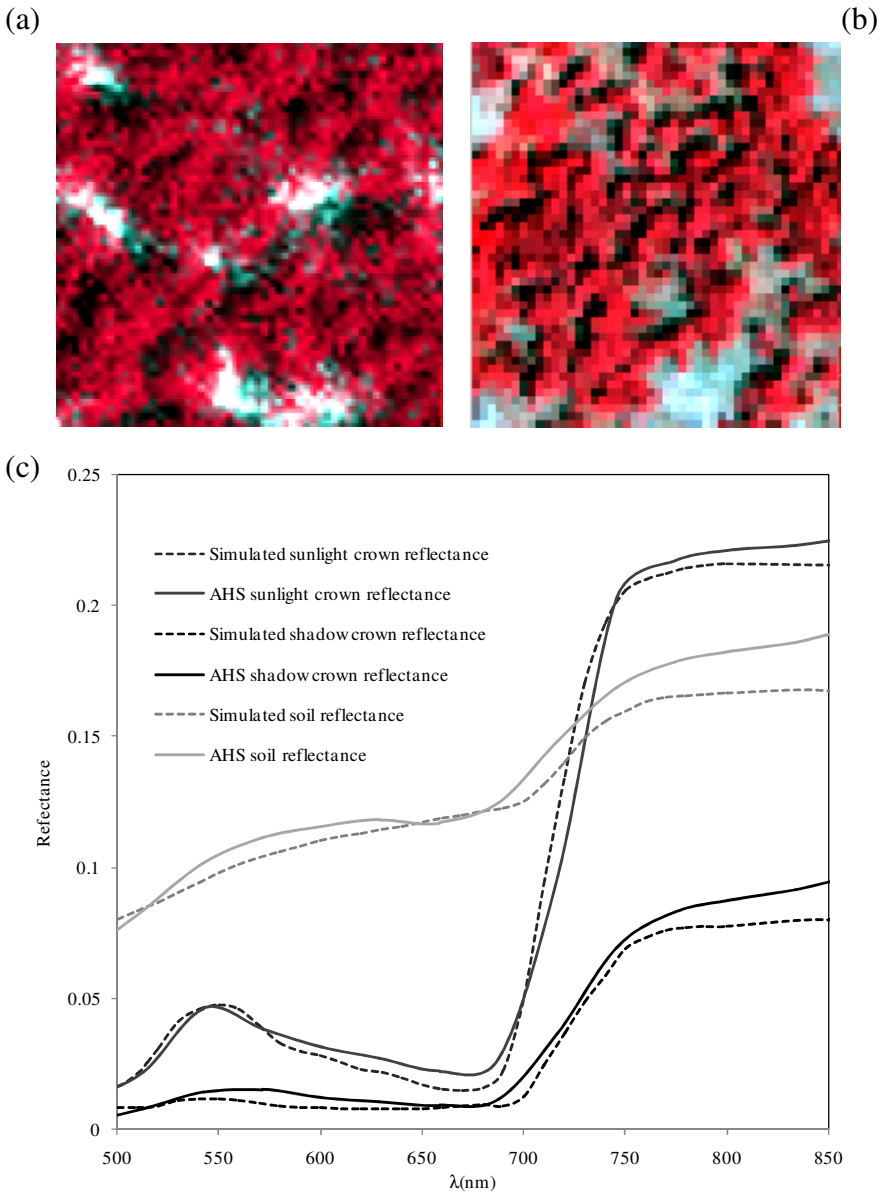

Figure 4.3. PROSPECT-5+DART simulated image (a); High-resolution multispectral image acquired from the AHS sensor (b) Tree crown and soil spectral reflectance obtained from the multispectral image and the simulated image (c).

The databases of spectral reflectance generated from radiative transfer modelling and infinite reflectance models were used for the estimation of Cab and Cx+c content using the optical indices mentioned above (TCARI/OSAVI, R_{750}/R_{710} and R_{515}/R_{570}). The synthetic spectra database was generated using 250 random inputs of Ca+b, Cx+c, N, LAI, soil reflectance and Cm (nominal values detailed in Table 4.2). 150 synthetic spectra were extracted for modelling based on infinitive reflectance approach and canopy DART simulations. 100 additional synthetic spectra were used to evaluate the Root Mean Square Error RMSE obtained for each scaling up approach.

3. Results

3.1. Modelling results

The relationships established between the simulations conducted with the coupled PROSPECT-5 + DART and the different canopy approximations through infinitive reflectance R_∞ models yield significant results ($p>0.0001$) to estimate Cx+c and Ca+b at the crown level. The regression models applied where obtained through quadratic models using R_{515}/R_{570}, and R_{750}/R_{710} or R_{515}/R_{570} and TCARI/OSAVI vegetation indices in the case of Cx+c estimations (2a, 2b, 2c) and using R_{750}/R_{710} or TCARI/OSAVI vegetation indices in the case of Ca+b estimations (3a, 3b,3c).

$Cx+c=f(R_{515}/R_{570})$ [2a]

$Cx+c=f(R_{515}/R_{570}; (R_{515}/R_{570})^{\wedge 2}; R_{750}/R_{710})$ [2b]

$Cx+c=f(R_{515}/R_{570}; (R_{515}/R_{570})^{\wedge 2}; TCARI/OSAVI)$ [2c]

$Ca+b=f(R_{750}/R_{710})$ [3a]

$Ca+b=f(R_{750}/R_{710}; (R_{750}/R_{710})^{\wedge 2})$ [3b]

$Ca+b=f(TCARI/OSAVI; (TCARI/OSAVI)^{\wedge 2})$ [3c]

The coefficient of determination (R^2) obtained from the relationship obtained between random pigments content (Ca+b, Cx+c) and the vegetation indices yield regression coefficients higher than $r^2>0.8$ for both pigments (Table 4.3, 4.4). The results obtained with the coupled PROSPECT-5+DART were similar than the results yielded with infinitive reflectance formulations. Among the different infinitive reflectance models tested, $R_{\infty 1}$ and $R_{\infty 2}$ showed superior results than $R_{\infty 3}$ formulations for both Ca+b (Table 4.3) and Cx+c (Table 4.4). Nevertheless, among the different canopy simulations proposed, no significant differences were found. In the case of Cx+c retrieval, the best coefficients of determination and RMSE values were obtained by using scaling methods based on the model regression (2b) (Table 4.3). Although, there is a consistent improvement of the statistical result obtained using models (2b and 2c) in comparison with the model (2a). For example, in the case of using the $R_{\infty 1}$ scaling method, the RMSE obtained for the model (2a) is 2.11 and for equation (2b) 1.35 ($\mu g/cm^2$) (Table 4.3).

For Ca+b retrieval, the best coefficient of determination and RMSE values were also obtained by using $R_{\infty 1}$, $R_{\infty 2}$ scaling methods and the model (2b). Although, in agreement with the results obtained for Cx+c estimation, results yielded from the different canopy approximations were very similar. The simulation demonstrated that the overall RMSE obtained using the R_{750}/R_{710} index was lower than using the TCARI/OSAVI. For example, in the case of using the $R_{\infty 1}$ scaling method, the RMSE improved from 6.97 to 4.41 ($\mu g/cm^2$) (Table 4.4). Among the different canopy reflectance approximations, the use of quadratic equations based on the R_{750}/R_{710} index

(model 3b) successfully improved the RMSE values of the estimated Ca+b content.

Summarizing, the simulation results obtained demonstrated that model simulation showed consistency for the retrieval of both Cx+c and Ca+b pigments with a significant improve of the estimations while using a model function of R_{515}/R_{570} and R_{750}/R_{710} vegetation indices.

3.2. Results from the Pigment content analysis based on hyperspectral imagery data.

Crown-level relationships established obtained between Cx+c content and the R_{515}/R_{570} index calculated from the airborne imagery showed significant results ($p<0.01$) yielding an average r^2 value of $r^2=0.57$ for Scotch and Black pine samples (Fig. 4.4). Relationships between Ca+b content and R_{750}/R_{710} or TCARI/OSAVI vegetation indices were evaluated separately. Fig. 4.5 and Fig. 4.6 shows the relationships obtained between Ca+b and the R_{750}/R_{710} index (Fig. 4.5) and between Ca+b and TCARI/OSAVI index (Fig. 4.6). For both vegetation indices and both species, the results provide evidence that narrow-bands vegetation indices calculated from hyperspectral imagery showed the capability to determine Ca+b content of the canopy. Further comparison between the performances of each vegetation indices showed that the coefficient of determination for R_{750}/R_{710} index was higher than for TCARI/OSAVI index. Although all relationships showed significant results ($p<0.001$), the mean coefficient of determination between Ca+b and R_{750}/R_{710} red edge was $r^2=0.63$, while a $r^2=0.50$ was obtained for using TCARI/OSAVI.

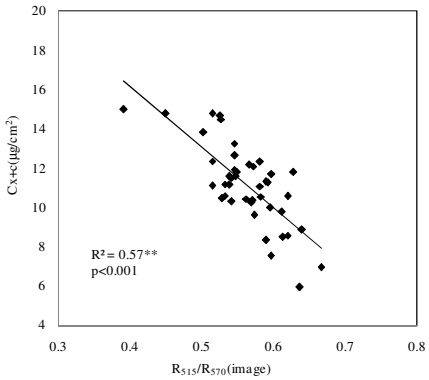

Figure 4.4. Relationships obtained at the crown level between the R_{515}/R_{570} index obtained from the airborne hyperspectral imagery and Cx+c measured in the field for *Pinus sylvestris* and *Pinus nigra*.

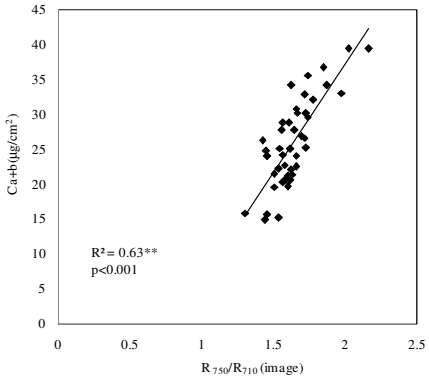

Figure 4.5. Relationships obtained at the crown level between the red edge index obtained from the airborne hyperspectral imagery and Ca+b content measured in the field for *Pinus sylvestris* and *Pinus nigra*.

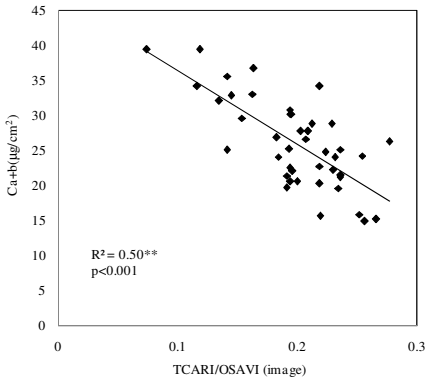

Figure 4.6. Relationships obtained at the crown level between the TCARI/OSAVI index obtained from the airborne hyperspectral imagery and Ca+b measured in the field for *Pinus sylvestris* and *Pinus nigra*.

Table 4.3. Simulation results obtained for crown carotenoid content (Cx+c) retrieval with PROSPECT-5 and different canopy approximations through infinitive reflectance R_∞ formulations and DART.

PROSPECT-5 + DART: Cx+c*, Ca+b*, N*, LAI*, ρsoil*					
Cx+c=f(R_{515}/R_{570})		Cx+c=f(R_{515}/R_{570}; $(R_{515}/R_{570})^{\wedge 2}$; R_{750}/R_{710})		Cx+c=f(R_{515}/R_{570}; R_{515}/R_{570}^2; TCARI/OSAVI)	
R^2	**RMSE (µg/cm²)**	**R^2**	**RMSE (µg/cm²)**	**R^2**	**RMSE (µg/cm²)**
0.62	2.44	0.81	1.7	0.83	1.6
PROSPECT-5 +$R_{\infty 1}$: Cx+c*, Ca+b*, N*					
Cx+c=f(R_{515}/R_{570})		Cx+c=f(R_{515}/R_{570}; $(R_{515}/R_{570})^{\wedge 2}$; R_{750}/R_{710})		Cx+c=f(R_{515}/R_{570}; R_{515}/R_{570}^2; TCARI/OSAVI)	
R^2	**RMSE (mg/cm²)**	**R^2**	**RMSE (µg/cm²)**	**R^2**	**RMSE (µg/cm²)**
0.77	2.11	0.91	1.35	0.89	1.45
PROSPECT-5 +$R_{\infty 2}$: Cx+c*, Ca+b*, N*					
Cx+c=f(R_{515}/R_{570})		Cx+c=f(R_{515}/R_{570}; $(R_{515}/R_{570})^{\wedge 2}$; R_{750}/R_{710})		Cx+c=f(R_{515}/R_{570}; R_{515}/R_{570}^2; TCARI/OSAVI)	
R^2	**RMSE (µg/cm²)**	**R^2**	**RMSE (µg/cm²)**	**R^2**	**RMSE (µg/cm²)**
0.77	2.11	0.91	1.36	0.88	1.45
PROSPECT-5 +$R_{\infty 3}$: Cx+c*, Ca+b*, N*					
Cx+c=f(R_{515}/R_{570})		Cx+c=f(R_{515}/R_{570}; $(R_{515}/R_{570})^{\wedge 2}$; R_{750}/R_{710})		Cx+c=f(R_{515}/R_{570}; R_{515}/R_{570}^2; TCARI/OSAVI)	
R^2	**RMSE (µg/cm²)**	**R^2**	**RMSE (µg/cm²)**	**R^2**	**RMSE (µg/cm²)**
0.72	2.28	0.79	1.86	0.89	1.42

Table 4.4. Simulation results obtained for crown chlorophyll content (Ca+b) retrieval with PROSPECT-5 and different canopy approximations through infinitive reflectance R_∞ formulations and DART.

PROSPECT-5 + DART: Cx+c*, Ca+b*, N*, LAI*, ρsoil*					
$Ca+b=f(R_{750}/R_{710})$		$Ca+b=f(R_{750}/R_{710}; (R_{750}/R_{710})^{\wedge 2})$		$Ca+b=f(TCARI/OSAVI; TCARI/OSAVI)^{\wedge 2}$	
R^2	**RMSE (µg/cm²)**	**R^2**	**RMSE (µg/cm²)**	**R^2**	**RMSE (µg/cm²)**
0.82	6.08	0.86	5.34	0.8	6.97
PROSPECT-5 +$R_{\infty 1}$: Cx+c*, Ca+b*, N*					
$Ca+b=f(R_{750}/R_{710})$		$Ca+b=f(R_{750}/R_{710}; (R_{750}/R_{710})^{\wedge 2})$		$Ca+b=f(TCARI/OSAVI; TCARI/OSAVI)^{\wedge 2}$	
R^2	**RMSE (mg/cm²)**	**R^2**	**RMSE (µg/cm²)**	**R^2**	**RMSE (µg/cm²)**
0.92	4.55	0.93	4.41	0.8	6.97
PROSPECT-5 +$R_{\infty 2}$: Cx+c*, Ca+b*, N*					
$Ca+b=f(R_{750}/R_{710})$		$Ca+b=f(R_{750}/R_{710}; (R_{750}/R_{710})^{\wedge 2})$		$Ca+b=f(TCARI/OSAVI; TCARI/OSAVI)^{\wedge 2}$	
R^2	**RMSE (µg/cm²)**	**R^2**	**RMSE (µg/cm²)**	**R^2**	**RMSE (µg/cm²)**
0.92	5.26	0.93	4.47	0.8	6.99
PROSPECT-5 +$R_{\infty 3}$: Cx+c*, Ca+b*, N*					
$Ca+b=f(R_{750}/R_{710})$		$Ca+b=f(R_{750}/R_{710}; (R_{750}/R_{710})^{\wedge 2})$		$Ca+b=f(TCARI/OSAVI; TCARI/OSAVI)^{\wedge 2}$	
R^2	**RMSE (µg/cm²)**	**R^2**	**RMSE (µg/cm²)**	**R^2**	**RMSE (µg/cm²)**
0.95	8.21	0.95	5.51	0.84	6.04

Ca+b and Cx+c content were them estimated by scaling-up the optical indices applied to hyperspectral imagery data. Models obtained from the model simulation analysis (Table 4.3, 4.4) were applied using the reflectance extracted from the airborne imagery. The results obtained for each method were compared based on the coefficients of determination and the Root Mean Square Error (RMSE). Table 4.5 shows the results obtained for Cx+c and Ca+b pigments content retrieval at canopy level for Scotch pine stands. According to the results, among all the canopy approximation analyzed, the estimation of Cx+c yielded a RMSE ranging from 1.4 to 2.12 $\mu g/cm^2$ when using quadratic models based on R_{515}/R_{570} and R_{750}/R_{710} indices (Table 4.5). The model performance for Ca+b using R_{750}/R_{710} yielded reasonable accuracy, ranging between 4.41 and 9.04 $\mu g/cm^2$. Although, best results were obtained when PROSPECT-5 was coupled to either DART radiative transfer model or through the $R_{\infty 3}$ infinitive reflectance simulation. In contrast, the analysis carried out introducing TCARI/OSAVI into the model for both, Cx+c and Ca+b pigment retrieval showed significant discrepancies, yielding poor RMSE values for all models analyzed. For example, the best results obtained for Scotch pine stands through the $R_{\infty 3}$ infinitive reflectance simulation yielded values of RMSE=22.76 and 4.78 $\mu g/cm^2$ respectively for Ca+b and Cx+c estimations. Similar results were obtained in the case of Black pine stands (Table 4.6). For this specie, pigment content retrieval yielded a RMSE ranging from 1.27 to 1.87 $\mu g/cm^2$, for Cx+c and from 3.75 to 14.28 $\mu g/cm^2$, for Ca+b using the R_{750}/R_{710} vegetation index into the models (Table 4.6). In agreement with the results obtained for Scotch pine, the best scaling-up results were obtained based on the coupled PROSPECT-5+DART and PROSPECT+ $R_{\infty 3}$ infinitive reflectance simulation.

Table 4.5. Coefficients of determination and RMSE obtained from airborne imagery for Cx+c and Ca+b estimation with models obtained through scaling up for *Pinus sylvestris* samples. Simulations used were PROSPECT-5 linked to three infinitive reflectance formulations ($R_{\infty 1}$; $R_{\infty 2}$; $R_{\infty 3}$) and DART.

CANOPY APPROXIMATION APPROACHES:	PROSPECT-5 +$R_{\infty 1}$		PROSPECT-5 +$R_{\infty 2}$		PROSPECT-5 +$R_{\infty 3}$		PROSPECT-5 +DART	
Regression models for the estimation of Cx+c and Ca+b content	R^2	RMSE (µg/cm^2)	R^2	RMSE (µg/cm^2)	R^2	RMSE (µg/cm^2)	R^2	RMSE (µg/cm^2)
Cx+c=$f((R_{515}/R_{570}; R_{515}/R_{570})^{\wedge 2}; R_{750}/R_{710})$	0,66	2.12	0,66	2.09	0,69	1.45	0,66	1.4
Cx+c=$f((R_{515}/R_{570}; R_{515}/R_{570})^{\wedge 2}$; TCARI/OSAVI)	0,66	6.55	0, 66	6.55	0,60	4.78	0,60	5.55
Ca+b=$f(R_{750}/R_{710}; (R_{750}/R_{710})^{\wedge 2})$	0,70	9.04	0,70	8.95	0,69	5.5	0,69	4.41
Ca+b=f(TCARI/OSAVI; (TCARI/OSAVI)$^{\wedge 2}$)	0,57	43.07	0,57	42.3	0,55	22.76.54	0,56	30.59

Table 4.6. Coefficients of determination and RMSE obtained from airborne imagery for Cx+c and Ca+b estimation with models obtained through scaling up for *Pinus nigra* samples. Simulations used were PROSPECT-5 linked to three infinitive reflectance formulations ($R_{\infty 1}$; $R_{\infty 2}$; $R_{\infty 3}$) and DART.

CANOPY APPROXIMATION APPROACHES:	PROSPECT-5 +$R_{\infty 1}$		PROSPECT-5 +$R_{\infty 2}$		PROSPECT-5 +$R_{\infty 3}$		PROSPECT-5 +DART	
Regression models for the estimation of Cx+c and Ca+b content	R^2	RMSE (µg/cm^2)	R^2	RMSE (µg/cm^2)	R^2	RMSE (µg/cm^2)	R^2	RMSE (µg/cm^2)
Cx+c=$f((R_{515}/R_{570}; R_{515}/R_{570})^{\wedge 2}; R_{750}/R_{710})$	0,43	1.87	0,43	1.84	0,37	1.27	0,42	1.54
Cx+c=$f((R_{515}/R_{570}; R_{515}/R_{570})^{\wedge 2}$; TCARI/OSAVI)	0,33	3.21	0,33	3.2	0,37	1.45	0,37	2.74
Ca+b=$f(R_{750}/R_{710}; (R_{750}/R_{710})^{\wedge 2})$	0,72	14.28	0,69	14.17	0,72	3.75	0,72	5.58
Ca+b=f(TCARI/OSAVI; (TCARI/OSAVI)$^{\wedge 2}$)	0,67	38.73	0,67	37.89	0,68	18.93	0,1	26.94

Among the data analysed for both species, Fig. 4.7 and Fig. 4.8 show the relationships between estimated and measured Cx+c and Ca+b pigment retrievals, respectively. In both cases, the lowest RMSE were obtained for the $R_{\infty 3}$ model (RMSE=1.37µg/cm^2) and DART (1.48 µg/cm^2) while $R_{\infty 1}$ and $R_{\infty 2}$ yielded lower RMSE values (RMSE=2.00 µg/cm^2 and RMSE =1.97

µg/cm^2, respectively). Those results agree with similar analysis performed on vineyards canopies (Zarco-Tejada et al., (submitted)).

Figure 7. Validation results obtained for the estimation of Cx+c from the airborne hyperspectral imagery using R_{515}/R_{570} and red edge based on infinitive formulations ($R_{\infty 1}$ and $R_{\infty 2}$) (a) and the infinitive formulation ($R_{\infty 3}$) and DART(b).

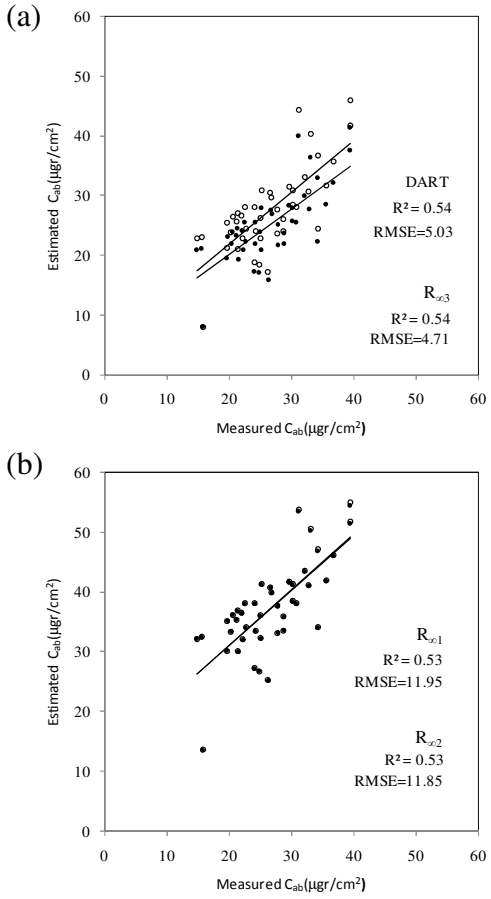

Figure 4.7. Validation results obtained for the estimation of Cx+c from the airborne hyperspectral imagery using R_{515}/R_{570} and red edge based on infinitive formulations ($R_{\infty 1}$ and $R_{\infty 2}$) (a) and the infinitive formulation ($R_{\infty 3}$) and DART(b).

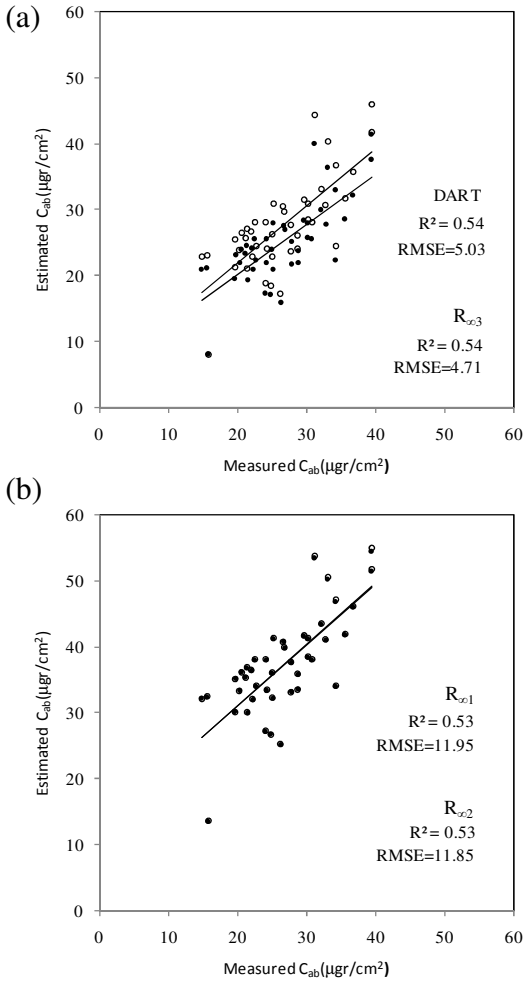

Figure 4.8. Validation results obtained for the estimation of Ca+b from the airborne hyperspectral imagery using red edge based on infinitive formulations ($R_{\infty 1}$ and $R_{\infty 2}$) (a) and the infinitive formulation ($R_{\infty 3}$) DART(b).

It is relevant to reinforce the high performance obtained on forest canopies with simpler infinitive reflectance models based on Hapke compared to the results obtained with more complex and computationally expensive approaches such as the DART model. Those results may be explained due pure crown reflectance extraction can be performed based on the high resolution of the images; therefore, model simulation of structural

parameters affecting the reflectance of the canopy are not required. Then, the models analyzed were applied at image level, mapping Cx+c and Ca+b with both the R_{515}/R_{570} and R_{750}/R_{710} vegetation indices acquired from the AHS hyperspectral imagery (Fig. 4.9 and 4.10). Mapping results enabled the estimation of both pigments at the crown level for the entire scene showing the spatial variability of caroteonoid content with areas with high content (Fig. 4.9) and low (Fig. 4.10) content of Cx+c.

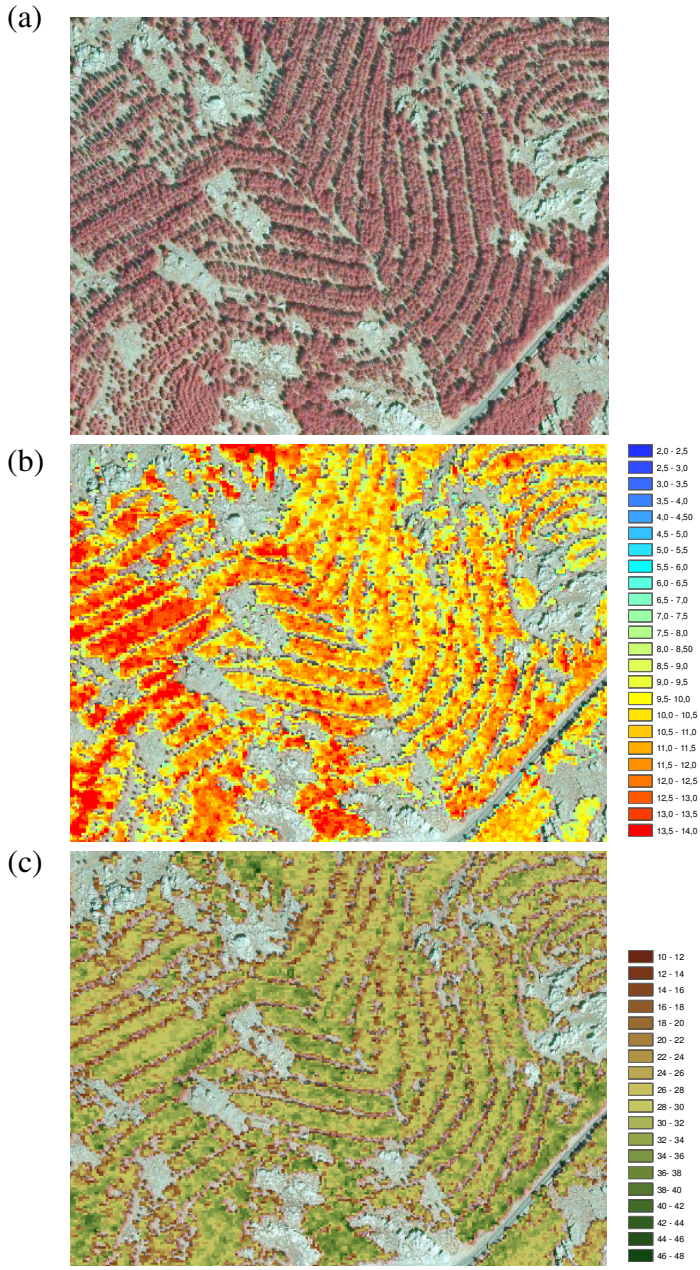

Figure 4.9. Mapping results obtained on two samples of *P. sylvestris* and *P. nigra* forest acquired with thy hyperspectral imager AHS in a sample area with high concentration of chlorophyll and carotenoid pigments. Color Infrared image (a), Cx+c content was estimated from indices R_{515}/R_{570} and R_{700}/R_{750} using $R_{\infty 3}$ (b), Ca+b content was estimated from R_{700}/R_{750} using $R_{\infty 3}$ (c).

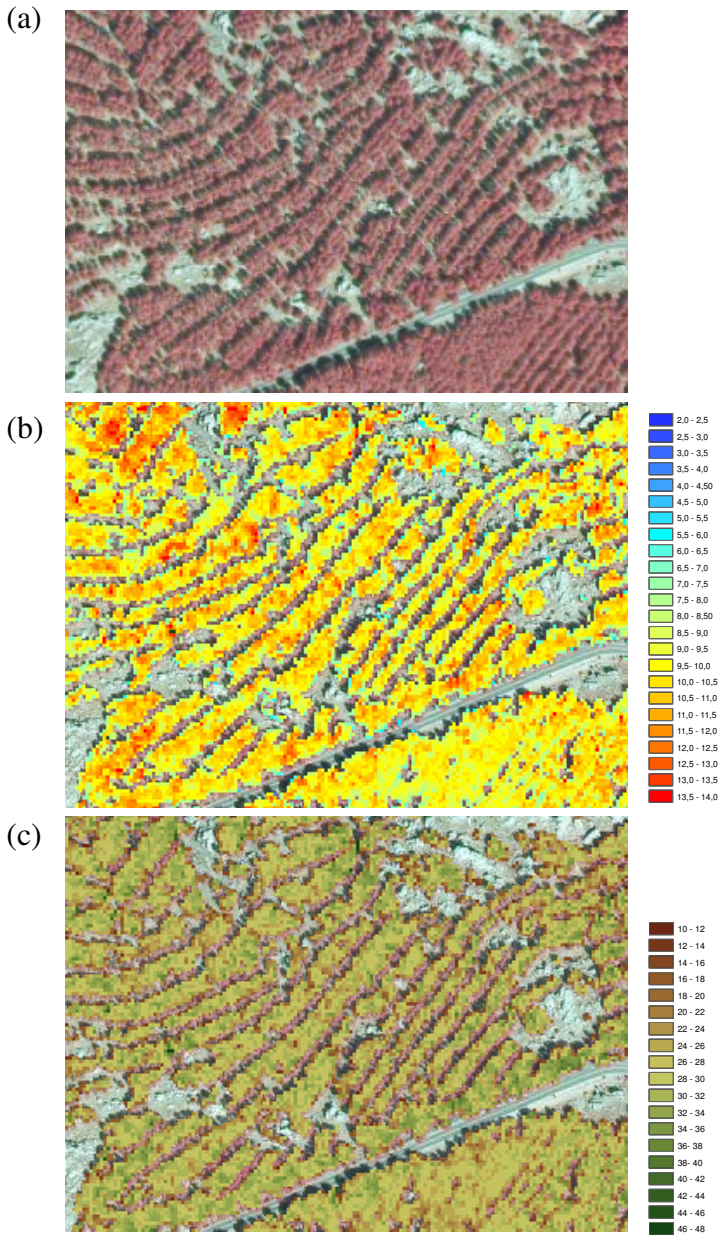

Figure 4.10. Mapping results obtained on two samples of *P. sylvestris* and *P. nigra* forest acquired with thy hyperspectral imager AHS in a sample area with low concentration of chlorophyll and carotenoid pigments. Color Infrared image (a), Cx+c content was estimated from indices R_{515}/R_{570} and R_{700}/R_{750} using $R_{\infty 3}$ (b), Ca+b content was estimated from R_{700}/R_{750} using $R_{\infty 3}$ (c).

4. Discussion

Model simulation analysis and experimental results achieved in this study at the crown level and from hyperspectral airborne flights confirmed the sensibility of R_{515}/R_{570} and R_{750}/R_{710} vegetation index for the simultaneous estimation of Cx+c and Ca+b respectively for Scotch and Black pine stands. The optical indices evaluated and related to Ca+b were previously analyzed by other authors (Moorthy et al., (2008) ; Zhang et al; 2002; Zarco-Tejada et al., (2001, 2004a)) for conifer forest. Recently, the R_{515}/R_{570} index was proposed by Hernandez-Clemente for Scotch pine sites, demonstrating to be significantly related to Cx+c content both at leaf (r^2>0.72; P<0.001) and canopy (r^2>0.72; P<0.001) based on imagery acquired from UAV platforms with spatial resolution less than 1m. Although these studies demonstrate the sensibility of specific narrow-band indices to pigment content, more studies for the successful retrieval of both pigments are needed at the crown level. This study present a methodology for the retrieval of both Ca+b and Cx+c content at the canopy level based of scaling-up the narrow vegetation indices for forest type canopies.

The estimation of pigment composition on forest canopies implies the analysis of the potential confounding effects of open canopies structures on narrow band vegetation indices (Zarco-Tejada et al., 2001). For this reason, different canopy simulation approaches were compared in this research; using simpler infinitive reflectance and 3-D canopy This work demonstrated the capability of scaling-up methods applied through infinitive reflectance approximations or DART canopy simulations using R_{515}/R_{570} and R_{750}/R_{710} index for the estimation of Cx+c and Ca+b content based on airborne hyperspectral imagery acquired at 2m spatial resolution on Scotch and Black

Pine stands. This results agree with the results obtained by Zarco-Tejada et al (2012), demonstrating the feasibility of scaling up methods based on infinitive reflectance approach. According to the analysis carried out in pine forest sites comparing the performance of TCARI/OSAVI and the R_{750}/R_{710} index, this study demonstrate the superior results obtained considering the R_{750}/R_{710} index for both Cx+c and Ca+b estimations. Those results differs from the relationship abstained between TCARI/OSAVI and canopy Ca+b content for crop canopies or open canopies (Haboudane et al., 2002; Zarco-Tejada et al.,2004b,2005). Although, the successful results obtained with the R_{750}/R_{710} index agree with the results obtained by Moothy et al., (2008) analyzing Ca+b content using hyperspectral observations on Jack Pine stands and Zarco-Tejada et al., (2001) studding the same pigment on Sugar Maple stands. However, both studies were carried out based on simple regression models while this study demonstrate a superior performance of pigment retrieval based on quadratic regression models.

In the case of Cx+c, the improvement obtained for the retrieval of Cx+c by quadratic regression models combining the R_{515}/R_{570} vegetation index and a Ca+b-releted optical index agree with the results obtained by Zarco-Tejada et al; (Submitted) for crops canopies. Although, this study demonstrates the higher performance of R_{750}/R_{710} from TCARI/OSAVI, in contrast to the results previously reported for crops canopies (Haboudane et al., 2002; Zarco-Tejada et al 2004b, 2005). This result may be explained by the higher effect that tree shadow pixels produce on TCARI/OSAVI index in comparison to the R_{750}/R_{710} index . As consequence, the quadratic regression model combining the R_{515}/R_{570} and the R_{750}/R_{710} index had been demonstrated to improve the estimations of Cx+c for dense conifer canopies.

It is remarkable the accuracy of scaling up methods applied to achieve Ca+b and Cx+c estimations based on infinitive reflectance approach. Despite our efforts analysing complex 3-D radiative transfer models to include the structural variations found on conifer forest, simpler approaches ($R_{\infty 3}$) yielded similar results. This may be due the fact that very high resolution was used to extract pure crown reflectance from high spatial resolution hyperspectral imagery, removing mixed pixels and shadows effects. Although, the spatial resolution is not a single factor affecting pure crown delimitation. It is important to highlight that the forest canopy analyzed in this study has a relative low heterogeneity as being the product of a systematic afforestation with relative null species mixture. Therefore, the results obtained with infinitive reflectance approach and DART simulation analysis might vary on other types of canopies, where the delimitation of pure crown is more complicated due the vegetation mixture or structural heterogeneity of the canopy. This implies that further studies should be carried out on more complex forest canopies comparing different simulation reflectance approach.

So far, the results obtained in this work demonstrate the feasibility of hyperspectral images for mapping Ca+b and Cx+c content at the crown level for Scot and Black pine afforestation using scaling up methods based on simplier infinitive reflectance models. In addition, the promising results obtained with 3-D model simulation demonstrated the capability of this methodology for more complex forest canopies. The generation of biochemical maps at the crown level could play a critical rule on the early

detection of forest decline processes enabling their application in precision forestry.

5. Conclusions

Results obtained in this paper indicate the feasibility of estimating needle simultaneous Ca+b and Cx+c by scaling-up methods of hyperspectral airborne reflectance data acquired from conifer canopies. Modelling analysis and experimental measurements were conducted for the estimation of pigment content at the crown level yielding mean errors of 1.42 μg/cm-2 for Cx+c retrieval and 4.87 μg/cm-2 for Ca+b retrieval. Those results were obtained based on the scaling up of pure crown vegetation indices (R_{750}/R_{710}, R_{570}/R_{515}) by using modelling simulations conducted with infinitive reflectance models based on Hapke and DART canopy reflectance modes linked to PROSPECT-5. Modelling and experimental results demonstrated the superior performance of the R_{750}/R_{710} index from the TCARI/OSAVI index for pigment retrieval on forest canopies.

The accuracy obtained by employing scaling up methods that used simpler approaches, such us the infinitive reflectance formulation proposed by Hapke was comparable to more complex canopy reflectance approximations such us DART model.

Finally, consistency was found between ground truth pigment at the study sites and canopy reflectance measured with the AHS hyperspectral sensor when using pigment related optical indices. The capability to remotely detect, assess and delineate areas of forest decline by airborne sensors would facilitate the study and ultimate understanding of the forest decline problem.

References

Allen, C., Macalady, A., Chenchouni, H., Bachelet, D., McDowell, N., Vennetier, M., Kitzberger, T., Rigling, A., Breshears, D., Hogg, E.; Gonzalez, P., Fensham, R., Zhangm, Z., Castro, J., Demidova, N., Lim, J., Allard, G., Running, S., Semerci, A., & Cobb, N. (2010). A global overview of drought and heat-induced tree mortality reveals emerging climate change risks for forests. *Forest Ecology and Management, 259,* 660-684

Batič, F., Kalan, P., Kraigher, H., Šircelj, H., Simončič, P., Vidergar-Gorjup, N., & Turk B. (1999). Bioindication of different stresses in forest decline studies in Slovenia. *Water, Air and Soil Pollution*, *116*, 377-382.

Carter, G.A. & Miller, R.L. (1994). Early detection of plant stress by digital imaging within narrow stress-sensitive wavebands. *Remote Sensing Environment*, 50, 295-302.

Carter, G. A. (1994). Ratios of leaf reflectances in narrow wavebands as indicators of plant stress. *International Journal of Remote Sensing*, *15*, 697-704.

Demarez V. & Gastellu-Etchegorry J.P. (2000). A modelling approach for studying forest chlorophyll content. *Remote Sensing of Environment*, *71*, 226-238.

Gastellu-Etchegorry, J. P., Martin E., & Gascon, F. (2004). DART: a 3D model for simulating satellite images and studying surface radiation budget. *Internation Journal of Remote Sensing*, *25*, 73-96.

Gitelson, A. A., Zur, Y., Chivkunova, O. B., & Merzlyak, M. N. (2002). Assessing carotenoid content in plant leaves with reflectance spectroscopy. *Journal of Photochemistry and Photobiology B-Biology*, *75*, 272-281.

Haboudane, D., Miller, J.R., Tremblay, N., Zarco-Tejada, P.J., & Dextraze, L. (2002). Integrated narrow-band vegetation indices for prediction of crop chlorophyll content for application to precision agriculture. *Remote Sensing of Environment*, *81*, 416-426.

Hapke, B. (1993). Theory of Reflectance and Emittance Spectroscopy. Cambridge, U.K. Univ. Press.

Hernández-Clemente, R., Navarro-Cerrillo, R. M., Suárez, L., Morales, F., & Zarco-Tejada, P. J. (2011). Assessing structural effects on PRI for stress detection in conifer forests. *Remote Sensing of Environment*, *115*, 2360-2375.

Hernández-Clemente, R., Navarro-Cerrillo, R.M., & Zarco-Tejada, P.J., Carotenoid content estimation in an heterogeneous conifer forest using narrow-band indices and PROSPECT + DART simulations, *Remote Sensing of Environment* (submitted).

Hoshizaki T, Rock BN, & Wong SKS. (1988). Pigment analysis and spectral assessment of spruce trees undergoing forest decline in the NE United States and Germany. *GeoJournal, 17*, 173-178.

Le Maire, G., François, C., Soudani, K., Berveiller, D., Pontailler, J.-Y., Bréda, N., Genet, H., Davi, H., & Dufrêne, E., (2008). Calibration and validation of hyperspectral indices for the estimation of broadleaved forest leaf chlorophyll content, leaf mass per area, leaf area index and leaf canopy biomass. *Remote Sensing of Environment, 112*, 3846-3864.

Lichtenhaler, H. K., (1998). The stress concept in plants: An introduction. *Annals of the New York Academy of Science*, *851*, 187-198.

Lippert M., Steiner K., Payer H.D., Simons S., Langebartels C., & Sandermann H. (1996) Assessing the impact of ozone on photosynthesis of European beech (Fagus syl6atica L.) in environmental chambers. *Trees*, *10*, 268–275

Main, R., Cho, M. A., Mathieu, R., O'Kennedy, M. M., Ramoelo, A. & Koch, S. (2011). An investigation into robust spectral indices for leaf chlorophyll estimation. *ISPRS Journal of Photogrammetry and Remote Sensing* , *66*, 751-761

Malenovsky, Z., Martin, E., Homolová, L.,Gastellu-Etchegorry, J. P., Zurita-Milla, R., Schaepman, M. E., Pokorný, R., Clevers, J. G. P. W., & Cudlín, P. (2008). Influence of woody elements of a Norway spruce canopy

on nadir reflectance simulated by the DART model at very high spatial resolution. *Remote Sensing of Environment*, *112*, 1-18.

Matyssek, R., M.S. Günthardt-Goerg, T. Keller & Scheidegger. C. (1991). Impairment of gas exchange and structure in birch leaves (*Betula pendula*) caused by low ozone concentrations. *Trees* , *5*, 5-13.

Meggio F., Zarco-Tejada, P.J., Núñez L.C., Sepulcre-Cantó G., Gonzalez M.R. & Martin, P. (2010). Grape quality assessment in vineyards affected by iron deficiency chlorosis using narrow-band physiological remote sensing indices. *Remote Sensing of Environment*, *114*, 1968-1986.

Moorthy I., Miller J. R., & Noland T. L. (2008). Estimating chlorophyll concentration in conifer needles with hyperspectral data: An assessment at the needle and canopy level. *Remote Sensing of Environment*, *112*, 2824-2838.

Peñuelas, J., I. Filella, & Gamon. J.A. (1995). Assessment of photosynthetic radiationuse efficiency with spectral reflectance. *New Phytologist*, *131*, 291-296.

Rock, B.N., Hoshizaki, T., & Miller J.R. (1988). Comparison of in situ and airborne spectral measurements of the blue shift associated with forest decline. *Remote Sensing of Environment*, *24*, 109-127.

Pinty B, Widlowski JL, Taberner M, Gobron N, Verstraete MM, Disney M, Lewis P, Gascon F, Gastellu JP, Jiang L, Li X, Su L, Tang S, Wang H, Wang J, Yan G, Zang H, Kuusk A, Nilson T, Ni-Meister W, North P, Qin W, Thompson R, & Verhoef W. (2004). RAdiation Transfer Model Intercomparison (RAMI) exercise: Results from the second phase. *Journal of Geophysical Research D: Atmospheres, 109,* 1-19.

Rondeaux, G., Steven, M. & Baret, F. (1996). Optimization of soil-adjusted vegetation indices. *Remote Sensing of Environment*, *55*, 95-107.

Tausz M., Jiménez M.S., Grill D. (1998). Antioxidative defense and photoprotection in pine needles under field conditions—a multivariate approach to evaluate patterns of physiological responses at natural sites. *Physiologia Plantarum*,104, 760–764.

Yamada, N. & Fujimura, S. (1991). Nondestructive measurement of chlorophyll pigment content in plant leaves from three-color reflectance and transmittance. *Applied Optics*, 30, 3964-3973.

Verhoef, W. (1984). Light scattering by leaf layers with application to canopy reflectance modeling: the SAIL model. *Remote Sensing of. Environment*, *16*, 125-141.

Zhang, Q., Xiao, X., Braswell, B., Linder, E., Baret, F., & Moore, B. (2005). Estimating light absorption by chlorophyll, leaf and canopy in a deciduous broadleaf forest using MODIS data and a radiative transfer model. *Remote Sensing of Environment*, *99*, 357-371.

Zarco-Tejada, P.J., Miller, J.R., Mohammed, G.H., Noland, T.L., & Sampson, P.H. (2001). Scaling-up and Model Inversion methods with narrow-band Optical Indices for Chlorophyll Content Estimation in closed Forest Canopies with Hyperspectral Data. *IEEE Transactions on Geoscience and Remote Sensing*, *39*, 1491-1507.

Zarco-Tejada, P.J., Miller J. R., Harron, J., Hu, B., Noland, T. L., Goel, N., Mohammed, G. H. & Sampson P. H. (2004a). Needle chlorophyll content estimation through model inversion using hyperspectral data from boreal conifer forest canopies. *Remote Sensing of Environment*, *89*, 189-199.

Zarco-Tejada, P.J., J.R. Miller, A. Morales, A. Berjón, & J. Agüera, (2004b). Hyperspectral Indices and Model Simulation for Chlorophyll Estimation in Open-Canopy Tree Crops. *Remote Sensing of Environment*, *90*, 463-476.

Zarco-Tejada, P.J., Berjón, A., López-Lozano, R., Miller, J.R., Martín, P., Cachorro, V., González, M.R., & Frutos, A., (2005). Assessing Vineyard Condition with Hyperspectral Indices: Leaf and Canopy Reflectance Simulation in a Row-Structured Discontinuous Canopy. *Remote Sensing of Environment*, *99*, 271-287

Zarco-Tejada, P. J., González-Dugo, V., & Berni, J. A. J., (2012). Fluorescence, temperature and narrow-band indices acquired from a UAV

platform for water stress detection using a micro-hyperspectral imager and a thermal camera. *Remote Sensing of Environment*, *117*, 322-337.

Zarco-Tejada, P.J., Guillén-Climent, M.L., Hernández-Clemente, R., Catalina, A., González, M.R., & Martín, P., Estimating carotenoid content in vineyards using high resolution hyperspectral imagery acquired from an unmanned aerial vehicle (UAV)., Submitted.

Chapter 4. Scaling-up methods for chlorophyll and carotenoid content estimation using narrow-band optical indices and radiative transfer model in conifer forest

5. Synthesis.

Chapter 5

5.1. General discussion

The primary objective of this research was to find operational tools for the early detection of forest decline processes. So far, remote sensing techniques had been widely applied in forest management (Schlerf et al., 2005; Waring et al., 2011). However, most of these works are focused on structural parameters, which are indicators of long-term stresses related to advanced states of damage and irreversible die-back processes. It is critical to seek pre-visual techniques to detect forest stress and determine latent diseases because early diagnostic of the damage can prevent from passing to more progressive stage (Sampson et al., 2000). This PhD research was focused on the analysis of the short-term physiological indicators of forest decline. The initial hypothesis of this work was to assume that one of the main reactions to stress condition is a decreasing of the photosynthesis rate produced by an alteration of pigment content and an increasing of the rate of stomatal closure. Remote sensing techniques have the capability of detect biochemical alterations based on specific narrow band indices and stomatal closure rate, based on thermal information. Different studies have demonstrated the sensibility of narrow band indices to specific pigment content at the leaf level (Chappelle et al., 1992; Gitelson et al., 2002). Although, according to the results presented in this research, leaf level results cannot be extrapolated to the canopy level due the confounding effects of BRDF produced by canopy structure, shadows and soil background. Those results agree with previous studies (Malenovsky et al., 2006; Suárez et al. 2008; Zarco-Tejada et al., 2001) and similar effects had been found working with thermal data (Sepulcré-Cantó et al., 2009).

Therefore, operational remote sensing tools based on the quantification of biochemical processes at the crown level requires further research to develop accurate methodologies considering structural properties of forest canopies.

The scientific contribution of this work was the analysis of the scaling-up of narrow-band vegetation indices related with the physiological status of the forest. Structural parameters affecting the performance of the spectral information from the leaf to the canopy level were assessed to ensure the robustness of vegetation indices formulations. Based on this work, appropriate algorithms for the retrieval of biochemical and biophysical properties of conifer canopies from high spatial resolution hyperspectral data are presented.

Radiative transfer simulation methods were applied using INFORM and DART as a canopy reflectance model linked with a modified LIBERTY and PROSPECT-5 leaf model in order to assess the effects of canopy structure on different formulations of vegetation indices related to pigment content. The simulations were conducted by computing canopy reflectance spectra with different values of structural parameters (LAI, tree density) and pigment content (chlorophyll and carotenoids), assessing the effects of these biochemical and structural inputs on the proposed vegetation indices formulations.

The primary approximation was focused on the Photochemical Reflectance Index (Gamon et al., 1992). Assessing plant physiological condition based on PRI at canopy scale is a difficult approach due to the different factors affecting this index, such as viewing and illumination geometry effects, crown architecture and shadow/sunlit fraction (Barton and

North, 2001; Hall et al., 2008; Hilker et al., 2008; Middleton et al., 2009; Suárez et al., 2008). The results presented demonstrated that the airborne-level PRI index is sensitive to the de-epoxidation of the xanthophyll pigment cycle caused by water stress levels (Chapter 2). Results showed that the airborne level PRI indices were sensitive to EPS but, as expected were also highly affected by structural parameters. A new formulation of PRI was proposed based on the analysis of structural parameters affecting the range of absorption spectra of photosynthetic pigments. The new index proposed (PRI_{512}) shows higher relationships with EPS (r^2=0.40) than previous formulations such us PRI_{570} (r^2=0.21), demonstrating with the EPS vs NDVI relationship that structural effects due to stress were not the major driver (r^2=0.13). Significant relationships were also found between T and EPS, although with lower coefficient of determination (r^2=0.37), this results agree with the results found by other authors in crops canopies (Sepulcré-Cantó 2006; Suárez et al., 2008). Simulation and experimental results were consistent with the mapping results obtained for PRI_{512}, showing its ability for accurately mapping stress at both pixel and object levels in conifer forests.

The second approach was to investigate total carotenoid content, usually represented by two (α- and β-) carotenes and five xanthophylls (lutein, zeaxanthin, violaxanthin, antheraxanthin and neoxanthin). The interest of analyzing Cx+c -related vegetation indices has been previously studied at the leaf level (Garrity et al. 2011; Gitelson et al., 2003, 2006). A complete review of traditional formulations and new simple ratios developed by combining bands sensitive to Cx+c absorption in the 500-600 nm region were evaluated based on modelling and experimental data (Chapter 3). Based on this work a new formulation for Cx+c estimation was proposed at

canopy level, assessing its performance with high-resolution airborne imagery. The new simple ratio vegetation indices proposed in this study were found to be significantly related with Cx+c content (r^2>0.6; P<0.001) at leaf and crown level. Nevertheless, this study confirms the robustness of other indices such as the CRI_{550} (r^2>0.93; P<0.001) and CRI_{700} (r^2>0.91; P>0.001) reported in previous studies at leaf level (Gitelson et al., 2003, 2006). Although, the robustness of these indices at leaf level was highly correlated to LAI and tree density values at crown level. These results agree with previous studies that have highlighted the need of assessing the structural and viewing geometry effects to properly scale-up physiological indices from leaf to crown level (Meggio et al., 2010; Suárez et al., 2008).

The final results presented in this thesis accomplish the estimation of biochemical content at the canopy level for conifer forest types. Based on this work a new methodology using scaling-up methods was proposed for the retrieval of Cx+c and Ca+b at canopy level, assessing its performance with high-resolution airborne imagery. This study was based on the methodology proposed by Zarco-Tejada et al.,(2012) for the retrieval of Cx+c content by combining narrow band vegetation indices sensitive to Cx+c and Ca+b simultaneously in order to reduce Ca+b effects. The performance of two Ca+b-related vegetation, the red edge and the TCARI/OSAVI index was compare through a scaling up approach. This study demonstrates the higher performance of the red ege index in comparison with TCARI/OSAVI, for the retrieval of both Cx+c and Ca+b content. This result may be explained by the effect that tree shadow pixels produce on TCARI/OSAVI index in comparison to the red edge index. As consequence, the quadratic regression model combining the R_{515}/R_{570} and the

red edge index had been demonstrated to improve the estimations of Cx+c for dense conifer canopies.

Despite our efforts analysing complex 3-D radiative transfer models to include the structural variations found on conifer forest, simpler approaches ($R_{\infty 3}$) yielded similar results. This may be due the fact that very high resolution was used to extract pure crown reflectance from high spatial resolution hyperspectral imagery, removing mixed pixels and shadows effects. Therefore, it is remarkable to highlight the accuracy of scaling up methods applied to achieve Ca+b and Cx+c estimations based on infinitive reflectance approach.

The early detection and diagnosis of forest decline processes has large potential and the ultimate goal of this dissertation was to face many challenges to explore the capability of remote sensing information to produce a more frequent spatial mapping of these quantitative properties for the status assessment of mountain and/or conifer ecosystems from space-borne image data. In light of the results, it can be concluded that this study demonstrates the possibility of obtaining physiological information of the status of the forest, the early detection of decline processes and the quantification of the main pigments regulating the photosynthesis system, Ca+b and Cx+c pigments based on high resolution hyperspectral data.

5.2. Conclusions

1. The simulation and experimental results demonstrated the sensitivity of PRI and modified PRI indices to canopy structural parameters and, therefore, the need for assessing robust PRI formulations with less structural effects.

2. Based on this work a new formulation of PRI (PRI_{512}) was demonstrated to be less sensitive to changes in LAI values, tree densities and chlorophyll content than PRI_{570}.

3. At the canopy level, experimental study confirms the radiative transfer modelling results, revealed that PRI_{512} was better correlated with EPS and physiological indicators, such as water potential and stomatal conductance, than PRI_{570}.

4. The sensitivity of the PRI indices to structural parameters is critical in conifer forests, where the heterogeneity allows greater influence due to the ground layer and shadows.

5. This work demonstrates the link between PRI_{512} and PRI_{570} with EPS in *P. sylvestris* and *P. nigra* at the leaf level, and it suggests the superior performance at the canopy level for PRI_{512} versus PRI_{570} when mapping previsual stress levels in conifer forests.

6. Traditional vegetation indices related to Cx+c content behave differently at the leaf and at crown level based on radiative transfer modelling and field and airborne data validation.

7. The modelling simulation analysis showed that a new narrow-band vegetation index tested in this study (R_{515} /R_{570}) was sensitive to Cx+c content variations at leaf level and were the most robust indices at canopy level.

8. The vegetation index R_{515} /R_{570} showed the best relationship with Cx+c at both leaf and canopy levels and was the least affected by the canopy

structure. The robustness of other indices at leaf level was highly correlated to LAI and tree density values at crown level.

9. The results obtained in this study show that when the scale increases to stand level, relationships between the spectral response and leaf chemistry tend to break down due to confounding factors related to the structure of the crown and background contributions.

10. The use of narrow-band multispectral cameras on board UAV platforms made it possible to validate this study and obtain high-resolution image data to map biophysical variables. These results demonstrate the feasibility of estimating Cx+c and Ca+b with narrow-band multispectral imagery and confirm the findings obtained by modelling methods.

11. Modelling and experimental results demonstrated the superior performance of the red edge index from the TCARI/OSAVI index for pigment retrieval on forest canopies.

12. This study proposed an specific methodology for estimating needle Ca+b and Cx+c by scaling-up methods of hyperspectral airborne reflectance data acquired from conifer canopies based on the scaling up of pure crown vegetation indices (Red edge, R_{515}/R_{570}) by using modelling simulations conducted with infinitive reflectance models based on Hapke and DART canopy reflectance modes linked to PROSPECT-5. The estimation of pigment content at the crown level carried out using airborne imagery and 3D RT model in conifer canopies yielded mean errors of 1.42 $\mu g/cm^{-2}$ for Cx+c retrieval and 4.87 $\mu g/cm^{-2}$ for Ca+b retrieval.

15. The accuracy obtained by employing scaling up methods that used simpler approaches, such us the infinitive reflectance formulation proposed by Hapke was comparable to more complex canopy reflectance approximations such us DART model.

16. The findings listed below should be useful tools in detecting forest decline processes at an early stage, and may also be regarded as warning signals for forest management and precision forestry. Consistency is found between ground truth pigment at the study sites and canopy reflectance measured with the hyperspectral sensors when using pigment related optical indices. The capability to remotely detect, assess and delineate areas of forest decline by airborne sensors would facilitate the study and ultimate understanding of the forest decline problem.

5.3. Recommendations for further research

The research conducted in this thesis has led us to identify and discuss the need for further research in the following lines:

-The methodology presented for biochemical quantification on conifer forest should be developed for other types of forest, including the same type of forest under natural ecosystems.

-Scaling up methodologies using 3-D radiative transfer modelling and simpler infinitive models should be further compare on different types of ecosystems with different landscape complexity ranges and different spatial resolutions.

-More research is needed on the analysis narrow band vegetation indices at the canopy level considering different types of forest.

- There is a need to evaluate other pigments like anthocyanin, from a physiological point of view (understanding the role on forest decline processes) and from the spectroscopy point of view (analysing robust narrow-band indices and methodologies for the retrieval of anthocyanin content at the image level).

-The analysis of the VAZ cycle and the capability of quantification of Ca+b and Cx+c rate should be used for monitoring physiological processes. Further research focused on the modelization of physiological trends of the vegetation under decline should be achieved.

-The underlying mechanisms behind the relationship between PRI, pigment content rate, and tree growth models should be studied and a standard methodology to assess forest dynamics using remote sensing data should be developed in a future precision forestry.

References

Barton, C.V.M. & North, P.R.J. (2001). Remote sensing of canopy light use efficiency using the Photochemical Reflectance Index. Model and analysis. *Remote Sensing of Environment*, 78, 264-273.

Chappelle, E.W.; Kim, M.S.; & McMurtrey, J.E., III (1992). Ratio analysis of reflectance spectra (RARS): An algorithm for the remote estimation of the concentrations of chlorophyll a, chlorophyll b, and carotenoids in soybean leaves. *Remote Sensing of Environment*, 39, 239-247.

Gamon, J.A.; Peñuelas, J.; & Field, C.B. (1992). A narrow-wave band spectral index that tracks diurnal changes in photosynthetic efficiency. *Remote Sensing of Environment*, 41, 35-44.

Garrity S.R.; Eitel, J.U.H.; & Vierling, L.A. (2011). Disentangling the relationships between plant pigments and the photochemical reflectance index reveals a new approach for remote estimation of carotenoid content, *Remote Sensing of Environment*, 115, 628-635.

Gitelson, A.A.; Zur, Y.; Chivkunova, O.B.; & Merzlyak, M.N. (2002). Assessing carotenoid content in plant leaves with reflectance spectroscopy, *Journal of Photochemistry and Photobiology B-Biology*, 75, 272-281.

Gitelson, A.A.; Gritz, U.; & Merzlyak, M.N. (2003). Relationships between leaf chlorophyll content and spectral reflectance and algorithms for non-destructive chlorophyll assessment in higher plant leaves, *Journal of Plant Physiology*, 160, 271-282.

Gitelson, A.A.; Keydan, G.P.; & Merzlyak, M.N. (2006). Three-band model for noninvasive estimation of chlorophyll, carotenoids, and anthocyanin content in higher plant leaves, *Geophysical Research Letters*, 33, L11402.

Hall, F.G.; Hilker, T.; Coops, N.C.; Lyapustin, A.; Huemmrich, K.F.; Middleton, E.M.; Margolis, H.A.; Drolet, G.G., & Black, T.A. (2008). Multi-angle remote sensing of forest light use efficiency by observing PRI variation with canopy shadow fraction. *Remote Sensing of Environment*, *112*, 3201-3211.

Hilker, T.; Coops, N.C.; Hall, F.G.; Black, T.A.; Wulder, M.A.; Nesic, Z.; & Krishnan P. (2008). Separating physiologically and directionally induced changes in PRI using BRDF models, *Remote Sensing of Environment*, 112, 2777-2788.

Malenovsky, Z.; Albrechtova, J.; Lhotakova, Z.; Zurita-Milla, R.; Clevers, G.P.W.; Schaepman, M.E.; & Cudlín, P. (2006). Applicability of the PROSPECT model for Norway spruce needles, International Journal of Remote Sensing, 27, 5315-5340.

Meggio, F.; Zarco-Tejada, P.J.; Núñez, L.C.; Sepulcre-Cantó, G.; González, M.R.; & Martin, P. (2010). Grape quality assessment in vineyards affected by iron deficiency chlorosis using narrow-band physiological remote sensing indices, *Remote Sensing of Environment*, 114, 1968-1986.

Middleton, E.M.; Cheng, Y.B.; Hilker, T.; Black, T.A.; Krishnan, P.; Coops, N.C.; & Huemmrich K.F. (2009). Linking foliage spectral responses to canopy level ecosystem photosynthetic light use efficiency at a Douglas-fir forest in Canada, *Canadian Journal of Remote Sensing*, 35, 166-188.

Schlerf, M., Atzberger, C.G. and Hill, J.(2005). Remote sensing of forest biophysical variables using HyMap imaging spectrometer data. In: *Remote sensing of environment*, *95,*177-194.

Sampson, P.H., Mohammed, G.H., Zarco-Tejada, P.J., , Miller, J.R., Noland, T.L., Irving, D., Treitz, P.M., Colombo, S.J., & Freemantle, J.,(2000). The Bioindicators of Forest Condition Project: A physiological, remote sensing approach**.** *Forest Chronicle*, *76,* 941-952.

Sepulcré-Cantó, G.; Zarco-Tejada, P.J.; Jiménez-Muñoz, J.C.; Sobrino, J.A.; de Miguel, E.; & Villalobos, F.J. (2006). Detection of Water Stress in an Olive Orchard with Thermal Remote Sensing Imagery, *Agricultural and Forest Meteorology*, 136*,* 31-44.

Suárez, L.; Zarco-Tejada, P.J.; Sepulcré-Cantó, G.; Pérez-Priego, O.; Miller, J. R.; Jiménez-Muñoz, J.C.; & Sobrino, J. (2008). Assessing Canopy PRI for Water Stress Detection with Diurnal Airborne Imagery. *Remote Sensing of Environment*, 112, 560-575.

Waring, R.H.; Coops, N.C.; & Running, S.W. (2011). Predicting satellite-derived patterns of large-scale disturbances in forests of the Pacific Northwest Region in response to recent climatic variation, *Remote Sensing of Environment*. 115, 3554-3566.

Zarco-Tejada, P. J.; Miller, J. R.; Mohammed, G. H.; Noland, T. L.; & Sampson, P.H. (2001). Scaling-up and model inversion methods with

narrow-band optical indices for chlorophyll content estimation in closed forest canopies with hyperspectral data, *IEEE Transactions on Geoscience and Remote Sensing*, 39, 1491-1507.

Zarco-Tejada, P. J.; González-Dugo, V.; & Berni, J. A. J. (2012). Fluorescence, temperature and narrow-band indices acquired from a UAV platform for water stress detection using a micro-hyperspectral imager and a thermal camera. *Remote Sensing of Environment*, 117, 322-337.

.